

3D Thermal Modeling of Built Environments Using Visual and Infrared Sensing

Ghassan Al Lafi

A Thesis in

The Department of

Building, Civil, and Environmental Engineering

Presented in Partial Fulfillment of the Requirements

For the Degree of

Master of Applied Sciences (in Building Engineering) at

Concordia University

Montreal, Quebec, Canada

February 2017

© Ghassan Al Lafi, 2017

CONCORDIA UNIVERSITY
School of Graduate Studies

This is to certify that the thesis prepared

By: Ghassan Al Lafi

Entitled: 3D Thermal Modeling of Built Environments Using Visual and Infrared Sensing

and submitted in partial fulfillment of the requirements for the degree of

Master of Applied Science in Building Engineering

complies with the regulations of the University and meets the accepted standards with respect to originality and quality.

Signed by the final Examining Committee:

_____ Chair

Dr. Tarek Zayed

_____ Examiner

Dr. Amin Hammad

_____ Examiner

Dr. Bruno Lee

_____ Supervisor

Dr. Zhenhua Zhu

Approved by _____

Chair of Department or Graduate Program Director

February 2017

Dean of Faculty

ABSTRACT

3D Thermal Modeling of Built Environments Using Visual and Infrared Sensing

Ghassan Al Lafi

Infrared thermography (IR) is a modern, non-destructive evaluation technology for monitoring and assessing built environments. It mainly relies on measuring surface temperature to identify any potential defects or damages. Currently, IR has been introduced widely in applications such as facility condition assessment and energy performance analysis of existing buildings. However, most of the current practices in IR rely only on 2D thermal images which are time-consuming and labor-intensive. On the other hand, the rapid improvement of high-defined IR cameras has become a powerful tool in infrared sensing. Accordingly, this has facilitated its implementation in 3D thermal modeling techniques to replace the current 2D approach in thermal inspection and building energy efficiency. Yet, further studies need to be performed to overcome 3D thermal modeling limitations such as the high cost, slow process, and the need of highly trained professionals.

The main objectives of this research are to (a) test the potentiality of using 2D visible and thermal images which were collected separately through digital and infrared cameras respectively, for the 3D thermal modeling of built environments, and (b) investigate the efficiency of the proposed methodology by comparing it to a developed experimental design in terms of evaluating density, time, and cost. In specific, the visible images were used in modeling 3D point clouds by applying the structure from motion (sfm) approach. In parallel, the overlapping thermal images were stitched to form a thermal panoramic image that covers a large surface area with an accurate temperature representation. The stitched thermal images were then mapped to the reconstructed 3D point cloud in order to generate both thermal and metric measurements of built environments. Correspondingly, the output was compared to another 3D thermal point clouds which were developed by a laser scanner and an infrared camera. The comparison was conducted by means of evaluating density, time, and cost. Finally, the comparison results of three different built environments in the city of Montreal, Canada; demonstrate that 3D thermal modeling using separate 2D thermal and visible images was able to generate a dense geometric and thermal information of built environments. Also, this approach is affordable in terms of cost and time.

ACKNOWLEDGMENTS

Words cannot express the respect and appreciation I feel towards my family, supervisors, and friends. You resembled the kind-hearted father to me, the strict architecture to reach perfection and the willing friend to cheer me up.

Special thanks to my Parents, family, fiancée and to the faithful friends who stood by my side. You have been exceptionally helpful and extraordinary throughout my journey.

My precious gratitude is addressed to my instructor and supervisor Dr. Zhenhua Zhu for his endless support, precious advice, and wisdom. I wouldn't be here without his supervision. In addition, I would like to thank my examiners, Dr. Amin Hammad, Dr. Tarek Zayed, and Dr. Bruno Lee for their time, advice and effort in reviewing my thesis. Commitment and perfection are your goals. God Bless you all.

My sincere thanks to all colleagues in the lab office especially, Wael El Hassan and Xiaoning Ren. Thank you all for your support. It was a pleasure working my thesis with you and sharing with your non-everlasting experience.

Lastly, I would like to show my gratitude to the Natural Sciences and Engineering Research Council of Canada (NSERC) for their financial support.

TABLE OF CONTENTS

TABLE OF CONTENTS.....	v
LIST OF FIGURES	viii
LIST OF TABLES.....	xiii
LIST OF ACRONYMS	xv
CHAPTER 1: INTRODUCTION.....	1
1.1. Background and Motivation	1
1.2. Problem Statement	5
1.3. Research Hypothesis.....	6
1.4. Objectives and Scopes	6
1.5. Expected Contributions.....	7
1.6. Thesis Organization	8
CHAPTER 2: LITERATURE REVIEW	9
2.1. Facility Condition Assessment	9
2.1.1. Condition Assessment.....	10
2.1.2. Infrared Sensing in AEC/O&M	14
2.1.3. Recent Technological Development	18
2.2. 3D Thermal Modeling Techniques	20
2.2.1. Mapping Infrared Image with 3D Models	23
2.2.2. Image Fusion and Matching of Infrared Image with Photogrammetry	24
2.2.3. Mapping Infrared Image with 3D Point Clouds	28
2.3. 3D Spatial Modeling.....	32

2.3.1.	Photogrammetry.....	32
2.3.2.	Laser Scanning.....	36
2.3.3.	Overview of Point Cloud Data.....	41
2.4.	Research Gap	42
CHAPTER 3: METHODOLOGY		43
3.1.	Overview of the Proposed Methodology	44
3.1.1.	Digital Imagery	45
3.1.2.	Infrared Thermography	47
3.2.	Overview of the Experimental Design.....	50
3.3.	Output models Comparison	52
3.3.1.	Density-Based Evaluation.....	52
3.3.2.	Time-Based Evaluation.....	53
3.3.3.	Cost-Based Evaluation.....	53
CHAPTER 4: IMPLEMENTATION AND RESULTS		54
4.1.	Implementation	54
4.1.1.	Environments	54
4.1.2.	Hardware.....	57
4.1.3.	Software	67
4.2.	Case Studies	70
4.2.1.	Case Study I – Subway Tunnel Segment.....	71
4.2.2.	Case Study II – Gymnasium at Loyola Campus	86
4.2.3.	Case Study III – Lab Office in EV Building.....	98
4.3.	Discussion and Remarks	105
4.3.1.	Output models Comparison	105

4.3.2. Remarks	108
4.3.3. Limitations of the Proposed Methodology	115
CHAPTER 5: CONCLUSION	117
5.1. Summary	118
5.2. Concluding Remarks.....	119
5.3. Future Work	120
BIBLIOGRAPHY	121
APPENDIX.....	132

LIST OF FIGURES

Figure 1-1: (a) Infrared in the Electromagnetic Spectrum, (b) Infrared Color Palettes (FLIR, 2016c)	2
Figure 1-2: 3D Thermal Point Cloud model example of a building, (Chao Wang, 2014)	4
Figure 2-1: Building Condition Assessment Main Process (Ahluwalia, 2008).....	11
Figure 2-2: Two indoor examples; (a) a structural thermal bridge, and (b) opening thermal bridge (Asdrubali et al., 2012)	13
Figure 2-3: Masonry texture detection of a historical building; (a) Visible image; (b) Thermal image (Binda et al., 2011).....	15
Figure 2-4: Factors that affect UAS-based thermal imaging process (FLIR, 2016c).....	19
Figure 2-5: The Electromagnetic Spectrum (Teachers Guide to the Infrared, 2016)	20
Figure 2-6: Main Color Palettes in Infrared Sensing (Teax T., 2014).....	21
Figure 2-7: Infrared mapping to a 3D modeled family house (Schreyer & Hoque, 2009).....	23
Figure 2-8: (a) mosaic from thermal images, (b) fusing mosaic into a pair of visible images, and (c) 3D thermal point cloud model (Lagüela et al., 2012).....	24
Figure 2-9: As-is 3D spatial and thermal point cloud models using image fusion (Ham, 2015) .	26
Figure 2-10: Other techniques; (a) laser scanner and IR camera (González-Aguilera et al., 2012), (b) UAS-based thermal modeling (Hsieh & Chio, 2015), and (c) Aerial geothermal image (Nishar et al., 2016)	27
Figure 2-11: (a) Mobile robot Irma3D and (b) 3D thermal model of a façade (Borrmann et al., 2013); (c) e-pack system and (d) human operator carrying e-pack system (Oreifej, Cramer, & Zakhor, 2014).....	29
Figure 2-12: (a) Arrayed thermal camera sensors mounted on a vehicle, and (b) panoramic thermal image of a facade (Essess, 2016).....	31
Figure 2-13: Sample file for a radiometric panorama stitching (FLIR, 2016b).....	31
Figure 2-14: Stereo-Photogrammetry	32
Figure 2-15: Case example on calculating coordinates (Stachniss, 2015).....	33
Figure 2-16: point cloud generation through sfm	35
Figure 2-17: ToF laser scanner principle.....	37
Figure 2-18: Phased-shift laser scanner principle in Faro 3D.....	38

Figure 2-19: (a) Flash LADAR SR-3000 (Hegde & Ye, 2008); (b) Self-positioning handheld laser ZScanner® 700 (BIBUS, 2016)	39
Figure 3-1: Flowchart of the proposed methodology	44
Figure 3-2: Two consecutive overlapping images	49
Figure 3-3: Flowchart of the experimental design	50
Figure 3-4: Flowchart for output models comparison and evaluation	52
Figure 4-1: (a) Map for Montreal Subway(stm, 2016),(b) Schematic Plan for the tunnel testing environment	54
Figure 4-2: (a) Gymnasium building located in Loyola Campus (Concordia University, 2016), (b) Gymnasium schematic plan	55
Figure 4-3: (a) EV building located in SGW Campus (Concordia University, 2012), (b) Lab office schematic plan	55
Figure 4-4: Images showing subway tunnel testing environment	56
Figure 4-5: Images showing gymnasium testing environment	56
Figure 4-6: Images showing lab office testing environment	56
Figure 4-7: Nikon Digital SLR Camera D600 (Nikon, 2016)	57
Figure 4-8: Faro Focus 3D x 130 (Faro Technologies Inc., 2011)	58
Figure 4-9: Deploying laser scanner and reference targets.....	58
Figure 4-10: UAS-based Thermal Imagery System: DJI Matrice100 equipped with Zenmuse XT Camera (DJI and FLIR, 2016)	60
Figure 4-11: Components of the DJI Matrice100 (DJI, 2016).....	61
Figure 4-12: Detailed DJI Matrice100 components (DJI, 2016); (a) Propellers, (b) Frame Arm, (c) Center Frame, (d) Expansion Bay, (e) GPS module, (f) Damper, and (g) Gimbal mounting plate.....	63
Figure 4-13: Gimbal profile (DJI, 2016).....	64
Figure 4-14: Thermal precision test at 100° and 0° C	65
Figure 4-15: Components of remote controller (DJI, 2016)	66
Figure 4-16: Ground control station in the case studies	67
Figure 4-17: Image-based point cloud generation using Autodesk Recap 360 software	68
Figure 4-18: Laser-based point cloud generation using Trimble RealWorks software	68
Figure 4-19: Radiometric panorama and image stitching using FLIR Tools Plus software.....	69

Figure 4-20: Thermal mapping using 3dreshaper software	69
Figure 4-21: Flowchart of the followed research work in all case studies	70
Figure 4-22: Sample of the images collected from the subway tunnel testing environment	71
Figure 4-23: Examples of the removed blurry images.....	73
Figure 4-24: Manual registration of images in Autodesk Recap 360	73
Figure 4-25: Scaling: (a) a measurement from the generated point cloud model, and (b) a known real measurement while data processing.....	73
Figure 4-26: 3D image-based point cloud Model of the Subway tunnel segment.....	74
Figure 4-27: As-is image-based ortho-photo for the subway tunnel segment environment.....	74
Figure 4-28: Five spherical targets deployed in the subway tunnel environment	75
Figure 4-29: Images while laser scanning the subway tunnel testing environment	76
Figure 4-30: Adjusting settings for scanning (similar in all case studies).....	76
Figure 4-31: Scanning positions in the subway tunnel environment.....	76
Figure 4-32: Automatic registration of scans using Autodesk Recap 360.....	77
Figure 4-33: Scan registration report	77
Figure 4-34: 3D Laser-based point cloud Model of the Subway tunnel segment	78
Figure 4-35: As-is laser-based ortho-photo for the subway tunnel segment environment	78
Figure 4-36: Sample of the light torches used as thermal targets	79
Figure 4-37: Sample of overlapping thermal images collected from the subway tunnel environment	80
Figure 4-38: A sample for feature extraction and matching	81
Figure 4-39: A sample for thermal image stitching	81
Figure 4-40: As-is 3D Thermal Model of the Subway tunnel segment; a) Image-based 3D thermal model, and b) Laser-based thermal model.....	81
Figure 4-41: As-is image-based thermal ortho-photo for the subway tunnel segment environment	82
Figure 4-42: As-is laser-based thermal ortho-photo for the subway tunnel segment environment	82
Figure 4-43: Checkerboards as reference targets in the Gymnasium environment	86
Figure 4-44: Sample of overlapping images collected from the gymnasium testing environment	86

Figure 4-45: 3D image-based point cloud model of the gymnasium testing environment.....	87
Figure 4-46: As-is image-based ortho-photo of the gymnasium testing environment	88
Figure 4-47: The scanning positions used in gymnasium testing environment.....	89
Figure 4-48: 3D Laser-based point cloud Model of the gymnasium testing environment	90
Figure 4-49: As-is laser-based ortho-photo of the gymnasium testing environment.....	91
Figure 4-50: Sample of overlapping thermal images collected from the gymnasium environment	92
Figure 4-51: As-is 3D Thermal Model of the gymnasium testing environment; a) Image-based 3D thermal model, and b) Laser-based thermal model.....	93
Figure 4-52: As-is image-based thermal ortho-photo for the gymnasium testing environment...	94
Figure 4-53: As-is laser-based thermal ortho-photo for the gymnasium testing environment	95
Figure 4-54: Visual markers attached to the walls of the lab office testing environment	98
Figure 4-55: Sample of overlapping images collected from the lab office testing environment..	98
Figure 4-56: 3D image-based point cloud model of the lab office testing environment	99
Figure 4-57: 3D laser-based point cloud model of the lab office testing environment	100
Figure 4-58: Thermal data collection in lab office testing environment; a) capturing images remotely, and b) sample of the collected thermal images.....	101
Figure 4-59: (a) Image-based 3D thermal point cloud model of the lab office testing environment, and (b) laser-based 3D thermal point cloud model of the lab office testing environment	102
Figure 4-60: Density-based evaluation for all generated thermal models	106
Figure 4-61: Sample for complete and incomplete surface generation of point clouds	106
Figure 4-62: Time-Based evaluation for all generated thermal models	107
Figure 4-63: Average cost-based evaluation for generated thermal models.....	108
Figure 4-64: Used systems in existing studies and the proposed methodology	110
Figure 4-65: Output models of related existing studies	111
Figure 4-66: Output models of the proposed methodology	112
Figure 4-67: Section selection between 2D thermal input and 3D thermal output.....	113
Figure 4-68: An example for color variation analysis	114
Figure 4-69: Narrow space dimension of the lab office testing environment.....	115
Figure 4-70: Incomplete surface modeling of walls with uniform textures.....	116

Figure 4-71: thermal modeling of incomplete surfaces	116
Figure 6-1: Fixed-wing UAS; a) Insitu Inc., USA-Integrator; b) General Atomics Aeronautical Systems, USA-Predator A; c) QinetiQ, UK-Zephyr; d) Lockheed Martin, USA-Morphing UAS. (Colomina & Molina, 2014)	136
Figure 6-2: Rotary wing UAS; a) Cheerson CX10 nano UAS (Andi, 2015), b) Phoenix 15 micro UAS (Stevenson, 2013), c) Phantom 3 professional mini UAS (dji, 2016), d) Skeldar 150 VTOL and e) Tricopter UAS (SAAB Aerosystems., 2006), f) Matrice 100 (DJI, 2016), g) s1000 octocopter UAS (Dji, 2014), h) MQ-8B Fire Scout by USnavy (Ben, 2015).....	136
Figure 6-3: UAS composition (McDougal, 2016)	138

LIST OF TABLES

Table 1-1: Title and Summary of each chapter of this Thesis	8
Table 2-1: Comparison between remote sensing techniques	40
Table 4-1: Technical data of the visible camera (Nikon, 2016)	57
Table 4-2: Technical data of the laser scanner (Faro Technologies Inc., 2014)	59
Table 4-3: Technical specifications of the DJI Matrice100 aircraft (DJI, 2016)	63
Table 4-4: Technical data of the infrared camera (DJI and FLIR, 2016)	64
Table 4-5: Technical specifications of the used tower machine	67
Table 4-6: summary of data collection for the subway tunnel segment image-based point cloud	72
Table 4-7: summary of thermal data collection for subway tunnel segment	81
Table 4-8: Density evaluation of the subway tunnel environment	83
Table 4-9: Time-based evaluation for image-based visible and thermal 3D point clouds generation	84
Table 4-10: Time-based evaluation for laser-based and 3D thermal point clouds generation	84
Table 4-11: Cost-based evaluation for image-based visible and thermal 3D point clouds generation	85
Table 4-12: Cost-based evaluation for Laser-based and 3D thermal point clouds generation	85
Table 4-13: summary of data collection for Gymnasium environment	87
Table 4-14: Laser scanning summary for the gymnasium testing environment	90
Table 4-15: summary of thermal data collection for gymnasium testing segment	93
Table 4-16: Density evaluation of the gymnasium testing environment	96
Table 4-17: Time-based evaluation for image-based visible and thermal 3D point clouds generation	96
Table 4-18: Time-based evaluation for laser-based and 3D thermal point clouds generation	97
Table 4-19: Cost-based evaluation	97
Table 4-20: summary of data collection for the lab office testing environment	99
Table 4-21: Laser scanning summary for the lab office testing environment	100
Table 4-22: summary of thermal data collection for the lab office testing segment	101
Table 4-23: Density evaluation of the lab office testing environment	103

Table 4-24: Time-based evaluation for image-based visible and thermal 3D point clouds generation.....	103
Table 4-25: Time-based evaluation for laser-based and 3D thermal point clouds generation ...	104
Table 4-26: Cost-based evaluation.....	104
Table 4-27: Density evaluation summary of all case studies.....	106
Table 4-28: Time evaluation summary in all case studies	107
Table 4-29: Differences between related existing studies and the proposed methodology	109
Table 4-30: Color variation analysis.....	114
Table 6-1: Total energy consumption (Mtoe) (Enerdata, 2016)	132
Table 6-2: Types and characteristics of UAS (Colomina & Molina, 2014)	135
Table 6-3: comparison between fixed-wing UAS and rotary-wing UAS (Siebert & Teizer, 2014)	135
Table 6-4: Regulations for UAS use in several countries (Nex & Remondino, 2014).....	140

LIST OF ACRONYMS

IR	Infrared
AEC	Architecture, Engineering, and Construction
O&M	Operation and Maintenance
Sfm	Structure from Motion
GPS	Global Positioning System
UAS	Unmanned Aerial Systems
FCA	Facility Condition Assessment
BIM	Building Information Modeling
CA	Condition Assessment
CI	Condition Index
HVAC	Heating, Ventilation, and Air Conditioning
EIFS	Exterior Insulations and Finish Systems
ETIC	External Thermal Insulation Composite Systems
ISPRS	International Society for Photogrammetry and Remote Sensing
PARS	Photogrammetry and Remote Sensing
MTOW	Maximum Take-off Weight
MC	Main Controller
FCU	Flight Control Unit
ESCs	Electronic Speed Controllers
FAA	US Federal Aviation Administration
EASA	European Aviation Safety Agency
EPAR	Energy Performance Augmented Reality

MSX	Multi-Spectral Dynamic Imaging
SIFT	Scale Invariant Feature Transform
LIDAR	Laser scanning, also known as Light Detection and Ranging
ToF	Time of Flight
PS	Phased-Shift
USD	US Dollars
FOV	Field of View

CHAPTER 1: INTRODUCTION

1.1. Background and Motivation

Infrared Thermography (IR) is a modern remote sensing, non-destructive technology that is used for monitoring and evaluating built environments. The main concept of infrared thermography is the ability to measure, record and show temperature scale patterns of an object exterior surface (Cho, Ham, & Golpavar-Fard, 2015; Farrag, Yehia, & Qaddoumi, 2015; Gamidi, 2009; Chao Wang, 2014). Infrared are heat radiations emitted from objects with a temperature above than zero absolute. In other words, even cold objects such as ice cubes can emit IR radiations. Heat radiations are different than visible light, which means that IR radiations are non-visible by the human eye (Figure 1-1-a). Accordingly, infrared sensing can detect the non-visible long-infrared ranges of the electromagnetic spectrum and then generate images with several color pallets known as thermal images (Figure 1-1-b). Thermal images give a 2D thermal visualization in the form of a clear color difference, representing an interval of the relative surface temperature of each pixel (FLIR, 2014b, 2014a, 2016c; Teachers Guide to the Infrared, 2016; Chao Wang, Cho, & Gai, 2012).

Recently, 2D thermal images were introduced in the condition assessment of architecture, construction, and engineering (AEC) industries and applications related to the energy efficiency of the existing facilities (Lagüela, Armesto, Arias, & Herráez, 2012; Plesu, Teodoriu, & Taranu, 2012). In specific, 2D thermal images were used in the 2D thermal inspection of facility models. Which facilitate the collection of the unseen information for condition assessment and repair management such as the structural crack detection. In addition, 2D thermal images were also applied in applications related to energy performance analysis of existing built environments. Several studies have already shown that AEC industries in North America are considered as the highest energy consumers (Enerdata, 2016; NRC, 2012; U.S. Department of Energy, 2012). Thus, the need for a more efficient approach to the energy efficiency of the existing facilities has become a target that would be achieved greatly by implementing infrared thermography. For example, 2D thermal images were used in studying the condition of building envelopes, and the justification of thermal transfer in buildings (Farrag et al., 2015; Chao Wang, 2014; Chao Wang et al., 2012).

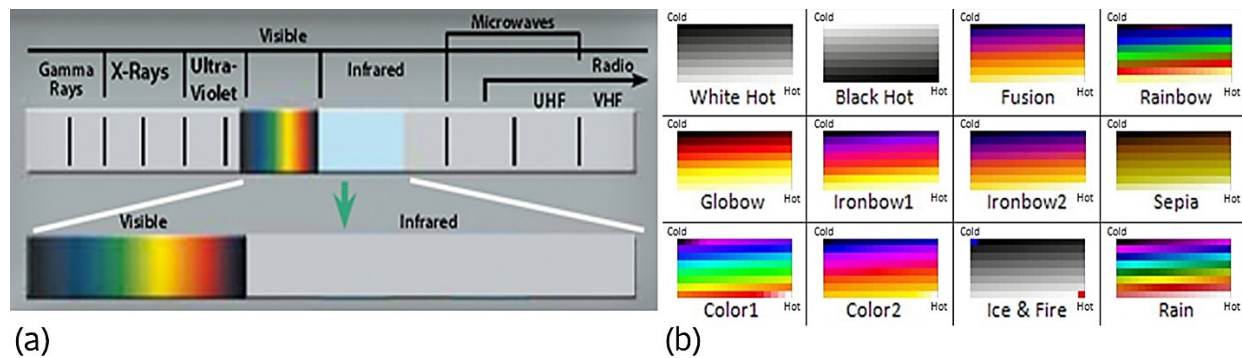


Figure 1-1: (a) Infrared in the Electromagnetic Spectrum, (b) Infrared Color Palettes (FLIR, 2016c)

However, relying on 2D thermal images for the thermal inspection is considered time-consuming, labor-intensive and insufficient (Chao Wang & Cho, 2011). First, applying only 2D thermal images for analyzing and reporting require more effort for searching and authorization. All of this would end in adding more time and effort to a project. Also, using selective 2D thermal images in thermal inspection and energy performance analysis does not include the entire geometry, materials, and the whole 3D as-is built environment condition. Therefore, 2D thermal images alone are considered as not sufficient to represent whole 3D as-is surrounding. Thus, the need for more reliable methods and techniques intended for AEC/OM facility models, as-is condition documentation, and energy efficiency analysis have become a necessary (Azhar & Brown, 2009; Chao Wang, 2014).

As a result, recent studies have proposed the use of infrared sensing in the generation of 3D thermal models to replace the current 2D thermal inspection (Chao Wang, 2014; Chao Wang & Cho, 2011). Using 3D thermo-graphic models to measure thermal information of buildings can be used widely by homeowners/users, contractors, consultants, and energy audits to help in the decision making of retrofit assessment (Chao Wang et al., 2012). 3D thermal models are reconstructed from thermal images and used widely in the sectors of building inspection, defect detection and energy efficiency analysis (Lagüela et al., 2012). Relatively, AEC industry has witnessed a huge development in remote and infrared sensing that could be implemented in 3D thermal modeling (González-Aguilera, Rodriguez-Gonzalvez, Armesto, & Lagüela, 2012). For example, modern high defined infrared- cameras have been improved in terms of performance, size, portability and cost (FLIR, 2013).

The implementation of the recent high defined IR cameras will surely have several advantages in 3D thermal modeling for defect detection and energy performance analysis (Ham, 2015; Lagüela, Martínez, Armesto, & Arias, 2011; Chao Wang, 2014). The list of advantages that could include but not limited to: (1) Fast image acquisition that covers large areas in a small duration; data collection using modern IR cameras can be achieved using the interval time collection feature. Thus, capturing multiple high still 2D thermal images can be achieved within seconds automatically. Unlikely, the old IR sensors require several seconds in order to process only one thermal image (FLIR, 2016a). Thus, old IR cameras were used mainly to capture only selective sections of an environment. (2) Enhanced spatial resolution; modern IR cameras can create thermal images with high spatial frequencies due to the integration of digital detail enhancement techniques. And, (3) Easiness in control and monitoring, in which modern IR cameras doesn't need any previous professional experience.

Related studies in reconstructing 3D thermal models have suggested several methods. For example, (Lagüela et al., 2012) proposed the image fusion of the textured surface of an exterior façade of a building with its thermal information using both digital and visible images. Next, the new fused images were applied under matching, 3D reconstruction algorithm to generate a 3D thermal building facade. Other researchers have tested the reconstruction of 3D thermal models through the as-is 3D point clouds represented by discrete point coordinates (x, y, and Z). Nowadays, photogrammetry and laser scanning are the most popular techniques in generating as-is 3D point clouds (Chao Wang, 2014; Chao Wang & Cho, 2011). Technically, reconstructing 3D thermal models through as-is point clouds require the mapping of infrared data with its relative spatial data. This could be achieved by superimposing infrared information, represented by thermal images collected using IR cameras, into a laser scanner-based point cloud. Mapping both thermal images and laser-based point clouds can solve problems related to image distortion and data acquisition. However, laser-based models are time-consuming when being tested within an environment of multiple confined spaces (Cho et al., 2015). Furthermore, infrared sensing was proved of being sensitive to neighboring bodies and the collection at different positions. Thus, mapping thermal images to a dense point cloud are still inaccurate due to the color variation of various thermal images. False thermal color variation can impress a wrong indication which in turn can lead to incorrect decisions.

An example of the color variation in the collected thermal images is shown in Figure 1-2. Where the IR camera was affected by the surrounding environmental factors such as shadows. Therefore, two thermal images being collected for two adjacent facades of an educational building (facades A and B, see Figure 1-2-a). Thermal image acquisition occurred at daytime in presence of sun heat and shadows. The output thermal images have shown different temperature visualization which was represented in a false thermal representation as shown in (Figure 1-2-b). Where “façade A”, being imposed to the sun heat has reflected a high temperature represented by the red hot color. While the adjacent “façade B”, covered by a shadow was represented as a colder area of green color. This can clarify that superimposing multiple thermal images of different thermal representation can lead to a false measurement (C Wang & Cho, 2014).

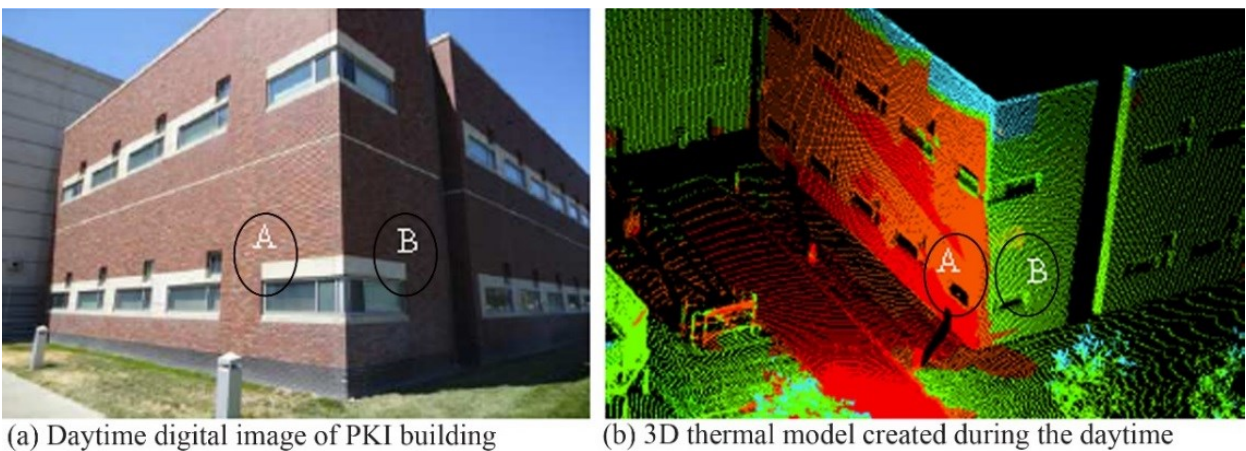


Figure 1-2: 3D Thermal Point Cloud model example of a building, (Chao Wang, 2014)

In addition, other researchers preferred the creation of as-is 3D thermal point clouds using photogrammetry. This process requires the collection of both visible and thermal images to generate 3D thermal point cloud models (Lagüela et al., 2012; Chao Wang, 2014; Chao Wang & Cho, 2011). Generating 3D thermal point clouds through photogrammetry is set to be more friendly, faster and cheaper (Colomina & Molina, 2014). The reconstruction of point clouds is done through both image overlapping and matching. Where applied algorithms in image matching are based on linking corresponding feature points of an object being collected from different positions. Consequently, the process of matching feature points in a 3D space based on their given projections onto two or more 2D images is called triangulation (Klein, Li, & Becerik-Gerber, 2012; Chao Wang, 2014).

Photogrammetry has become an affordable approach in representing the spatial information of as-built facilities due to the dramatic enhancements in visual sensing. Old practices of photogrammetry, known as softcopy photogrammetry, are dependent on the camera position coordinates at the time of collecting images. The collection is done mainly by a camera that is equipped with a Global Positioning System (GPS) and electric compass (Elhassan, Nejad, Daliri, & Zhu, 2015). However, (Klein et al., 2012) stated that current practices of photogrammetry can detect the coordinates and position of each image automatically, in an algorithm usually referred to as Structure from Motion (sfm). Advantages of using image-based 3D thermal modeling include but not limited to the reduction of relevant time and cost in reconstructing as-built facility models (Lagüela et al., 2012). Also, the introduction of commercial software related to sfm and mapping (e.g, Autodesk Recap360, Pix4dmapper, Postflight Terra 3D, etc...) made it more user-friendly for users to process the collected data.

1.2. Problem Statement

Infrared thermography has been introduced widely in areas such as facility condition assessment, energy performance analysis, and defect detection, etc. However, current practices in thermal thermography are heavily dependent on 2D thermal images which are considered as time-consuming, labor-intensive, and insufficient in representing 3D as-is built environment conditions. As a result, the need for a more effective approach in replacing the current practices in the thermal inspection of built environments using 2D thermal images has become a necessary.

Consequently, several researchers have suggested 3D thermal modeling as a replacement for the current 2D thermal inspection technique in defect detection and energy performance analysis. Relatively, infrared sensing has witnessed a remarkable development by means of efficiency, accuracy, size, and cost; in addition to the presence of efficient software related to photogrammetry and mapping. This has encouraged several researchers to implement these technologies in 3D thermal modeling as an approach. Yet, the existing studies in 3D thermal modeling are limited to different factors such as the highly cost of used laser scanners, slow data processing, and the need for highly trained professionals and experts. Therefore, there is still a gap in the literature regarding an affordable method in the 3D thermal modeling of built environments that can be accurate, reliable and easy to accomplish.

Correspondingly, the innovative improvements in generating as-is 3D image-based point clouds using 2D visible images have become a feasible way in generating the spatial information of the as-built environments. Consequently, the integration of infrared thermal imagery with the spatial information generated using photogrammetry has been a preferable solution for modeling 3D thermal point clouds of built environments. However, until the time of conducting this research, it is still not clear in the literature whether 2D thermal and visible images collected separately, by both infrared and digital cameras respectively, can be used to generate dense and accurate 3D thermal models of the built environments.

1.3. Research Hypothesis

With respect to the research hypothesis, several questions are suggested and need to be answered within this research, questions are as follow:

- [1] Can 2D visible, and infrared images collected separately be used in the generation of as-is 3D thermal models of built environments?
- [2] If yes, are these models feasible enough to be implemented in the field? And, Why?
- [3] Can this method facilitate the replacement of 2D thermal inspection by 3D thermal models? And, How?

1.4. Objectives and Scopes

The main objectives of this research are to; (a) test the possibility of using 2D visible and thermal images which were collected separately through digital and infrared cameras respectively, for 3D thermal modeling of built environments. And (b), investigate the efficiency of the proposed methodology by comparing it to a developed experimental design in terms of evaluating density, time, and cost. To accomplish these objectives, a novel method was developed that consist of two main stages as follows:

(1) In order to reconstruct 3D thermal models of built environments, a digital imagery sensor and an infrared thermal imagery sensor were deployed to capture 2D visible and IR images respectively. Next, the visible images were used in modeling image-based 3D point cloud model by applying the structure from motion (sfm) approach, which represent the spatial information of

the built environment. In parallel, the overlapping thermal images were stitched to form a thermal panoramic image that covers a large surface area with an accurate temperature representation. The stitched thermal images were then mapped to the reconstructed image-based 3D point cloud model in order to generate both thermal and metric measurements of the built environments.

(2) Respectively, the output model representing both metric and thermal measurements of built environments was compared to another 3D thermal point clouds which were developed by a laser scanner and an infrared camera. The comparison was conducted by means of evaluating density, time, and cost. Thereafter, investigating the density of the output model was done through the study of the total number of 3D points in a point cloud model. While time and cost evaluation were fulfilled by recording the time required for generating each model and the relative cost of equipment and software needed. To achieve research objectives, three different case studies were conducted in the city of Montreal, Canada: (1) Subway tunnel-Green Line; connecting station Frontenac and station Papineau, (2) Gymnasium of Loyola Campus at Concordia University, and (3) A lab office at the second basement floor level of the EV building at Concordia University. The purpose behind selecting such unlike environments was to test the proposed method within different variables such as the geometry of environments, materials, and lighting conditions. At the end of this research, a set of recommendations will be defined for further development and future work. In addition, limitations of this research will be presented and argued.

1.5. Expected Contributions

The findings of this research showed that both 2D visible and thermal images collected by a separate digital and infrared camera respectively; can be used effectively in the 3D thermal modeling of built environments. Moreover, the output models indicated that the generated 3D thermal point clouds were successful in the complete surface reconstruction of a surrounding. Also, the density of the generated point clouds was acceptable. In addition, the results of the proposed methodology designated that this approach is feasible in terms of time and cost. Furthermore, the research findings can encourage other researchers to develop new applications using both digital and infrared imagery. For example, a UAS or a robot can be implemented in this method for post-disaster modeling without the need of sending a human team for control and operating. Where, affected facilities by a disaster can be examined easily and remotely in cases like (earthquake, war, flood, etc.).

In addition, a remote control system could facilitate the study of dangerous facilities with high-security precautions such as (nuclear plants, military bases, prisons, etc. Besides, such remote-based system could be useful for rapid inspection assessment of long and large areas such as tunnels and large structures. For example, unseen defects and/or cracks can be detected easily for critical areas. This can help engineers and inspectors to identify serious building and infrastructure components for retrofits. Moreover, this method can also facilitate the boost of energy performance in a facility. In other words, this method could be implemented in several applications related to energy efficiency such as; the justification of thermal transfer, air leakage source inspection, Moisture detection and sick- building syndrome diagnosis, and HVAC systems performance evaluation. All of this could minimize the total energy cost and a waste of facility.

1.6. Thesis Organization

Table 1-1: Title and Summary of each chapter of this Thesis

Chapter	Summary
1) Introduction	The introduction summarizes the main idea of this thesis, highlight the gaps and shows the goals and targets. Also, it states the proposed objectives and the expected contributions of this thesis. In the end of this chapter, a thesis organization part is present.
2) Literature Review	This chapter reviews the main ideas in 3D thermal modeling and provides the closely related work to this research
3) Methodology	This chapter explains the framework of the proposed methodology that will be followed to achieve the objectives of this thesis.
4) Implementation and results	In this chapter, three case studies are described in details. Starting from setup environment to the execution of experiments, and finally providing results and findings for discussion.
5) Conclusion	This chapter summarizes the outcomes of this research and its findings. Define the outlines for further future works.

CHAPTER 2: LITERATURE REVIEW

This chapter will conduct a review of the recent studies and technologies related to facility condition assessment for the AEC and/or O&M. Followed, by studying the implementation of infrared thermography techniques. Besides, there will be a detailed evaluation of the related methods in the reconstruction of 3D thermal models. In the end, a summary of all will highlight the research gaps and needs. As a part of this task, three main classifications of literature reviews will be presented that includes but not limited to:

1. Condition assessment in AEC/O&M
2. Infrared sensing and 3D thermal modeling
3. Point cloud collection methods

2.1. Facility Condition Assessment

Improving facility condition assessment (FCA) and conducting effective retrofits to the existing buildings and infrastructures are considered among the biggest challenges to the AEC/O&M industries. Governments, engineers, and audits are trying to develop modern and efficient techniques to control and asses of existing built facilities. Currently, 2D spatial-based condition assessment is considered as the basis of any decision making in maintaining and renovating buildings and infrastructures (National Centre for Education Statistics, 2013). In other words, 2D inspection is the tool for the physical inspection system of built environments. However, there are no well-known based standards in such practice that can satisfy the desired objectives of owners and landlords (Chouinard & Andersen, 1996; Kaiser & Davis, 1996; Sadek, Kvasnak, & Segale, 2003). In North America, the public infrastructure is aging and overused; hence, the building sector requires a rapid intervention in maintenance and renovation (Ahluwalia, 2008; Grussing & Liu, 2013). In Canada, (Mackenzie, 2013) indicates that most of the public infrastructure buildings are currently showing an increasing rate of deteriorating, especially buildings of education and healthcare facilities, this raised the alarm to Canadians that their safety standards of daily living are in risk and danger. This can be illustrated by factors such as age, over capacity, and harsh environmental factors (Grussing & Liu, 2013). As a result, a serious challenge of conducting a proper inspection and appropriate condition assessment arose.

Currently, condition assessment methods are considered labor intensive, time-consuming, cost inefficient and subjective (Ahluwalia, 2008). On the other hand, 2D-based condition assessment is considered inaccurate, slow and old fashioned. Therefore, researchers and audits started to test new methods to satisfy the need of more reliable and efficient condition assessment practices. Here is a comprehensive overview of the related building and infrastructure condition assessment practices, process, and their different applications.

2.1.1. Condition Assessment

Building and infrastructure condition assessment can be handled through different parties as contractors, home-owners, audits, and mainly specialized inspectors. The performance of building and infrastructure inspection are measured and characterized in a relation of many standards and factors. However, the cost is considered as the major factor in the assessment process. Also, inspection requires a trained condition assessment team that seize a good knowledge about their tasks (Ahluwalia, 2008). Generally, condition assessment data includes inspection data, prediction, the short and long range of repairs and maintenance, work packages and budgeting. These data are transformed into meaningful condition metrics that can help in the decision making and retrofits (Amekudzi & McNeil, 2008). Currently, inspection surveys mainly deal with the recorded deficiencies, which makes the assessment only a response practice that only minimizes the damaging effect on civil infrastructure. As a result, a more advanced practice is required to allow inspection not only detect current defects but also to predict any expected deficiencies in the future. Where, maintaining weak points and any expected defects before taking place are much easier, faster and cost effective (Ahluwalia, 2008; Amekudzi & McNeil, 2008). Since current practices in condition assessment rely mainly on visible inspection, it is nearly impossible to predict for any expected deficiencies.

Technically, the traditional practice of inspecting building structures is heavily dependent on the manual and visual investigation of civil and engineering structures; that uses old fashioned techniques such as large access units, scaffoldings, truck cranes, and other related tools. These practices are considered time-consuming, expensive, and hard to handle especially for inaccessible and dangerous environments. In addition, these practices are inaccurate since the recognition and analysis process are highly dependent on the knowledge of inspectors which is error prone (Morgenthal & Hallermann, 2014).

Some of the approaches that can be applied in the building retrofit assessment and decision-making efficiency are the deficiency-based assessment; in which, the inspector will investigate visually and manually to recommend the weak points and work deficiencies. Another possible approach is the interval rating assessment; where an inspector appoint a numerical scale for measuring and assigning the condition state after an inspection (Grussing & Liu, 2013). Subsequently, the main function of condition assessment and repair for buildings and infrastructures can be categorized into main four levels. First, a current condition assessment of an asset; second, prediction of any expected defects in the future; third, choosing the best strategies and criteria's for maintenance, and finally applying the retrofits (Eweda, Zayed, & Alkass, 2013). In Figure 2-1, a summary of a facility condition assessment and repair is shown. The first step is the evaluation technique, which is considered as the most important stage, in which it will be used as the base for any later analysis, prediction, and decision-making. Finally, retrofits are applied in response to the final decisions. In summary, and based on the outcomes of both (Ahluwalia, 2008; Eweda et al., 2013), Current 2D-based inspection practices are considered inconvenient.

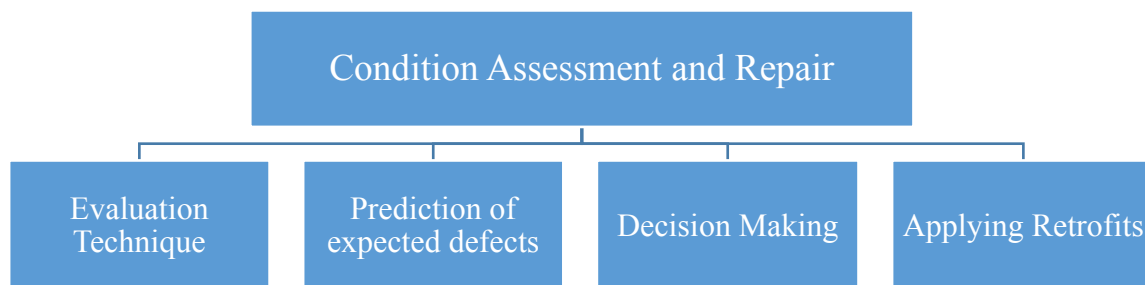


Figure 2-1: Building Condition Assessment Main Process (Ahluwalia, 2008)

On the other hand, AEC industries are considered as the main consumer of the primary energy consumption in North America (Maldague, 2001). The United States of America ranked as the second country, right after china, in energy consumption for the year 2014. While it was ranked first in North America with 90% of the total energy consumption. Canada, ranked ninth in the world and second in North America with 10% out of its total energy consumption. Still, Canada is considered among the highest in the world with some stability since 2009. North America alone including USA and Canada has a total energy consumption that is equal to 18 % of the total consumption of the world (Goswami & Kreith, 2015).

Due to the fact that north America is one of the biggest energy consumers in the world, Canada decided to enact and update laws related to energy saving and implement new codes in its building sector. This would be reflected in a more energy efficient environment. For example, some programs like “eco-energy efficiency for buildings”, for new and existing buildings in the commercial and institutional sector, is founded to preserve the implementation of energy standards in the building code. While “eco-energy efficiency for housing program”, especially for low-rise residential housing, aims to support the retrofit in the housing to be more energy efficient (NRC, 2012). On the other side, USA has decided to lower its energy consumption in the building sector by a range of (40%-70%). The building sector in the USA including both residential and commercial buildings consumes about 41% of the total energy consumption of the country (U.S. Department of Energy, 2012). Meanwhile, in Canada, housing sector consumes about 17% of energy consumption and “institutional and commercial” buildings consumes about 12% of the total energy consumption. Thus, the building sector in Canada consumes about 29% of the total energy consumption (NRC, 2012). This arises the need of quick and rapid actions toward energy efficient buildings implied ineffective solutions and corrective measures. Accordingly, the improvement of building energy efficiency and reducing environmental impacts relies mostly on the improvement of existing residential and commercial buildings (Chao Wang, 2014).

As a result, researchers and inspectors have suggested infrared thermography as a modern and reliable approach in building condition assessment and energy analysis. Infrared thermography is a promising non-destructive evaluation technique in monitoring and assessing building and infrastructure environments. The main concept of applying IR thermography in condition assessment is to detect defects using information being collected by infrared camera sensing. Where, thermal images collected by infrared sensing can read, show and record the temperature measurements of a surface. These temperature measurements are represented by a color scale scheme known as color pallets (FLIR, 2014b; Teachers Guide to the Infrared, 2016). Many advantages could be achieved by using the IR thermography in building and infrastructure inspection; firstly, it is considered as a rapid assessment model. Second, it is very easy in collecting preliminary data about defects and deficiency points in the built environments. Third, it can be very efficient in predicting defects that are non-obvious through the visible inspection. On the contrary, there are many challenges that could limit the performance of IR practice related to environmental conditions and material properties (Farrag et al., 2015; Plesu et al., 2012).

In summary, IR thermography is very efficient to facility's energy analysis, since it allows the detection of thermal bridges (Chao Wang & Cho, 2011). Thermal bridges, also known as heat or cold bridges, are the areas in which demonstrates a higher heat transfer with respect to its surrounding materials which results in a decrease in the performance of thermal insulation of that area. The presence of thermal bridges can be related to three main causes: (1) the big difference in heat conductivity between materials, (2) weak points in the thermal envelopes that permit for heat losses, and (3) absence or gaps in the insulation layers. Figure 2-2, shows two examples on how thermal images can detect thermal bridging of indoor environments. First, a structural thermal bridging in (Figure 2-2-a) demonstrates a decrease in surface temperature while heating. While in (Figure 2-2-b), a decrease in temperature is obvious at the level of coupling a door of glass and a frame (Asdrubali, Baldinelli, & Bianchi, 2012).

Consequently, many researchers have presented related studies in using infrared thermography technology in the building, infrastructure condition assessment, and energy analysis. (Plesu et al., 2012) Introduced infrared technology as a non-destructive application for building investigation in fields as structural systems and energy performance analysis. On the other hand, (Farrag et al., 2015) investigated the effect of mix variation of several concrete mixtures on the defect detection ability using the infrared thermography. Moreover, (Chao Wang & Cho, 2011) presented infrared sensing as a non-invasive thermal application that can show accurate thermal images.

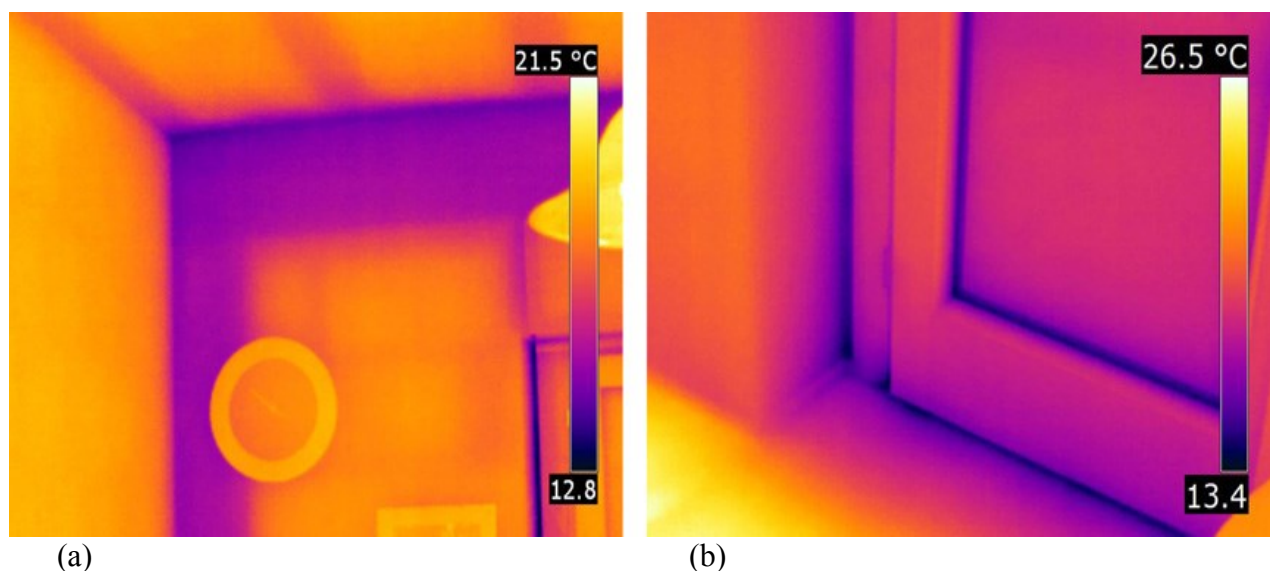


Figure 2-2: Two indoor examples; (a) a structural thermal bridge, and (b) opening thermal bridge (Asdrubali et al., 2012)

2.1.2. Infrared Sensing in AEC/O&M

Generally, any object with a temperature above than zero absolute is applicable of emitting heat in the form of electromagnetic radiations that represents its surface temperature. Consequently, infrared thermography technologies can be used for building and infrastructure investigation, by viewing the temperature distribution of the heated surface of an object (FLIR, 2014b; Gamidi, 2009; Teachers Guide to the Infrared, 2016). Technically, there are two methods for measuring the temperature difference of object surfaces; the passive (static) method and the active method. In summary, IR thermography can be used in applications related to facility condition assessment of existing built environments such as the investigation of structural systems and the justification of thermal transfer (Plesu et al., 2012). In the following section, a brief description of the different methods and applications of IR thermography in facility's condition assessment are explained.

IR Thermography Methods in Facility Condition Assessment

Passive (static) method: This technique is applied by using solar radiations at the stage of collecting thermal images without the need of applying any external system heating or cooling. The efficacy of this technique is based on three main factors; (1) Surface configuration: it detects the thermal conductivity by measuring the density areas. Where low density or sparse areas mean a lower thermal conductivity. (2) Surface conditions: defines the surface as rough or smooth; where rough surfaces have high emission values while smooth surfaces have low emission values. Thus, rough surfaces are more favor to be detected and collected. (3) Environment systems: environment factors which affect the accuracy and efficacy of infrared sensing. Factors are known as: “cloudy and windy weathers, high moisture levels, extreme cold and hot temperatures, and solar radiations”. As a result, the recommended condition of collecting thermal images could be at a clear night time, avoiding the harmful influence of environmental factors. Also, results from thermal images collected at a daytime and a nighttime are reversed. This can be justified by the fact, at night a defect detection area in thermal images will be reflected as the cooler temperature in comparison to its surrounding. While at a daytime defect detection areas are represented as the hottest (having higher temperature values) areas in comparison to its surrounding. This method is generally used since it is more consistent and even with the surfaces assessment results (Farrag et al., 2015; Plesu et al., 2012; Chao Wang, 2014).

Active method: Active IR thermography method usually requires an external source of IR radiations to heat-cool the object surfaces under study. The heated-cooled surfaces emit back an IR radiations that could be collected and recorded to view their temperature values, where a difference in temperature values could be identified representing a defect area detection. Also, heating and cooling process of object surfaces differ with respect to their materials. However, this technique is limited to the type of IR radiation used for the cooling and heating process. Additionally, active IR thermography method can be performed only in controlled spaces which mean it is limited only to the confined interior spaces. This technique requires more time for heating-cooling process thus it is considered as time-consuming. As a result, a passive (static) method is more reliable and preferable over the active method which is considered limited to the geometry and material of the testing surrounding (Plesu et al., 2012).

IR Thermography Applications in Facility Condition Assessment

Investigation of building structural systems

Recently, the use of IR thermography as a non-destructive evaluation technique in the inspection of building structures has been improved in a tremendous way (Plesu et al., 2012). In Figure 2-3, a masonry texture detection of a historical building is performed using both visible and IR thermal images. Where a comparison between the two collected visible and thermal images taken for the same building shows how a thermal image can show and visualize a hidden layer of hollow bricks. On the other hand, the visible image can only view the end layer texture of the paint. Where the shadow areas in the visible image are defined as the coolest areas in the thermal image, the coolest areas are represented by the blue color from the color scheme (Binda, Cantini, & Cucci, 2011; Plesu et al., 2012).

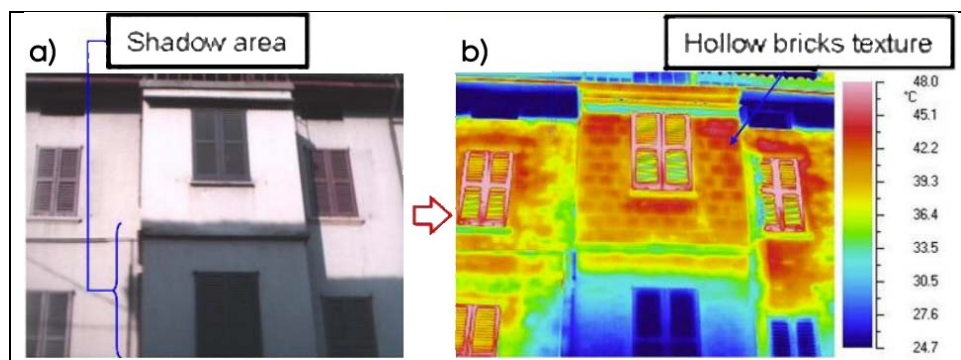


Figure 2-3: Masonry texture detection of a historical building; (a) Visible image; (b) Thermal image (Binda et al., 2011)

Justification of thermal transfer

Another important application of IR thermography in a facility condition assessment is energy analysis. Usually, the ideal energy performance of a facility is to maintain a temperature difference between interior and exterior environments with a range of (10° to 20° C). Relatively, the best condition of using thermography is when temperature fluctuating at zero degrees. At this point, the detected thermal bridges from outside represent heat bridges, while those recorded from the inside represents cold bridges. Cold bridges can be detected on walls, roofs, ceilings, frames of openings, and levels separating areas (Asdrubali et al., 2012; Wild, 2007). In summary, applying IR thermography to justify the thermal transfer in the facility can be categorized into five main applications described as follow:

1. Calculating heat losses for buildings envelopes

With the assumption that heat transfer is stable over space elements as (Walls, roofs, ceilings, and floors), it is possible to calculate the temperature distribution over the enclosed surfaces of a space. As a result, a set of mathematical algorithms is applied to measure the thermal losses over the air temperature from inside to outside. This process allows the categorization of buildings with respect to their energy efficiency (Plesu et al., 2012; Vavilov, 2010; Chao Wang et al., 2012).

2. Insulation inspection

Insulation in buildings is very sensitive to damages (i.e, cracks and shrinkage) as a result of aging, deterioration, and poor installations. This may lead to harmful problems like heat leaks accompanied with an increase in energy consumption, or the presence of molds and water leaks affecting the structure of a building. Consequently, IR thermography is used as a non-destructive approach to investigate the building insulation layers. Investigation process in the exterior environment must be done at a clear, non-windy day at day-time. Also, to take the advantage of solar heat that helps in displaying and detecting anomalies in insulation layers. In addition, this method is also used in moisture detection of Exterior Insulations and Finish Systems (EIFS) and External Thermal Insulation Composite Systems (ETIC). Furthermore, this method is applicable for indoor inspection; for example, the detection of the expanded foam insulation boards that have high risks of absorbing water by time (Barreira & Freitas, 2005, 2007; Plesu et al., 2012).

3. Air leakage source inspection

Relative problems with air leakage are mainly related to a failed window seal, other complex air pathways in walls, ceilings and floors, pipes and sanitary open holes, HVAC wires fixation holes, etc. These anomalies could be a deficiency in preserving air inside closed enclosures. The resulted air leakage are accompanied with a high energy consumption that means an increase in cost. Detecting the air leakage sources by manual visual inspection is considered very difficult since they are very small, hidden and hard to reach. As a result, thermal imaging is a reliable non-destructive inspection technique that can record air leakage sources easily. This method can be applied through different seasons if the temperature difference between inside/outside is more than few degrees (Asdrubali et al., 2012; Plesu et al., 2012).

4. Moisture detection and sick- building syndrome diagnosis

Improper insulation installation and other water leak problems can result in a mold growth and the presence of moisture in walls and roofs. IR thermography is very efficient in investigating and detecting the sick components of a facility with moisture and mold. The detection technique is easy since water has high thermal conductivity and high heat capacity; thus, can be easily detected using infrared sensing. But the challenge relies on the detection of moisture sources that have mostly the same sources of air leakage and water pipes installation anomalies (Asdrubali et al., 2012; Plesu et al., 2012).

5. HVAC systems performance evaluation

IR thermography can be a helpful tool for verifying the correct position and performance of devices that are required to afford heating and ventilation. Usually, this is accomplished using hot water and electric cables. Thus, pipe leaks can be easily detected in walls, ceilings, roofs, and floors (Plesu et al., 2012).

In conclusion, IR thermography is considered as a reliable non-destructive evaluation method in the inspection, investigation, and justification of the thermal transfer in existing buildings and infrastructures. As temperature index varies, this indicates the presence of anomalies and defects like (cracks, voids, hollows, etc.), poor insulation, air leakage sources, heat loss, and moisture. As a result, IR sensing can be a powerful tool over the visible inspection technique in facility condition assessment and energy efficiency (Barreira & Freitas, 2005, 2007; Plesu et al., 2012; Wild, 2007).

2.1.3. Recent Technological Development

Recently, technology has witnessed a remarkable high-tech development by means of equipment and its applications; especially in the last decade. Among these improvements, UAS technology market is growing rapidly and effectively. Technically, the US Department of Defense (DOD) has defined Unmanned Aerial systems (UAS) as generic unmanned aircraft that needs no human pilot on board. UAS exists in different types, models, sizes and system configurations (Siebert & Teizer, 2014). Unmanned aircraft are also known under many names and acronyms, such as Unmanned Aerial Vehicle (UAV), aerial robots or drones. Recently, the manufacturing of UAS has improved rapidly and spread intensively in the worldwide marketplace (Colomina & Molina, 2014). Latest studies show that UAS market will expand and escalate heavily in the upcoming few years, it will expand from 6,762\$ million in 2014 to 10,573\$ million by 2020 (Markets & Markets, 2014). Moreover, academic researchers and agencies started to invest in unmanned aircraft within many aspects and fields including construction process, building sector quality control and condition retrofits. Academically, UAS influenced researchers and projects. For example, the International Society for Photogrammetry and Remote Sensing (ISPRS) congress showed an increase in the submitted papers that reached the double between 2008 and 2012 (Colomina & Molina, 2014; Eisenbeiß, 2009).

On the other hand, another notable advancement is taking place in Remote Sensing. Spatial and infrared sensing pose an extraordinary technological enhancement by means of efficiency, accuracy, size, mobility, fast processing and cost. Consequently, and due to the high-tech development, recent UAS are equipped with a high-definition infrared camera. The modern trend has been successfully implemented in many applications including the AEC/O&M industries. However, UAS thermal imaging system has to overcome some of the challenges related to the environmental factors when navigation, and the oblique view angle of the UAS. Also, these prototypes were all designed for outdoor purposes and don't have the ability to capture both visible and thermal images simultaneously. As a result, UAS-based spatial and thermal sensing has multi-abilities; thus, it is predicted to be the next revolutionary technology in AEC/O&M industries. Below is a common background for UAS technology and its integration with the recent development in remote sensing. Followed by a description of its advantages and applications especially in the condition assessment of existing facilities (FLIR, 2013, 2014a, 2014b).

UAS-based Infrared Sensing

Recently, a notable collaboration between drone manufacturing and thermal imaging system was successfully established in developing a UAS-based thermal imaging system which is also known as UAS-based infrared sensing. The new high defined infrared sensing can be mounted on drones and are considered as the most current powerful thermal cameras. The main concept of remote infrared sensing is the ability to detect and record surface temperature taking into consideration the characteristics of surfaces, atmospheric interference, and the imaging system. Where the main surface characteristics that can alter the process of thermal measuring are surface emissivity and reflectivity. While the atmospheric interference is represented by the distance between the camera and surface and any composition in between. Finally, the imaging system which is represented by main factors like image focus, image blurry, and the pixel of the resolution (FLIR, 2016c). Figure 2-4, Show the effect of these factors on the process of UAS-based thermal imaging and the accuracy of temperature measurements of surfaces.

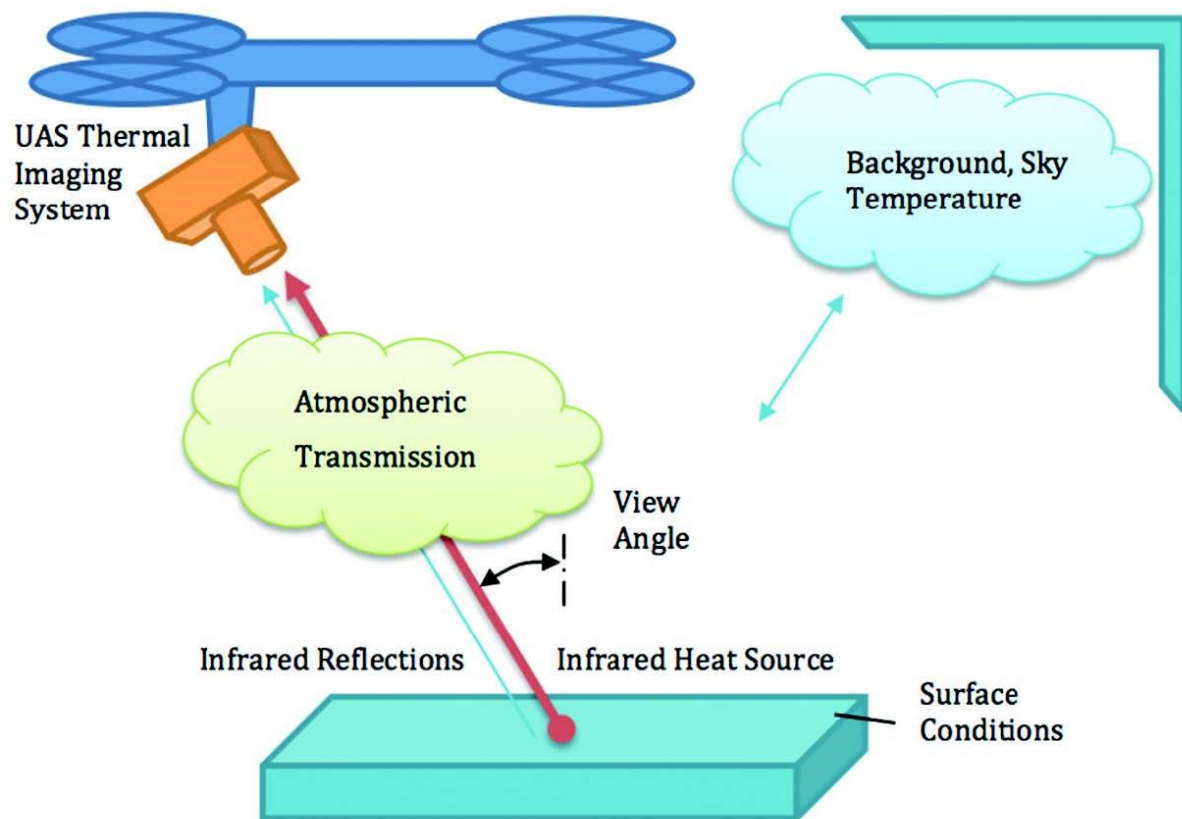


Figure 2-4: Factors that affect UAS-based thermal imaging process (FLIR, 2016c)

2.2. 3D Thermal Modeling Techniques

The discovery of infrared radiation and its thermoelectric effect goes back to the period between 1800 and 1821 by William Herschel and Thomas Johann Seebeck. Since that time and until now, scientists started to study and develop this technique implementation in various fields and applications (Plesu et al., 2012). The main concept of IR thermography is the ability to calculate and measure the surface temperature index of an object. The accuracy of this technique is too high, in which it can record and view the small differences in temperature as a few hundredths of a degree Celsius (Gamidi, 2009). Mainly, the implementation of IR thermography technique in the construction field is applied for building condition assessment of its structural systems, in addition to the justification of its thermal transfer such as the inspection of insulation layers, air leakage sources, and the calculation of heat loss for building envelopes (Plesu et al., 2012). The efficiency of this technique has been proven by means of efficacy, performance, feasibility, and easiness. IR thermography is a nondestructive evaluation technology that can be applied at daytime or nighttime taking in consideration some environmental conditions that can affect the results of this method (Ahluwalia, 2008; Amekudzi & McNeil, 2008). Thermal testing techniques are considered accurate, repeatable, feasible, and user-friendly (Gamidi, 2009). Recent technological developments facilitate the collection methods and techniques in implementing the infrared thermography for several applications (Cho et al., 2015).

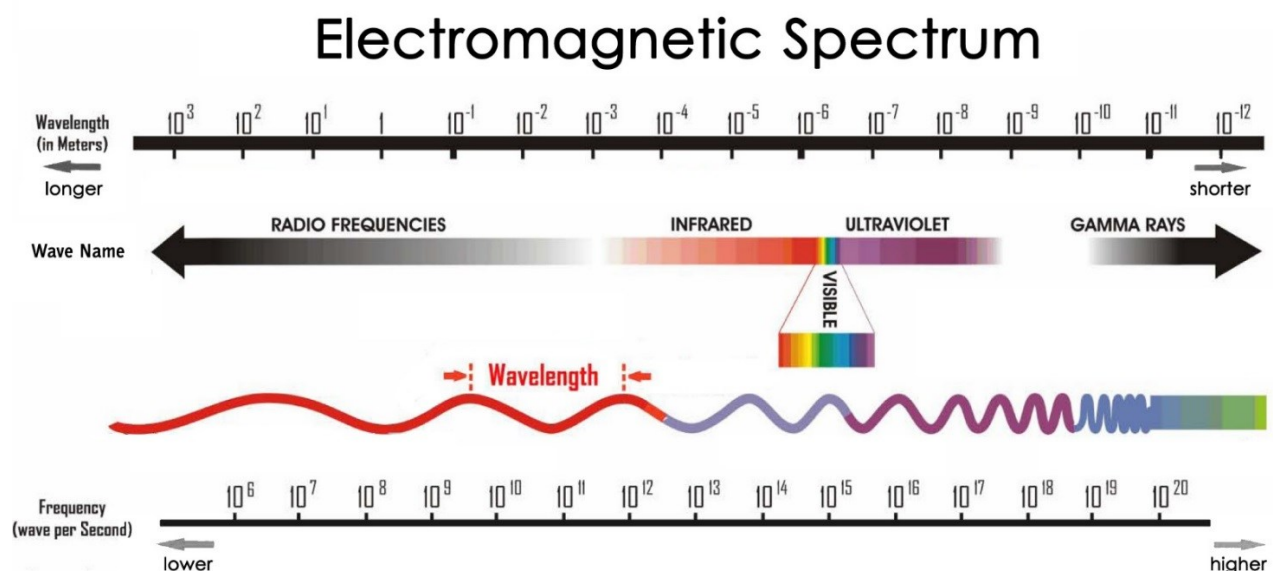


Figure 2-5: The Electromagnetic Spectrum (Teachers Guide to the Infrared, 2016)

Scientists have proved that human eyes can see a very small range of light waves known as the visible radiations, while other light waves do exist but are not visible to human eye. In Figure 2-5, the electromagnetic spectrum shows all the discovered light waves up to date, these various types of radiations differ in their wavelength and frequency. Infrared radiations refer to the heat energy or in other words the temperature of an object. Infrared sensing can record the surface temperature of an object. IR radiations have longer wavelengths and lower frequencies than visible radiations. In general, IR wavelengths ranges from $0.78\text{ }\mu\text{m}$ (IR shortest wavelength) to $1000\text{ }\mu\text{m}$ (IR longest wavelength). Consequently, infrared sensing has a combination of both IR imagery and lens detectors that give a visual illustration of the surface temperature of an object. Most of the infrared sensing operate in two common wave intervals of $3\text{ to }5\text{ }\mu\text{m}$ or $8\text{ to }12\text{ }\mu\text{m}$. Moreover, the most efficient condition for building inspection is to use long wavelengths of wave intervals between $8\text{ to }12\text{ }\mu\text{m}$. In specific, infrared sensing is able to detect IR energy and then convert them into electric signals that can be produced as thermal images or in another word “a false-color image” (Lo & Choi, 2004; Plesu et al., 2012; Teachers Guide to the Infrared, 2016).

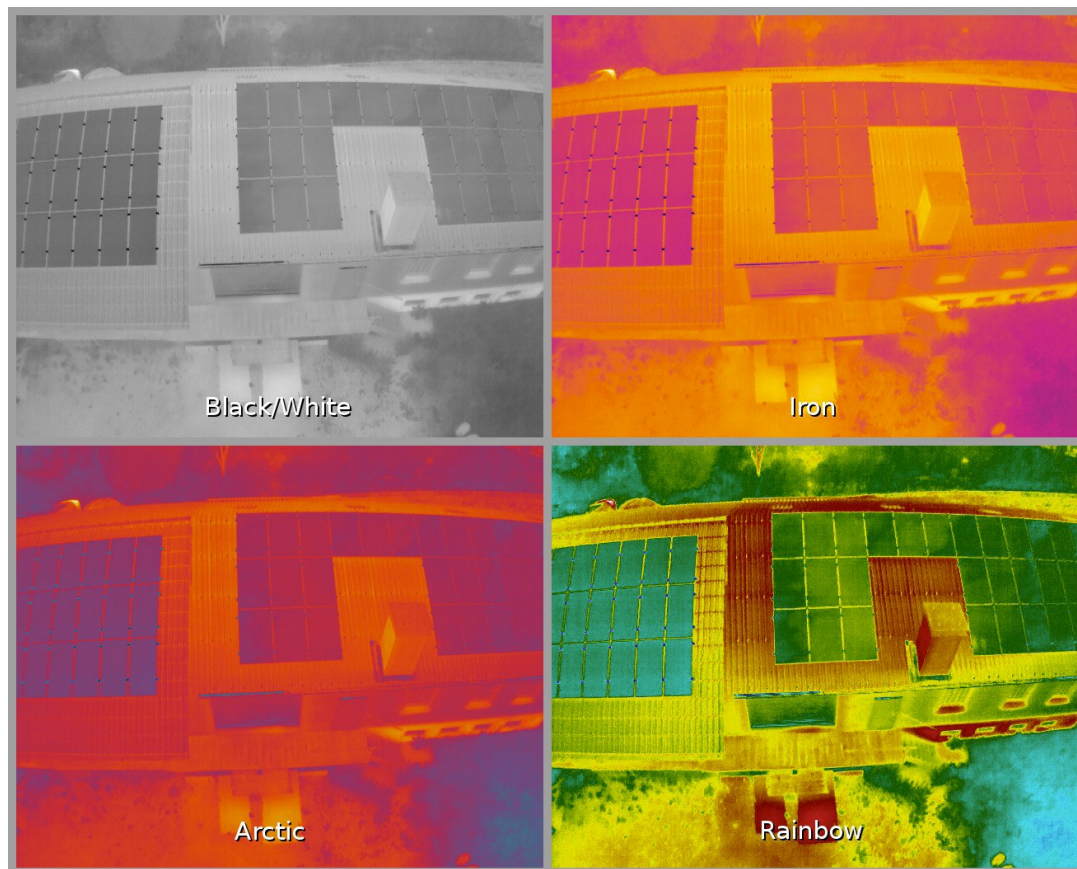


Figure 2-6: Main Color Palettes in Infrared Sensing (Teax T., 2014)

Since IR radiations are invisible and cannot be detected by our human naked eye, a technique was developed to convert temperature indications with a relatively visible color scale. These representations known as thermal images are in reality a false-color image representation. In which the variation of colors are transferred into a detectable color palette that represents the brightness difference variation of the detected object wavelengths (Teachers Guide to the Infrared, 2016). Many color palettes can be found in thermal cameras as a representation of false-colors, usually red and yellow colors are used as an indication of hot temperatures and blue is used for cold temperature representation. Eventually, colored images without its related color bar at the side are useless; there are four main color palettes that can be inverted creating eight possible color palettes ranges from iron, contrast, arctic, grayscale, hottest, coldest and rainbow (Vollmer & Möllmann, 2010). Figure 2-6 show the main four color palettes available in infrared sensing (Teax T., 2014)

Recently, infrared sensing was improved in an impressive way in terms of effectiveness, accuracy, size, and cost. In parallel, many software has taken place which is related to photogrammetry and mapping. As a result, researchers and audits started to develop as-is 3D thermal modeling techniques as an approach that can replace the existing 2D practices of thermal inspection and condition assessment. Adding to this, the innovative technological improvements in many fields have made as-is 3D thermal modeling an effective approach for energy efficiency. Consequently, the integration of thermal images captured using infrared sensing in the generation of as-is 3D thermo-graphic models have become a preferable solution for inspection and energy analysis, especially for built environments. However, existing techniques in 3D thermal modeling are much harder than 3D spatial modeling. Current methods in 3D thermal modeling have huge gaps for many reasons. For example, there are only a few tests have been accomplished in the area of as-is 3D thermal modeling, especially for the indoor built environments. Also, previous researchers didn't achieve encouraging results comparing to the promising capabilities of IR thermography. In summary, there are three categories in generating 3D thermal models using thermal images collected by infrared sensing. (1) Thermal imaging mapping to 3D models; (2) image fusion and matching between thermal and visible imaging captured by infrared and spatial sensing respectively; and (3) thermal imaging mapping to 3D point cloud models (C Wang & Cho, 2014; Chao Wang, 2014; Chao Wang et al., 2012)

2.2.1. Mapping Infrared Image with 3D Models

Current practices in 2D IR thermography are considered old fashioned since most of the 2D thermal images are low in resolution and can be confusing for audits and clients. Also, the representation of a fully 3D environment with 2D images is considered useless and ineffective. One way to visually represent thermal information on a 3D model is to map Infrared images collected by an infrared camera into a 3D modeled environment. Modeling 3D environments can be done using a variety of commercial software available such as: (Autodesk's 3ds max, AutoCAD, Revit, Maya, Blender, Google Sketch up and others). Next, thermal images can be mapped to the model as a thermal texture. To do so, multiple images are used to construct the full model. (Schreyer & Hoque, 2009; Chao Wang, 2014).

In Figure 2-7, an example of 3D thermal modeling is shown by mapping collected thermal images to a 3D model. First, (Schreyer & Hoque, 2009) used google sketch up software to remodel a single-family house using its footprint. Next, collected thermal images were mapped to the modeled geometry by assigning texture from images. This method shows successfully the visualization of thermal color variation on a 3D modeled geometry. However, many limitations can be addressed from this approach such as; (1) remodeling a building can't be used to represent an as-built model, thus the resulted 3D thermal visualization can't be used in the representation of as-is 3D thermal models. (2) Using multiple images in mapping one surface can be challenging. Where results show a lower-quality surface texture which in turn can reflect a false indication.

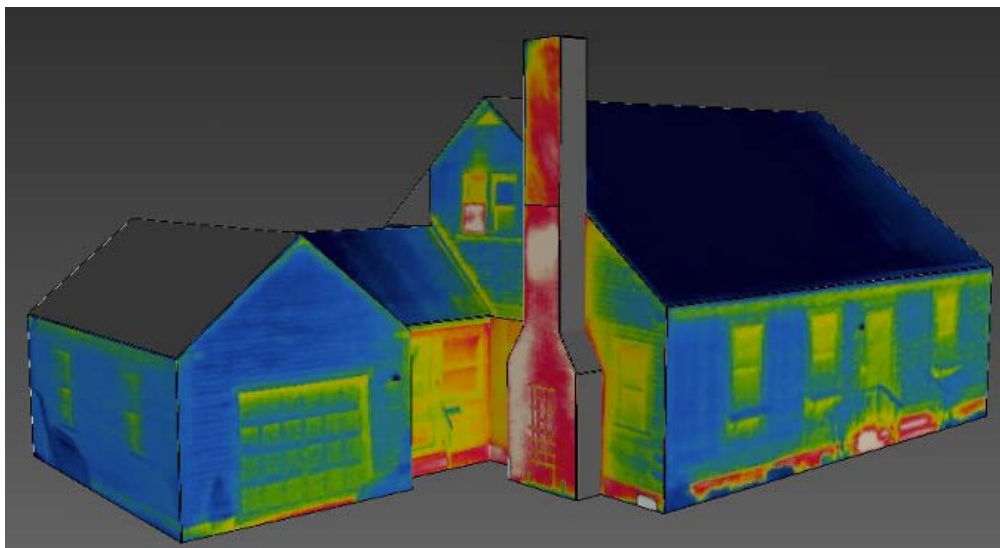


Figure 2-7: Infrared mapping to a 3D modeled family house (Schreyer & Hoque, 2009)

2.2.2. Image Fusion and Matching of Infrared Image with Photogrammetry

Another 3D thermal modeling approach was introduced by (Lagüela et al., 2012), which can be applicable for as-is facility environments. This research can be summarized into three main steps; (1) both a digital and thermal cameras were used to capture highly overlapped visible and thermal images respectively for an exterior façade of a building. (2) As shown in Figure 2-8, thermal images were registered together to form a large mosaic (Figure 2-8-a). Next, the registered mosaic was successfully fused to the multiple overlapping visible images using developed algorithms (Figure 2-8-b). (3) Finally, 3D surface reconstruction was applied using image matching techniques for a pair of overlapping fused images. Figure 2-8-c shows the resulted dense 3D thermal point cloud model.

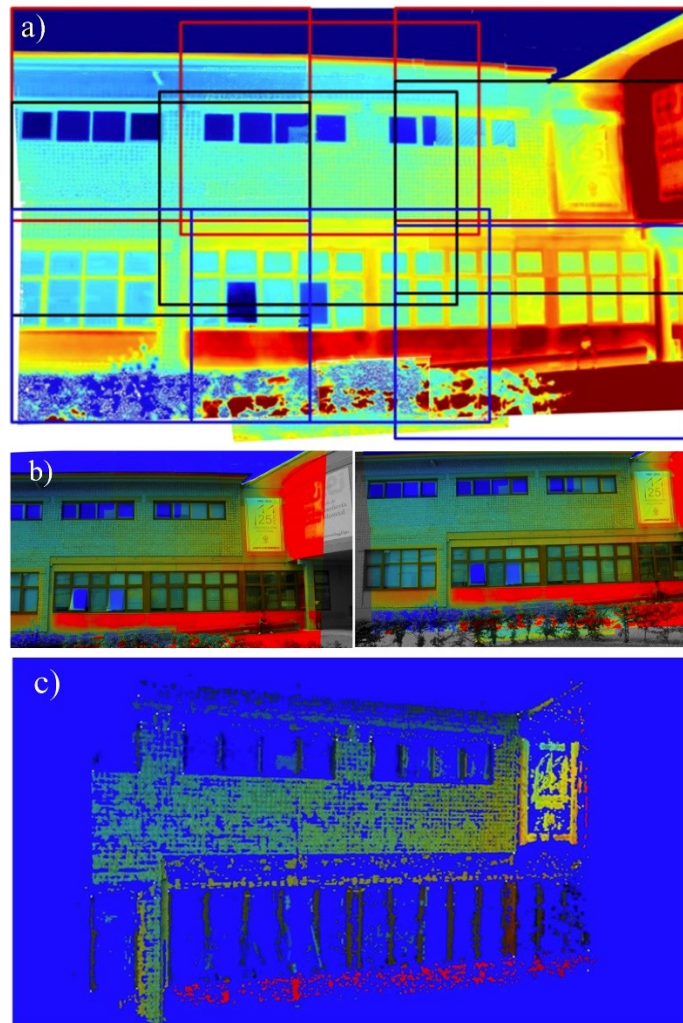


Figure 2-8: (a) mosaic from thermal images, (b) fusing mosaic into a pair of visible images, and (c) 3D thermal point cloud model (Lagüela et al., 2012)

Although (Lagüela et al., 2012) was successful in creating as-is 3D thermal point cloud model from fused thermal and visible images. Still, the output point clouds are not dense enough in case of using it later by engineers and audits for the purpose of inspection and retrofit assessment. Moreover, when collecting thermal images, IR camera was affected by the surrounding environment which caused a difference in the temperature scale of the same wall surface. This can be clear shown in the color variation of the represented mosaic and cloud model respectively (Figure 2-8-a, and c). To avoid or lessen the surrounding effects on the radiometric acquisition, (Ham & Golparvar-Fard, 2012; Lagüela et al., 2011; Schreyer & Hoque, 2009) and many others have proposed several suggestions. For example, one suggestion was to collect the thermal images in parallel of the studied surface and try to stabilize the height from the ground. Others suggested switching to normal mode when capturing images. Another suggestion is to unify the maximum and minimum temperature within a selected thermal scale. Even though the proposed suggestions were clearly useful in minimizing the effect of distortion and color range variation among multiple overlapped thermal images. Yet, most of the thermal cameras have at least (+1/-1 co) temperature error which can affect the representation of thermal information.

Another study in generating as-is 3D thermal point cloud models, Energy Performance Augmented Reality (EPAR), was presented by (Ham, 2015; Ham & Golparvar-Fard, 2012) Where one infrared sensing camera was used to collect both thermal and visible images simultaneously. This means that each captured image consists of one pair of visible and thermal images that have the same corresponding camera location and orientation. Next, each pair of images including spatial and thermal information were fused together to form one image containing spatial and thermal information. After that, a set of fused images were processed together using sfm approach to generate a 3D thermal point cloud model. (Ham, 2015) Presented about eight case studies including exterior facades and indoor environments of an instructional facility and a residential building. Unlike (Lagüela et al., 2011), this method was useful in creating indoor and confined environments. However, the resulted models failed to compute the complete surfaces of an environment creating some hollow areas in the generated models. Also, digital images are imperfect at night and within dark conditions, while thermal images are encouraged to be collected at nighttime to avoid lighting conditions. This has made this method limited to the surrounding lighting environments. On the other hand, indoor environments were affected by the reflective materials and neighboring objects (Chao Wang, 2014).

In Figure 2-9, (Ham, 2015) has tested an indoor environment of a kitchen in a residential building and the exterior façade of an instructional facility. In the first experiment, 165 pairs of images were collected for the indoor kitchen. After image fusion, sfm approach was applied to run the 165 visible images alone in (Figure 2-9-a) and the 165 fused images in (Figure 2-9-b). Only 93 visible images were successfully registered in creating the 3D point cloud, this corresponds to 0.56 success ratio in registering visible images. On the other hand, 678 pairs of images were collected to the exteriors facades of an instructional facility. Next, image fusion was applied to run the 678 visible images alone in (Figure 2-9-c) and the 678 fused images in (Figure 2-9-d). The corresponding 3D point cloud was successful in registering 672 images with a relative 0.99 success ratio in the registration of visible images. These experiments reflect the high success of this method within outdoor environments, while it is very limited for indoor environments. In summary, this method failed in reconstructing the reflective and uniform materials such as tiles and walls. Also, 3D thermal point clouds are considered sparse when compared to its relative 3D spatial point clouds. For example, in (Figure 2-9-a) the number of spatial point clouds is 2,262,349 points while it is only 220,428 thermal points in (Figure 2-9-b). Similarly, (Figure 2-9-c) has 28,552,261 points while it is only 2,489,117 thermal points in (Figure 2-9-d)

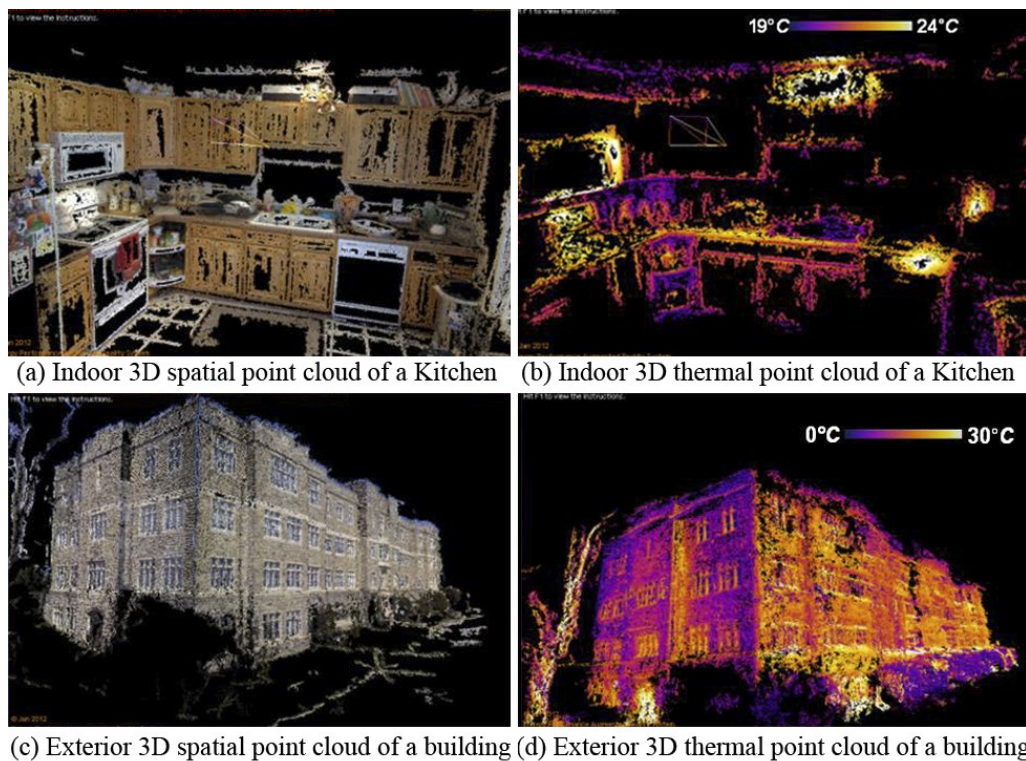


Figure 2-9: As-is 3D spatial and thermal point cloud models using image fusion (Ham, 2015)

Furthermore, other researchers have developed new techniques within image fusion. For example, In Figure 2-10-a, (González-Aguilera et al., 2012) used a laser scanner and a thermal camera to create a thermal orthophoto for building exteriors. First, a range image of the scanned point cloud was obtained using a laser scanner. Next, visible and thermal images were fused together and registered on the range image using feature extraction technique. In the end, a thermal orthophoto of the building exterior was created. On the other hand, recent commercial companies have developed UAS-based thermal camera sensors that can be used in generating semi-automatic 3D thermal aerial mosaic for agriculture and geothermal environment applications. (Hsieh & Chio, 2015) Conducted a study to create a thermal mosaic for an outdoor gym using a quadcopter UAS equipped with an FLIR tau thermal sensor as shown in Figure 2-10-b. Another study in UAS-thermal based imaging was done for a geothermal environment at Wairakei - Tauhara field, New Zealand by (Nishar, Richards, Breen, Robertson, & Breen, 2016). The resulted thermal mosaic is shown in Figure 2-10-c. However, UAS-thermal imaging for 3D modeling of building and infrastructure facility's is still very limited within outdoor environments and does not exist for indoor environments. Nevertheless, recent modern thermal cameras are more advanced in a way that can provide automatically fused images that contain both spatial and thermal information. This technology of thermal image enhancement is known as the multi-spectral dynamic imaging (MSX). The main concept of this technology is to add key details from the visible sensor to thermal images (FLIR, 2014b). Still, applying previous methods for indoor environments have failed or at best can give very sparse results that are ineffectual in any further assessment.

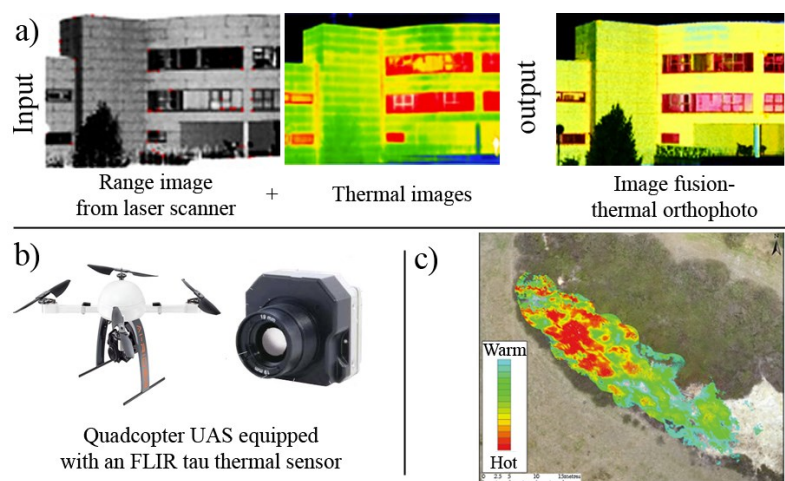


Figure 2-10: Other techniques; (a) laser scanner and IR camera (González-Aguilera et al., 2012), (b) UAS-based thermal modeling (Hsieh & Chio, 2015), and (c) Aerial geothermal image (Nishar et al., 2016)

2.2.3. Mapping Infrared Image with 3D Point Clouds

Another technique in creating as-is 3D thermal models for existing buildings and infrastructures is by mapping 2D thermal images to 3D point cloud models. Thus, fusing captured thermal information to the generated spatial information models. Previous studies using this approach have shown more advanced results over the above-mentioned techniques (Chao Wang, 2014). Following, a detailed review of the recent promising studies in using this approach is presented. To begin, a “Bi-camera” system was introduced by (Alba, Barazzetti, Scaioni, Rosina, & Previtali, 2011), a system which consists of IR camera sensor, digital camera, and a laser scanner. First, thermal information of a facility was collected by the IR camera sensor while 3D point cloud scans were generated using a laser scanner. Then, both a digital camera and laser scanner were used to detect and measure control points manually. Finally, thermal information was fused to point clouds using control points. The output 3D point cloud model successfully showed a thermal color range variation. However, the bulkiness of this system at data acquisition have resulted in a very time-consuming process. Also, with the fact that digital sensors are sensitive to lighting conditions, this system is limited in darkness and advised to take place only at daytime.

Another approach was presented by (Lagüela et al., 2011) using a calibrated IR camera sensor. First, the infrared sensor was calibrated to minimize image distortions while a laser scanner was used to scan and generate 3D point clouds. Next, processed thermal images were entered into a commercial software. Later, images were mapped and textured the laser-based point cloud. Mapping process was done manually for each image using at least six different control points. The resulted model positively displayed a visualized thermal color range difference for an exterior façade of a building. Yet, several limitations can be deduced, in order to avoid image distortion and minimize thermal color variation from one thermal image to another; (1) the infrared camera sensor must be in a perpendicular shooting direction with the facing façade. And, (2) the distance between an IR shooting camera sensor and a façade is fixed with high overlapping manner more than 50%. (3) Data collection is advised to take place at nighttime in order to reduce surface heating by the sun heat. In summary, (Lagüela et al., 2011) has proposed a more efficient and user-friendly approach, it is still unclear how this approach can perform in confined indoor environments. Also, mapping images manually are both time-consuming and labor intensive especially for large-scale projects and multiple closed spaces.

Additional approach was provided via (Borrmann et al., 2012; Borrmann, Elseberg, & Nüchter, 2013) by developing a mobile robot (Irma3D), Figure 2-11-a, that consists of a Light Detection and Ranging (LIDAR), a digital webcam sensor and a low-resolution thermal camera sensor (160 x 120 pixels) mounted on the top of the robot. Data collection process using Irma3D robot was conducted by taking multiple scans at different locations. First, a laser scanner was used to scan a surrounding environment while the mounted thermal camera sensor rotated over the vertical axis of the laser scanner and captured nine images that covered the whole 360° scene. After, thermal information was automatically mapped to the scanned models using the 6D simultaneous localization and mapping technique (SLAM). The corresponding approach was applied on the town hall façade in the city of Bremen, Germany (Borrmann et al., 2013). The result is shown in (Figure 2-11-b). However, this system is inadequate when collecting information over 100 vertical degrees due to the limited camera field of view. Consequently, tall buildings need to be scanned from a faraway distance which would affect the resolution and accuracy of the collected thermal information (Cho et al., 2015).

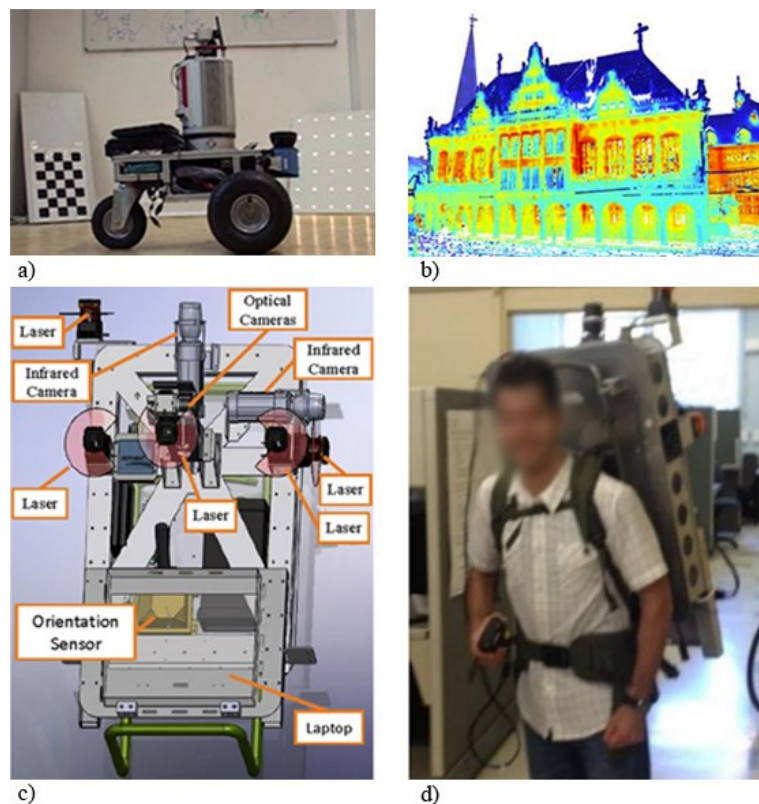


Figure 2-11: (a) Mobile robot Irma3D and (b) 3D thermal model of a façade (Borrmann et al., 2013); (c) e-pack system and (d) human operator carrying e-pack system (Oreifej, Cramer, & Zakhori, 2014)

While most of the studies focused on 3D thermal visualization of exterior environments and building facades, (Oreifej et al., 2014) presented a study for 3D thermal mapping of building interiors. To do so, a new system called “e-pack”, (Figure 2-11-c) was developed. The system consisted of five 2D laser sensors, two infrared camera sensors, two optical camera sensor with fisheye lenses, an orientation sensor, and a laptop. Figure 2-11-d shows the massive system that can be carried by a human operator. For data acquisition, an operator carried the system and walked through an interior environment to collect information. Next, the collected data were processed offline and the traversed environment was generated as a 3D point cloud model. Then, co-registration was applied to texture both the visible and thermal information to the point cloud model. Output models showed aligned spatial and thermal point cloud models. The advantages of interior thermal mapping can be summarized in the applications of inspection and energy efficiency analysis. However, this method is limited to the inaccessible places that are hard for a human to reach. Also, the “e-pack” system is extremely expensive and require the integration of several sensors. Furthermore, a hybrid LIDAR system was developed and introduced by (Chao Wang et al., 2012), this system consists of two robotic Infrared camera sensors (320x240 pixels) integrated with a laser scanner. Similar to previous studies, thermal information were fused to laser-based point clouds representing a 3D thermal point cloud models. In addition, window detection algorithms were applied to generate thermal points on the transparent glass surfaces.

Methods that facilitate the collection of thermal images:

While most of the studies focused on the developing techniques related to data processing, only few who tried to enhance and improve data collection process. (Essess, 2016) Introduced a technique that enhances the process of collecting the very large amount of overlapping thermal images for building facades at night. To do so, several arrayed thermal camera sensors were mounted on a car to capture multiple overlapping thermal images at the same, Figure 2-12-a. Next, overlapping images were stitched together to create a large panoramic thermal image of a building façade represented in Figure 2-12-b (Cho et al., 2015). Moreover, FLIR systems have developed a platform tool that can stitch radiometric images into large thermal panoramas. Stitching requires minimum 30% overlapping thermal images, then using the feature extraction method that can identify the exact overlapping areas ready to stitch (FLIR, 2013). However, this technique is only available for the modern thermal camera sensors with high resolution as shown in Figure 2-13.

This practice was also available in other commercial software like IRT stitch developed by GRAYESS Inc (GRAYESS Inc, 2016). Hence, the advantage of such technique is the possibility of creating wide thermal images at the collection stage without losing any of the thermal information. Also, with the fact that recent modern thermal cameras are integrated with digital detail enhancement techniques, modern thermal images were enhanced dramatically as high spatial frequencies are boosted. This improved feature detailing and made it more precise. So, radiometric stitching has become more efficient and promising as a tool that can be invested in thermal mapping and 3D thermal reconstruction. Correspondingly, other recent studies also suggested the implementation of UAS in collecting thermal images for the purpose of 3D thermal modeling. (Roca, Martínez-Sánchez, Lagüela, & Arias, 2016) Used UAS-based thermal imagery to automatically extract building geometries that will be later used in the modeling of 3D buildings.

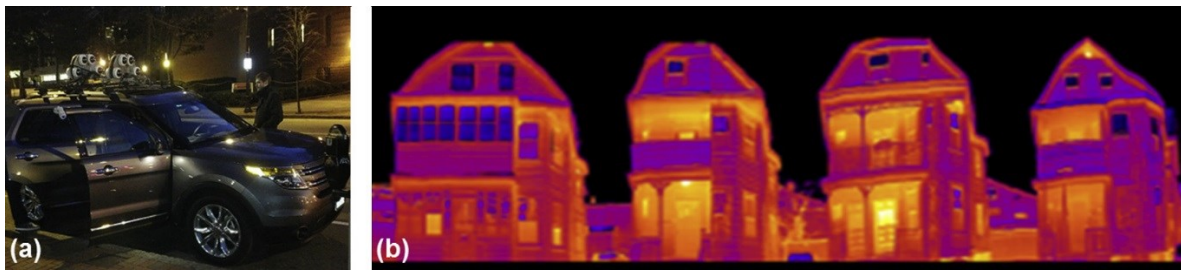


Figure 2-12: (a) Arrayed thermal camera sensors mounted on a vehicle, and (b) panoramic thermal image of a facade (Essess, 2016)

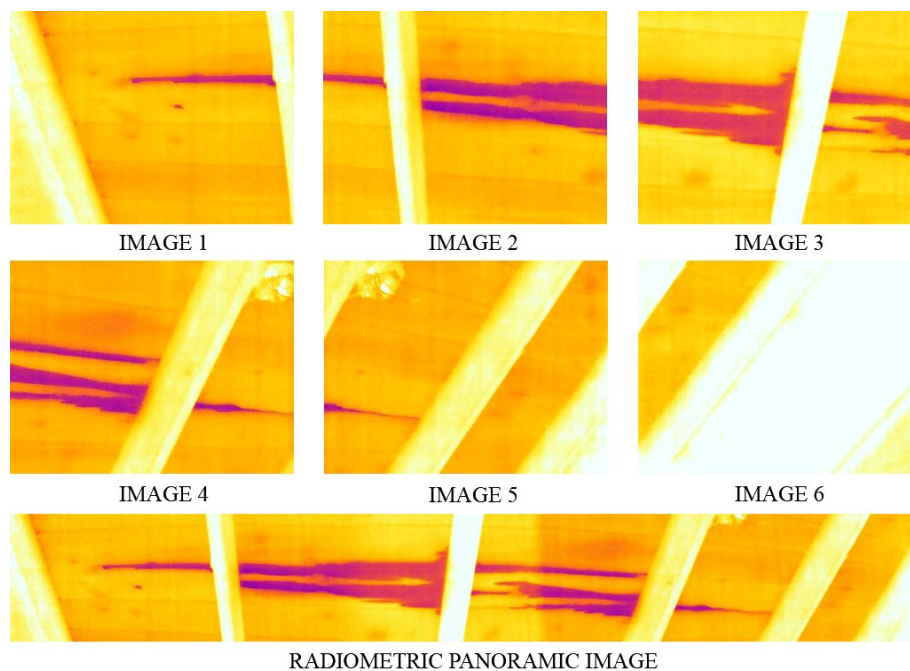


Figure 2-13: Sample file for a radiometric panorama stitching (FLIR, 2016b)

2.3. 3D Spatial Modeling

Point cloud consists of a group of points that resembles the outer surface of an object, in which each of these points has its coordinates (x,y,z) confined in one discrete coordinate system. The most common and popular techniques for generating point cloud is known for remote sensing solutions that include but not limited to photogrammetry and laser scanning. The main concept of point cloud generation is known as registration; where multiple sets of images (photogrammetry) or scans (laser scanning) are grouped and combined into one common coordinate system. Recently, point clouds were implemented in the construction sector for reconstructing as-is models of the existing buildings and infrastructures (Eisenbeiß, 2009).

2.3.1. Photogrammetry

The main concept of photogrammetry relies on measuring the spatial features distances and localizing its positions, for any visible surface using collected overlapping images. This approach consists of four steps, the first is to identify and extract common feature points among images, the second is to match the extracted feature points that are known as stitching, the third is to identify the camera location with respect to each image, the fourth is to intersect these feature points and reconstruct a 3D data model in one coordinate system which is known as triangulation (Klein et al., 2012). Photogrammetry is also known as Stereo vision or stereo-photogrammetry, in which softcopy triangulation algorithms are applied on the overlapping stereo-pairs (Westoby, Brasington, Glasser, & Hambrey, 2012). The term stereo-photogrammetry is referred to the method of identifying the 3D coordinates of common points found in different images being collected from different positions (Chao Wang, 2014; Westoby et al., 2012).

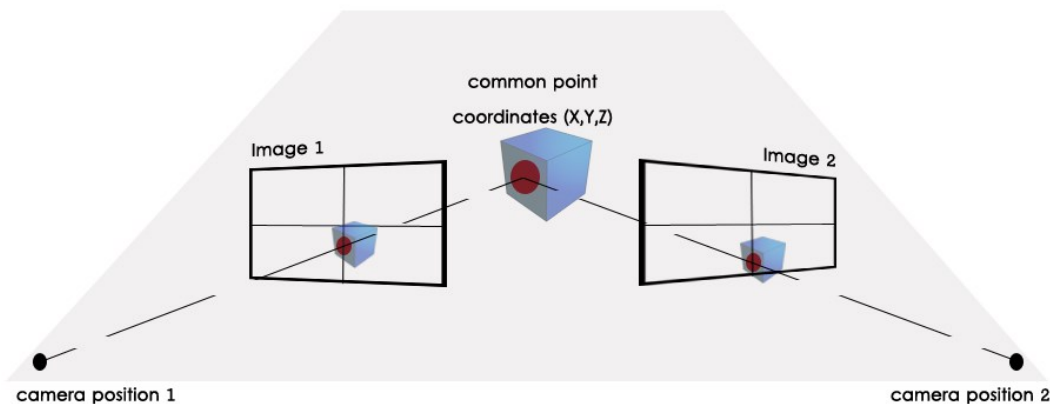


Figure 2-14: Stereo-Photogrammetry

In Figure 2-14, a cube appears in two different images (Images 1 and 2) taken from two different positions (camera position 1 and 2), the same common point (the red point) appears in the two different images of different locations and orientations. Triangulation is the method of using the two overlapping images 1 and 2 to identify the position (3D coordinates) of the common point (the red point). To simplify a basic calculation case example, two images (I and II) were taken at the same focal length f , same height, and orientation method. Thus, the two images share the same Y and Z coordinate but different X coordinate. Thus, translating the calculation into a simplified 2D problem can be done by ignoring the Y-axis. In Figure 2-15, I and II are two images were taken respectively with the same focal length f . P is a real feature point that is projected into P' in the image I and P'' in image II. O' and O'' are the focal points for the two images respectively. Thus, B is the distance between O' and O'' . While the X-coordinates of P' and P'' are x' and x'' respectively. First, Z-coordinate must be calculated. Thus, $O'P$ can be projected to O'' (represented as the red line). Using the intercept theorem in Equation 1, P_x is the difference in the x-coordinate of P' (x') and P'' (x''). By substituting this into Equation 2, the Z-coordinate of point P can be deduced. While Equation 3 is the corresponding theorem to calculate the X-coordinate of point P. Thus, by substituting the z from Equation 2 into Equation 3, the X-coordinate can be deduced in Equation 4 (Stachniss, 2015).

$\frac{Z}{f} = \frac{B}{Px}$	Equation 1	$Z = f \frac{B}{x' - x''}$	Equation 2
$Z = f \frac{B}{x' - x''}$	Equation 3	$X = x' \frac{B}{x' - x''}$	Equation 4

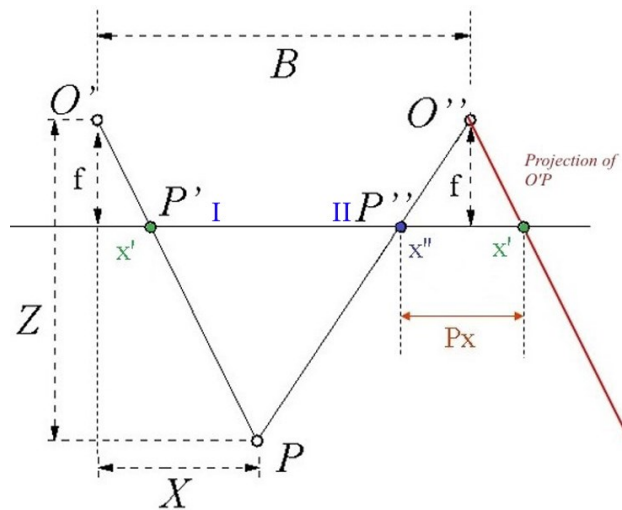


Figure 2-15: Case example on calculating coordinates (Stachniss, 2015)

Consequently, photogrammetry relies on the calculation of 3D coordinates of common feature points, using the identification of location and orientation for each of the collected images (Klein et al., 2012). Thus, photogrammetry was applied to transform images rich with spatial information into as-built 3D models (Chao Wang, 2014). Old practices achieved this manually using a GPS (for location) and electric compass (for orientation), but it's said to be ineffective by means of effort and time (Klein et al., 2012). Recently, a modern photogrammetric survey method was introduced to identify and extract feature points automatically. This method is known as structure from motion (sfm), in which related algorithms can automatically identify the location and position of each captured image. Then, feature points can be detected and extracted semi-automatically for matching and the reconstruction of 3d models. Sfm commercial software was developed to generate image-based point cloud models. Steps of generating point clouds via sfm are shown in Figure 2-16 and are summarized as follow (Klein et al., 2012; Westoby et al., 2012):

- A. Data collection: overlapping images are collected from different positions and orientations {camera1... camera8) preserving an overlap of 80% or more. The collection process is preferred to finish at the starting location (closed loop).
- B. Feature points detection: Detection of key features such as vertices and edges.
- C. Feature points extraction and matching: similar feature points are matched using the Scale Invariant Feature Transform (SIFT) recognition system.
- D. Identifying camera position and orientation for each image: Linking a bundle of light from feature points to the center of the camera, this process is known as the “bundle adjustment”.
- E. Generating a 3d point model: through triangulation method.

Automatic registration of image-based point clouds requires a lot of close overlapping images to identify and extract feature points for later stitching. This automated process will result in a denser and accurate point cloud (thousands of points). However, automatic identification and extraction of feature points will cover unwanted areas in the background, this will increase the error and noise in the generated point cloud model. To solve this issue, manual filtering is required to remove the unwanted points of the model. Manual registration needs fewer images to apply manual identification of feature points between images, but it results in a sparse and inaccurate point clouds (hundreds of points) (Klein et al., 2012).

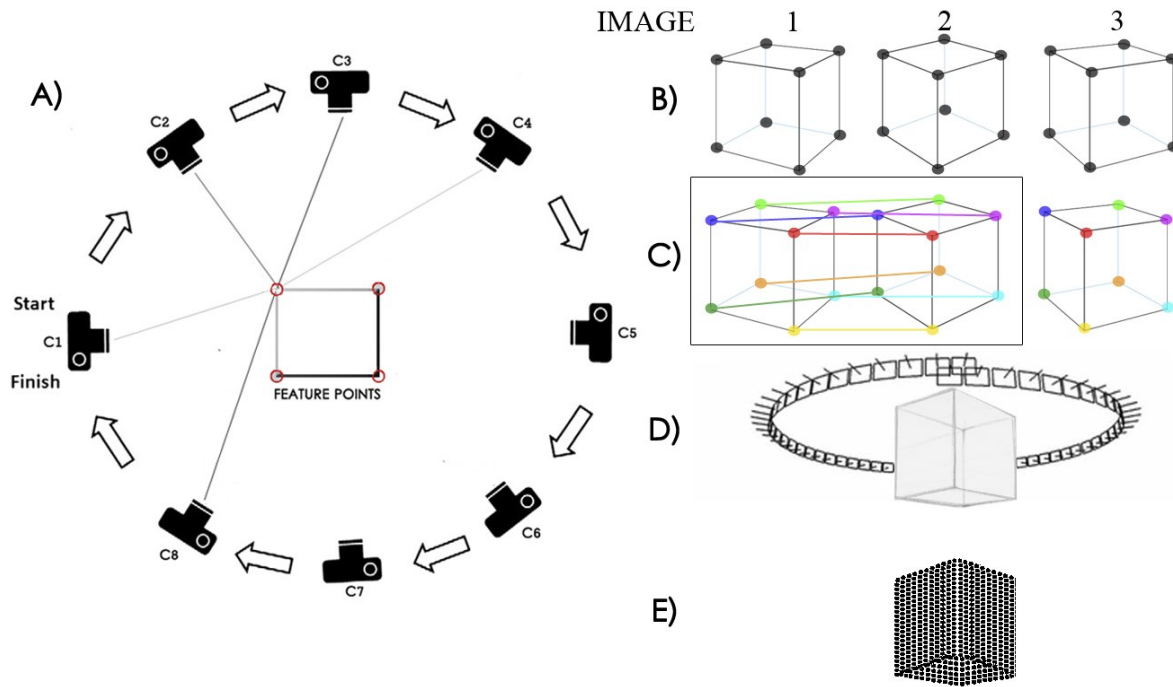


Figure 2-16: point cloud generation through sfm

Due to the fact that even commercial software allows an automatic generation of point clouds, manual registration and filtering are still required to enhance the quality of the resulted point clouds. Moreover, some environmental factors can affect the quality of the generated point cloud models such as lighting, occlusions (moving objects, equipment's), and other factors (e.g., smoothness, reflective materials, and featureless surfaces) (Klein et al., 2012). Some researchers have suggested relative solutions that could enhance the quality of a point cloud; for example, collecting images at night can exclude the sunlight effect and avoid some of the moving objects (e.g., people, mobile furniture, and equipment at the site through the construction phase). Also, some visual markers can be added to the featureless surfaces to improve feature points (Snavely, Simon, & Goesele, 2010). Photogrammetry was improved in a tremendous way in the past few years. Therefore, the enhancements developed the ability of fast data collection of colorful and textural images. Also, improvements showed an advanced processing of a large amount of data for object recognition. This progress allowed the implementation of image-based 3D clouds in the reconstruction of existing built environments. Developed as-is 3D image-based point cloud models have the ability to identify the as-is condition of a built environment. Consequently, this method can be used effectively in facility monitoring and quality control (Bhatla, Choe, Fierro, & Leite, 2012; Chao Wang, 2014).

2.3.2. Laser Scanning

Laser scanning is also known as Light Detection and Ranging (LIDAR), it is an optical sensor dependent technique that uses laser scanners to scan the exterior surfaces of objects. The main concept of laser scanning relies on transforming the spatial data of object surfaces into a 3D point cloud (Bhatla et al., 2012). Technically, laser scanners emit a laser beam that reflects with objects surfaces and returns back to calculate the distance between the scanner center and the object. By measuring the distance between the center of the scanner and the object, it is possible to detect the accurate position (coordinates X, Y, and Z) of objects with respect to the scanner position (Klein et al., 2012). Laser scanners are very expensive, efficient and high accurate machines. They can scan hundreds of meters away, and measures in millimeters accuracy generating very dense point clouds (millions of points). It's very efficient for complicated and complex projects that require the visualization of small details of the high resolution. Recently, laser scanners are used to reconstruct the Point clouds of the as-is conditions in Architecture, Engineering and Construction (AEC) fields (Bhatla et al., 2012).

However, the huge price and the need for some operating skills are considered as the main limitations of using this technique. Additionally, laser scanners are bulky, not portable, requires some professional experience and also considered as time-consuming in means of data collection and data processing. Also, other factors can affect the whole process within the area of coverage, required a number of scans, and the needed software for registering, editing, and texturing the scans. As other remote sensing techniques, laser scanning is affected by weather conditions, lighting, reflective materials, featureless surfaces and mobile objects. Laser scanning based point clouds can be also implemented in various applications such as rapid modeling, real-time safety management on site, construction progress monitoring and defect detection (Bhatla et al., 2012). Laser scanners systems have photon source that emits either continuous laser signals or a series of laser pulses that can scan and detect objects in its environment, or objects that rely on its line-of-sight. After that, a rotating photon source can collect 3D points of a surrounding environment and generates 3d columns. After, a panoramic image range of a surrounding is created. This image is used in registration and generation of 3D point cloud model. In summary, the two common types of laser scanners that are present in the market nowadays are either a time of flight (TOF) laser scanners or the phased-shift (PS) laser scanners (Chao Wang, 2014).

Time of Flight (TOF) laser scanners:

The main principle of time of flight laser scanners is based on laser beam emitting and receiving. First, the scanner (emitter) emits continuous laser pulses that will be reflected by a built-in mirror. Next, these pulses will bounce off of an object (receiver) and return back to the mirror once again which will reflect it back to the scanner, as shown in Figure 2-17. The pulses are then collected and the time difference between the emission phase and the reception phase will be calculated. Equation 5, shows that the difference in distance can be measured depending on the time of the beam has traveled and the speed of light in air. Moreover, scanners can emit hundreds of laser pulses per second which can be collected and used to reconstruct a 3D point cloud model for a surrounding environment. ToF scanners are a fast data collection systems with a high rate of data collection. ToF laser scanners can detect several thousands of points per second (up to 50,000). Thus, it's mainly used for real-time applications and other uses that require a very high resolution and can be collected in a small time-frame. Some factors as data resolution and photon source frequency can control the time required for one station scan to another and that may vary from few minutes to several hours. An example for the tof is leica scan-station c10 laser scanners (Faro Technologies Inc., 2014; Klein et al., 2012; Chao Wang, 2014; Westoby et al., 2012).

$$d = \frac{(Et * v)}{2} \quad \left| \quad \text{Equation 5} \right.$$

Where: d: distance between the scanner and the object target.

V: is the speed of light in air

Et: is the required time needed to emit and receive a light beam

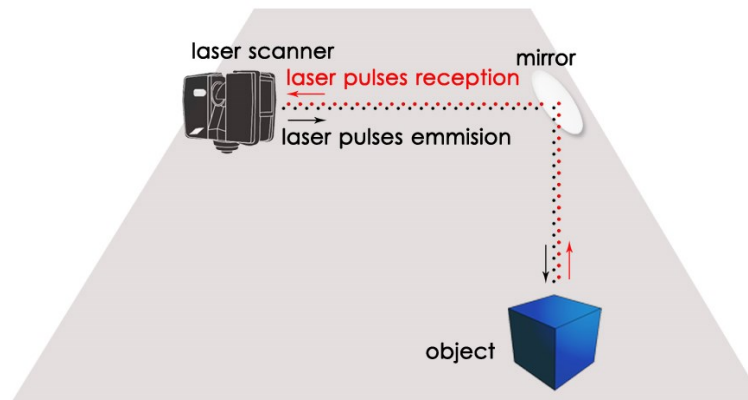


Figure 2-17: ToF laser scanner principle

Phased-shift (PS) laser scanners:

The main principle of the phased-shift laser scanner is that the scanner (emitter) emits outward laser pulses by means of light waves and records the phase wavelengths emitted. Then upon the contact of the pulses with an object (the receiver), it returns back to the scanner to be collected by the sensor. The phase shift between the returning pulses and the stored pulses are compared, then it is possible to calculate the distance of the beam that represents the distance between the scanner and the object. By calculating the light traveling time and the corresponding distance, the spatial information of the surrounding environment can be collected. The phased-shift system is considered as ten times faster than tof systems. However, phased-shift scanners are less accurate with low reflective materials like glass, aluminum, steel and other materials that reflect noise points. Also, phased-shift scanners are inaccurate and can collect a lot of noise points for long ranging scans greater than 100 m (Klein et al., 2012; Chao Wang, 2014; Westoby et al., 2012). Figure 2-18, Shows the angle measurement of the emitted laser pulses in PS system, where the vertical rotation angle is 305° and the horizontal rotation angle is 360°. Emitted laser pulses from the scanner (emitter), represented by black dots, bounces off the object (the cube as a receiver) and returns back to the scanner, represented by red dots.

$$T(\text{Time of Flight}) = \frac{(\text{Phase shift})}{2\pi * \text{modular frequency}} \quad \Bigg| \quad \text{Equation 6}$$

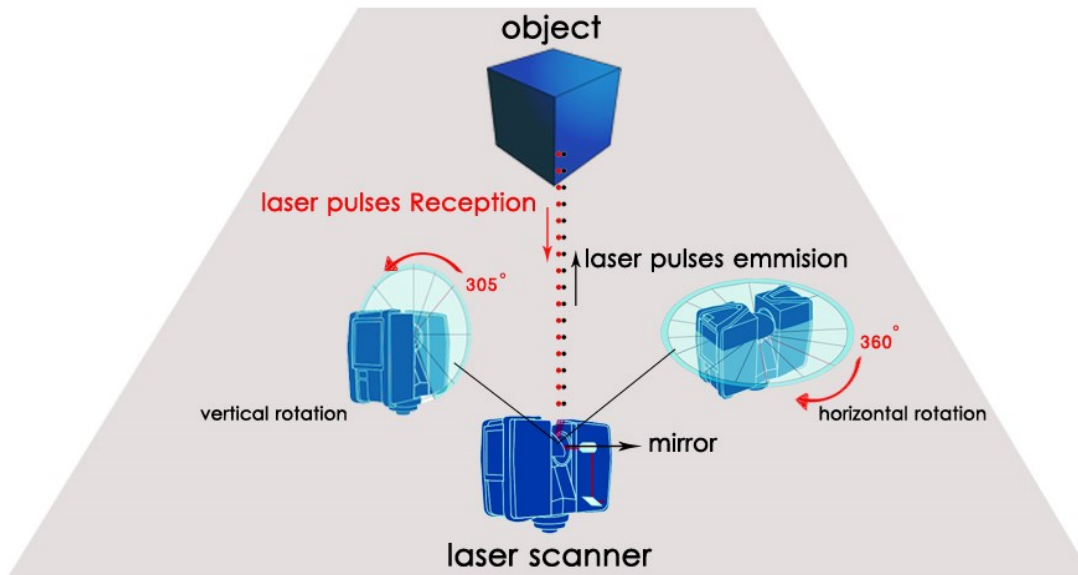


Figure 2-18: Phased-shift laser scanner principle in Faro 3D

Other types of the unfamiliar laser scanning remote sensing techniques in the industry of construction are (the Flash Ladar system or 3D range cameras) and (the self-positioning handheld laser scanner) shown in Figure 2-19 respectively (Chao Wang, 2014). Flash Ladar systems function using Tof principle, but the main difference is that they use flash frame method instead of collecting 3D points while scanning. Where it emits non-continuous laser flashes which capture a sort of images for each flash, this process is known as flash frames (Hegde & Ye, 2008). On the other hand, the self-positioning handheld laser scanners are an easy way to obtain 3D spatial data. It is present in fields as manufacturing, aerospace, and medicine. Self-positioning handheld laser scanners are mobile scanners that support automatic calibration, registration and automatic localization for self-positioning (BIBUS, 2016).

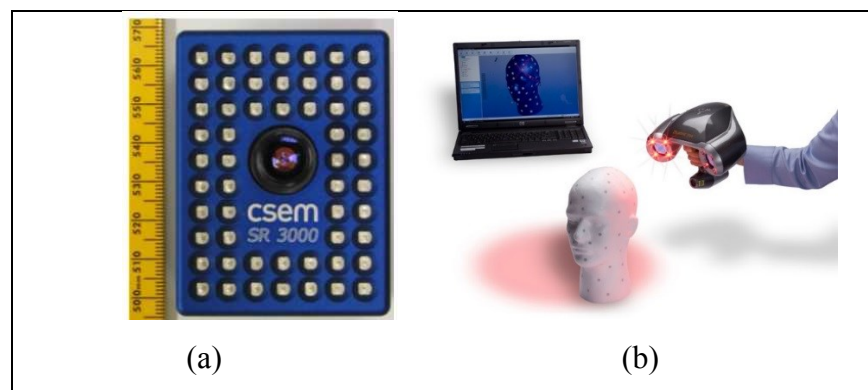


Figure 2-19: (a) Flash LADAR SR-3000 (Hegde & Ye, 2008); (b) Self-positioning handheld laser ZScanner® 700 (BIBUS, 2016)

Comparing between Photogrammetry and Laser Scanning

Remote sensing techniques include both photogrammetry and (tof and ps) laser scanning that are different in concept, this encouraged some researchers to compare the two techniques. To determine their efficiency in generating as-is 3D point cloud models for built environments, (Giel & Issa, 2011) proposed different variables for comparison. For example, using laser scanning in measuring the accuracy in as-built building information modeling (BIM's), is considered more efficient than photogrammetry by means of accuracy and resolution. Firstly, the accuracy of photogrammetry is measured in centimeters, while the error range in laser scanning is limited within millimeters. Secondly, photogrammetry generates a sparse point cloud model that contains hundreds to thousands of points, while laser scanning generates a dense point cloud model that contains millions of points (Giel & Issa, 2011; Klein et al., 2012). Moreover, laser scanning registration software can automatically mesh and extract shapes, while registration software of

photogrammetry requires a manual modeling in the generation 3D point cloud models. However, other researchers considered photogrammetry is preferable by means of equipment cost, required skills, and portability. Firstly, laser scanners are very expensive machines that their cost ranges within tens of thousands American dollars (USD), while cameras used in photogrammetry are priced in hundreds USD. Secondly, laser scanners require a medium to high level of operation skills while cameras are very easy equipment that requires a minimal level of skills. Thirdly, laser scanners are bulk, large in size and immobile, while cameras are considered very handy, portable and are user-friendly (Bhatla et al., 2012; Eisenbeiß, 2009; Snavely et al., 2010; Westoby et al., 2012). Finally, both photogrammetry and laser scanning have some limitations that affect their quality such as surface reflectivity and smoothness, featureless surfaces, occlusions, line-of-sight, edges, weather conditions, etc. (Klein et al., 2012; Chao Wang, 2014).

Laser scanning techniques other than (tof and ps) laser scanners, such as flash lidar systems and self-positioning handheld scanners, are very limited and rarely used in construction; still, some researchers discussed their advantages and disadvantages in construction. Flash lidar systems are small in size and less expensive than the traditional laser scanners, but it is inaccurate enough, very sensitive to the line-of-sight and outdoor conditions such as lighting and weather. On the other hand, self-positioning handheld laser scanners are more accurate in location detection and portable, but it is very limited for short ranges of data collection (Hegde & Ye, 2008; Chao Wang, 2014). Consequently, researchers used mainly photogrammetry and laser scanners for the generation of as-is 3D point clouds of buildings and infrastructures. In summary, a comparison between both photogrammetry and laser scanners is presented in Table 2-1 below.

Table 2-1: Comparison between remote sensing techniques

Remote Sensing Technique	Laser scanning	Photogrammetry
Error Measurement	millimeter	Centimeters
Density	Dense	Sparse
Resolution	Millions of Points	Hundreds to thousands of Points
Cost (USD)	Tens of Thousands	Hundreds
Weight and Portability	Heavy and not portable	Light and Portable
Operation Skills	Medium to High	Low

2.3.3. Overview of Point Cloud Data

Point cloud models can be generated and reconstructed using different remote sensing techniques. Generated point cloud models consist of a group of points that resembles the spatial information of an environment which relies on the line-of-sight of the scanner. The processes of reconstructing a point cloud model depend heavily on the data structure of the collected points. Mainly, the data structure of collected point cloud can be classified into two types known as organized and unorganized point cloud. Organized point clouds are a simplified ordered 2D grids converted into an ordered 3D points that have a similar data structure of an image. This means that each point has its index of columns and rows. Thus, each point has a recognized reference and a known relationship to its neighbor points which is defined as the nearest points (Holzer, Rusu, Dixon, & Gedikli, 2012). As a result, the data processing of point cloud models using organized points is much easier, efficient and needs less time. Consequently, organized point clouds are very useful in applications related to 3D registration and object recognition. An example is the application of organized points in the data collection method used in stereo cameras or other tof cameras and laser scanners (Chao Wang, 2014). On the other hand, unorganized points are points that have no reference and no data structure because of the variation in their size, resolution, density and points order. Thus, the relationship between a certain point and its adjacent points is unfamiliar and unknown. As a result, the data processing of unorganized point clouds is much harder, inaccurate, requires manual enhancement and need more time (Chao Wang, 2014)

Data processing of point clouds is also known as registration, it defines the spatial information of each point of the collected data then combines them in one discrete system. After registering and generating a 3D point cloud of the scanned environment, a second consecutive process called triangulation takes place, in which the 3D point cloud model is converted into a solid 3D model. Triangulation concept relies on connecting relative points with their nearest in order to generate geometric primitives such as planes, cylinders, and spheres. Consequently, a solid 3D model representing the as-is condition is reconstructed. Recently, 3D Point cloud become a powerful technology that has improved in a tremendous way and has been applied in the building sector. Some researchers used point cloud for building condition assessment, others implement it along with thermal imaging techniques in aspects such as facility condition assessment and energy performance analysis (Klein et al., 2012; Chao Wang, 2014).

2.4. Research Gap

The implementation of infrared thermography in 3D thermal modeling has been studied by many researchers. Such as, (Ham & Golparvar-Fard, 2012; Lagüela et al., 2012; Chao Wang & Cho, 2011). However, most of these studies focused only on the exterior facades of buildings and outdoor environments. Only few who tried to test infrared thermography in the reconstruction of as-is 3D thermal models of indoor built environments such as, (Borrmann et al., 2012; Oreifej et al., 2014). Yet, these studies were dedicated to building indoor environments only. However, this is insufficient since AEC sectors require the method to be tested within different environments, and under different variables. Also, these researchers used developed systems that integrate multiple methodologies and requires sophisticated knowledge for the execution of their methods.

Thus, until the date of conducting this research, separate data collection and data processing of infrared thermography is considered not enough and not convenient in generating 3D thermal models. Unlikely, a more user-friendly technique is needed that involve a minimum effort by means of least number of technologies, fewer tools, separate image acquisition and separate data processing. In addition, some of the proposed systems as (Irma3D and e-pack) are bulk, large in size, heavy, expensive, and unaffordable. And some requires direct operation of a human by wearing the system on the back of the operator. Consequently

As a result, and to the best knowledge of the author, (a) no one has tested the implementation of 2D IR and visible images, collected separately by an infrared and a digital camera sensing respectively, in the generation of as-is 3D thermal models of built environments. On the other hand, built environments are considered different by means of geometric shape, lighting conditions, and material textures. (b) Accordingly, and until the date of this research, no existing researchers have studied the generation of 3D thermal models of indoor infrastructure environments. Both gaps (a, and b) are to be expressed and reviewed in this research. Finally, and in order to evaluate the efficiency of the proposed method; different output models will be compared with respect to an experimental design by means of density, time and cost.

CHAPTER 3: METHODOLOGY

The main objective of this research is to reconstruct as-is 3D thermal models of built environments using 2D IR and visible images. Several researchers have studied the reconstruction of 3D thermal models Such as, (Ham & Golparvar-Fard, 2012; Lagüela et al., 2012; Chao Wang & Cho, 2011). However, most of these researchers have applied the 3D reconstruction of outdoor environments and exterior building facades. Only a few researchers who tried to focus their studies in the reconstruction of 3D models for indoor built environments such as (Borrmann et al., 2012; Oreifej et al., 2014). Still, their studies were dedicated only for indoor buildings. This provoked the need for more studies within different environments of different variables like the geometry, lighting condition and the materials of built environments. Also, most of the suggested methods were dependent on equipment as laser scanners that are bulky, heavy, cost-intensive, and time-consuming. Consequently, this arouses the need for more affordable methods in terms of mobility, cost, time and accuracy. As a result, this chapter will present a novel method to overcome the above-mentioned gap. Therefore, the following part will be categorized into three main sections.

The starting section will highlight and review the proposed methodology to achieve the main objective of this research. Also, the proposed methodology will be presented in a flowchart diagram that can summarize the whole method visually. Moreover, a detailed explanation of each stage of the proposed method will be present.

Second, the output model of the proposed method will be compared with respect to an experimental design. The aim of the experimental design is to compare its output with that of the suggested methodology in order to estimate the efficacy of the last-mentioned. The experimental design will also be shown in a flowchart diagram that can summarize the whole process. Besides, a complete review of each stage will be present.

Finally, the comparison between the two output models will be modeled in terms of evaluating density, time, and cost. In conclusion, the comparison of the output model can validate the hypothesis of the suggested method. Finally, output models comparison will be also presented in a flowchart diagram that will review the several variables under study.

3.1. Overview of the Proposed Methodology

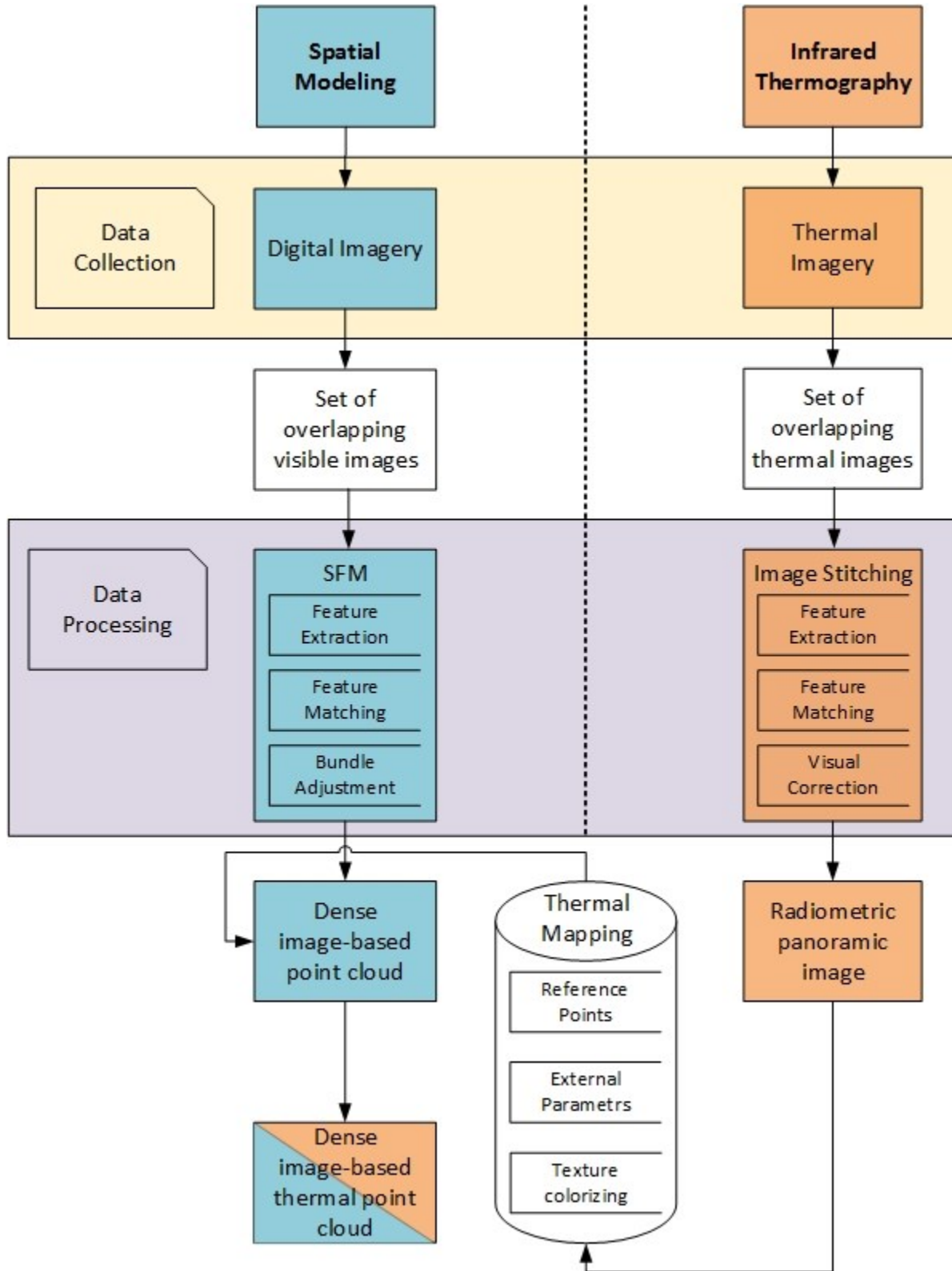


Figure 3-1: Flowchart of the proposed methodology

To begin, an overview of the suggested method is presented in the above flowchart (see Figure 3-1). Also, in this section, the proposed methodology will be described and discussed in details. The main concept of the suggested method is to create 3D thermal point clouds using 2D IR and visible images which are collected and processed separately. To do so, first, all the required equipment and tools will be prepared and deployed for separate data collection. In which, a digital camera will be used to capture a set of overlapping visible images preserving an overlap of 80% or more. Next, an infrared camera will be used separately in collecting a set of overlapping thermal images with an overlap of 50% or more. The second stage will be data processing, where a set of visible images will be processed using sfm approach to generate an image-based point cloud representing the spatial information of an environment. Finally, a set of overlapping thermal images will be filtered and stitched together to form large panoramic images. After, stitched radiometric panoramic images will be mapped to the generated image-based point cloud model using reference points. As a result, as-is 3D spatial and thermal point clouds will be generated which reflect both metric and thermal measurements of a built environment.

In the next section, a detailed discussion of 3D spatial modeling using photogrammetry and image processing is present. In which, all the related stages of data collection and data processing will be reviewed. Following is a detailed explanation for infrared thermography. Which, includes both thermal data collection and later thermal data processing stages.

3.1.1. Digital Imagery

Digital imagery has been used by several researchers in the modeling of 3D thermal point cloud models such as (Lagüela et al., 2012; Oreifej et al., 2014; Westoby et al., 2012). However, none of the studies have studied the implementation of digital imagery separately in the generation of 3D thermal models. The research methodology of this research propose the implementation of digital imagery as a separate technique in both data collection and processing stages; then, the output model from this technique will be used in reconstructing 3D thermal models of built environments. To accomplish this objective, both hardware and software need to be selected carefully. Relatively, advanced commercial software and improved digital cameras were enhanced dramatically. Thus, selecting the proper tools for applying photogrammetry in the reconstruction of as-is 3D point cloud models is an important stage that will affect the outputs of the proposed methodology.

In specific, a mobile digital camera will be used to capture overlapping visible images of the built environments. Technically, a setup process will take place before collecting any data. In which, control points and reference targets will be added at different locations of the built environment. This can be referred for several reasons. (1) Environments that are rich in details and features are preferable to give better results in any 3D reconstruction. Consequently, and in order to enhance the results of the studied environments; random visual markers will be added to featureless surfaces or to the surfaces that have a low number of features. For example, surfaces with one unvarying color, a reflective material such as glass, aluminum surfaces, and stucco walls. (2) In order to control the scale accuracy of the reconstructed models, a reference target or a built-in tag need to be assigned in the model with an accurate realistic dimension.

Therefore, control points or checkboard references will be added for the proper scaling of the model, and visual markers will be added to the featureless surfaces. Next, and after setting up the environments, data collection will begin starting by image acquisition. Thus, images will be captured at different locations and orientations. Also, an overlap of 80% or more is needed between consecutive images. After, a set of overlapped visible images will be filtered, where all blurry images and images that contain moving objects will be removed. Next, the filtered set of overlapping visible images will be used for later processing. Images will undergo sfm approach, where key features are extracted from images and linked with its corresponding match among the different images. After, the location of camera and orientation will be figured out corresponding to each image in a process known as bundle adjustment. Therefore, multiple 2D images will be used to generate 3D points of the same coordinate system. Lastly, the extracted feature points of known location and orientation will be matched together in a process known as triangulation. The result will be the reconstruction of a dense “as-is 3D spatial image-based point cloud model”. The final output will be filtered by removing any unwanted points and scaled using previously deployed reference target and/or built-in tags of known dimensions. In summary, a set of overlapping visible images will be both collected using a digital camera sensing and processed separately. The end result of this step is the generation of a dense image-based point cloud model as shown in Figure 3-1. Finally, the visible point clouds will be orthogonally projected to form an orthogonal image. In which, it represents an adequate layout with direct metric measurements using a graphic scale to measure distances and areas.

3.1.2. Infrared Thermography

Recent studies of using infrared thermography for the 3D reconstruction of thermal models, have shown the integration of infrared sensing and other data collection sensing techniques, such as laser scanners and digital camera sensing simultaneously (Borrmann et al., 2012; Ham & Golparvar-Fard, 2012; Lagüela et al., 2012; Oreifej et al., 2014; Chao Wang & Cho, 2011). However, none of the researchers have studied a separate collection and self-processing of the collected thermal information. To achieve this objective, a novel method is proposed in thermal imagery collection and thermal data processing. First, thermal data collection will be performed using a modern thermal imagery system for built environments. Nowadays, standalone high defined thermal cameras are a recent modern technology that has a limited number of prototypes in the world market. Yet, none has used these high defined infrared cameras separately in the 3D thermal modeling of built environments. To achieve this objective, an appropriate hardware should be selected. First, the chosen infrared camera sensing should be adequate to small and confined spaces of an indoor environment. Thus, it should have an advanced image stabilization characteristics that will lessen image distortions. Besides, the camera must have the ability to capture and show images in site for fast revision. Finally, time is considered as a vital factor in data collection, so the system has to operate effectively and execute the work needed within the required time and without any disturbances. Hence, old thermal cameras are considered very slow and time intensive especially when covering large areas. Thus, the needed infrared camera must have the ability to automatically capture multiple thermal images within an interval time of seconds.

After choosing the suitable hardware for accomplishing the proposed task, the selected thermal imagery system will be installed and deployed for data collection. To do so, an environment will be set by adding light control points such as light torches. Next, the settings of the selected infrared camera will be adjusted to the appropriate features corresponding to the surrounding environment. Following, thermal camera is ready for image acquisition and images will be captured in a modular manner with a consistent distance from the facing plane surfaces. This process will be repeated back and forth for several times until the collection of the whole scene of an environment is complete. The modular capturing manner of thermal images is very important in minimizing the temperature variation between images.

Also, the infrared camera will be switched within a maximum and a minimum temperature to preserve a consistent temperature scale range. During image acquisition, captured images can be viewed and altered automatically. Blurry images can be removed directly in site and more images can be captured if needed. Also, an overlap of 50% or more must be preserved between consecutive images. This can be achieved by collecting overlapping images in a regular grid pattern or a planned modular manner as a guideline. At the end of this stage, a set of overlapping thermal images will be ready for processing.

Consequently, each set of overlapping thermal images will be processed together for image stitching, to create a big radiometric panoramic image. These panorama images cover a large surface area with an accurate temperature representation. Technically, key features of each image will be identified and extracted using features from accelerated segment test (FAST) algorithm. Detectable key features can be a point of interests which are different than its neighboring points such as corners and edges. Next, a feature matching will take place which can identify the exact corresponding points between the overlapping areas of consecutive images. After, a visual correction will validate the previous matches before transforming the images for image registration. To acquire multiple images a unified coordinate system and image characteristics, it will be adjusted with relative to its parameters of calculating the exact position and orientation of each image with respect to the other.

Finally, the radiometric correction will take place to overlay the color variation between the overlapping regions using the linear transition method. For example, two consecutive images overlapping at the same row, then X_{\max} is the highest value of X of the overlapping area while X_{\min} is the minimum value of X of the same overlapping area. While a pixel value is A_i in the first image A , the same pixel will have a value of B_i in the second image B . Correspondingly, the new pixel value S_i for the stitched image. For an X coordinate of X_i the values are calculated as shown in equation 7 and Figure 3-2. On the other hand, if two images are overlapping vertically at the same column, then the equation will be used in the Y coordinates and values (Y_{\max} , Y_{\min} , and Y_i) are used (Lagüela et al., 2012; Liu, Shen, & Chen, 2009).

$$S_i = (X_{\max} - X_i) / (X_{\max} - X_{\min}) * A_i + (1 - (X_{\max} - X_i) / (X_{\max} - X_{\min})) * B_i \quad (\text{Equation 7})$$

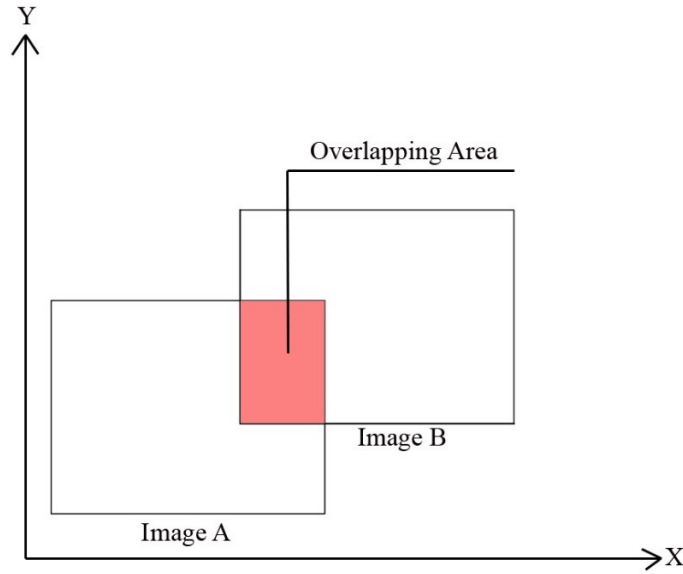


Figure 3-2: Two consecutive overlapping images

Later on, the processed panoramic thermal image will be mapped to the generated image-based 3D point cloud model using reference points that are common feature points between both the panoramic image and a 3D model surface. These reference points can be vertices, corners, and edges. Next, the external parameters (position and orientation) of the image will be computed. To do so, (3DReshaper, 2016) recommends at least four common reference points that could be for example the four corners of an image and its relative surface corners. This justifies the importance of collecting images in a modular manner that is parallel to the testing surface. After, superimposing the temperature color visualization using texture colorizing and model sampling will take place in order to produce a 3D thermal point cloud model using both spatial and infrared information. In summary, thermal visualization will be based on the collected 2D thermal images, while the density of the output model will be based on the dense point cloud model reconstructed from 2D visible images. At the end, all surface planes are projected orthogonally to create an ortho-thermogram image that generates both thermal and metric measurements using a temperature scale and a metric graphic scale respectively.

In order to test the feasibility of this method, three different environments will be tested that resembles different variables; (1) Different geometric volumes such as (long tunnels, rectangular volume, and rectangular volumes of high ceilings. (2) Different lighting conditions such as (dark and artificial lighting). And (3) different materials like (rough concrete, reflective metal, and uniform stucco).

3.2. Overview of the Experimental Design

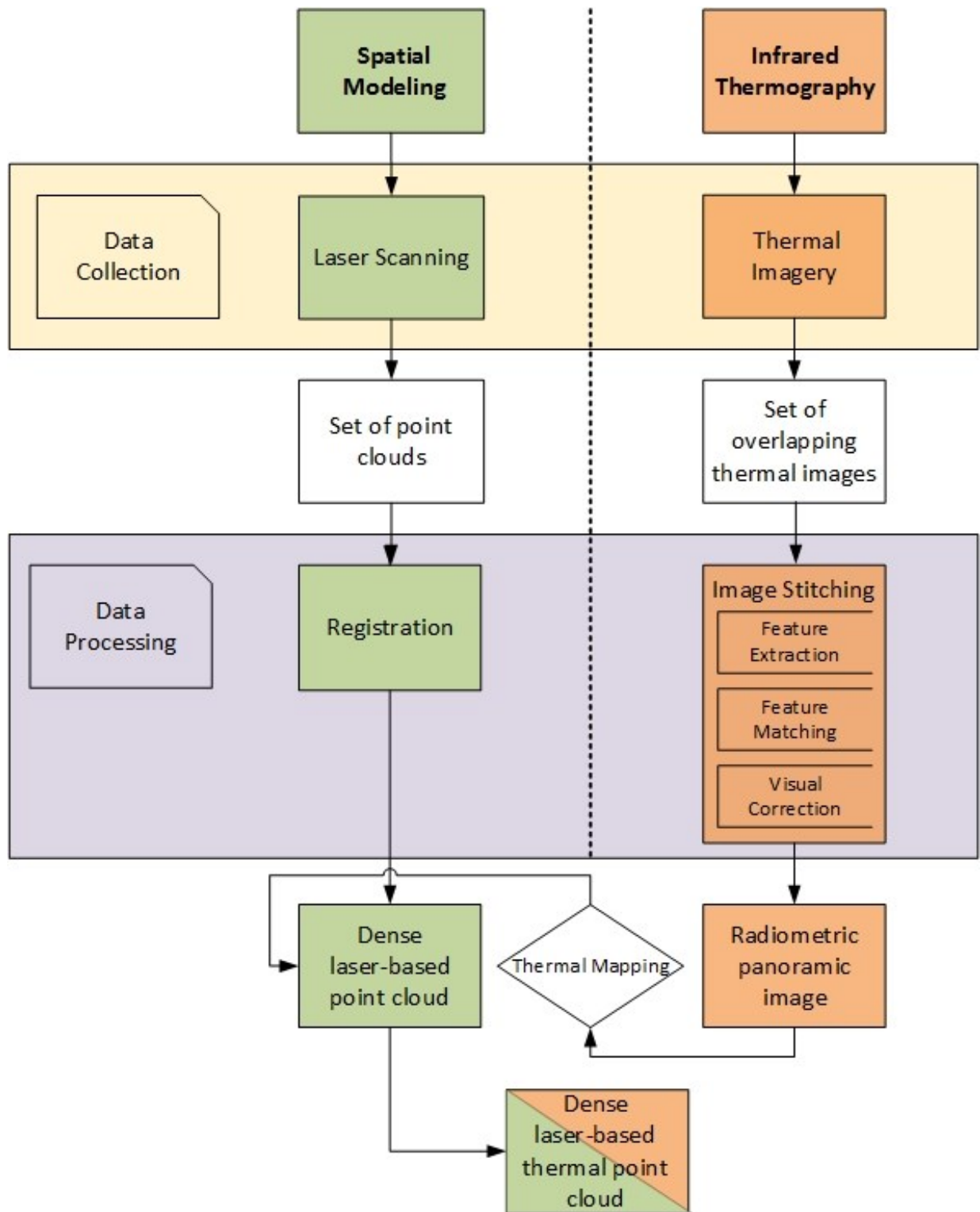


Figure 3-3: Flowchart of the experimental design

In order to test the efficacy of the proposed methodology, the output models will be compared with an experimental design as the ground truth. The main concept of an experimental design that it uses a proven technique which can be compared with; when evaluating the outputs of a proposed methodology (Key, 2016). Figure 3-3, shows the flowchart diagram that can summarize the whole process of the used experimental design.

Laser scanning is considered as an accurate practice in reconstructing as-is 3D point clouds of buildings and infrastructures (Bhatla et al., 2012; Klein et al., 2012). Mainly, most of the studies in 3D thermal modeling rely on mapping thermal information to the spatial information being collected using laser scanners (Lagüela et al., 2011; Chao Wang et al., 2012). Therefore, in order to test the feasibility of the proposed methodology, a laser scanner will be used as an experimental design to generate 3D laser-based point clouds for the built environments. To do so, a laser scanner will be positioned at different locations in the built environments. Also, control points will be placed in the same built environment before performing data collection. Some of the examples for control points and targets are the spherical references or the plain checkboard targets. After, multiple scans will collect the spatial information at each position and generate a panoramic range image for each scan. Next, an offline process will take place by grouping the different sets of point cloud models into one complete model of the same coordinate system. This process is known as registration, in which multiple scans can be aligned together using previously deployed control points. This post-processing step can assure the fusion of multiple point cloud models by matching relative control targets and feature points. Modern automated technologies can automatically detect the deployed targets and align the different scans together. Also, a deviation analysis report will be present to show the error percentage which ranges in less than few millimeters. Thus, laser-based point cloud models are considered very accurate. Finally, the registered 3D laser-based point cloud will be filtered by removing any unwanted points. At the end, all surface planes are projected orthogonally to create ortho-gram images that generate an adequate layout with direct metric measurements using a graphic scale to measure distances and areas.

Finally, infrared thermography will be used similarly as in the proposed methodology. The only difference is the last stage of superimposing thermal information. In another word, mapping of the stitched radiometric images will be applied to a laser-based point cloud model. Thus, the output of this experimental design is a 3D thermal laser-based point cloud model.

3.3. Output models Comparison

In order to evaluate the outputs of the proposed methodology, it will be compared with the output model of the experimental design. Evaluation will be developed in terms of density, time and cost for both laser-based and image-based thermal point cloud models as shown in Figure 3-4.

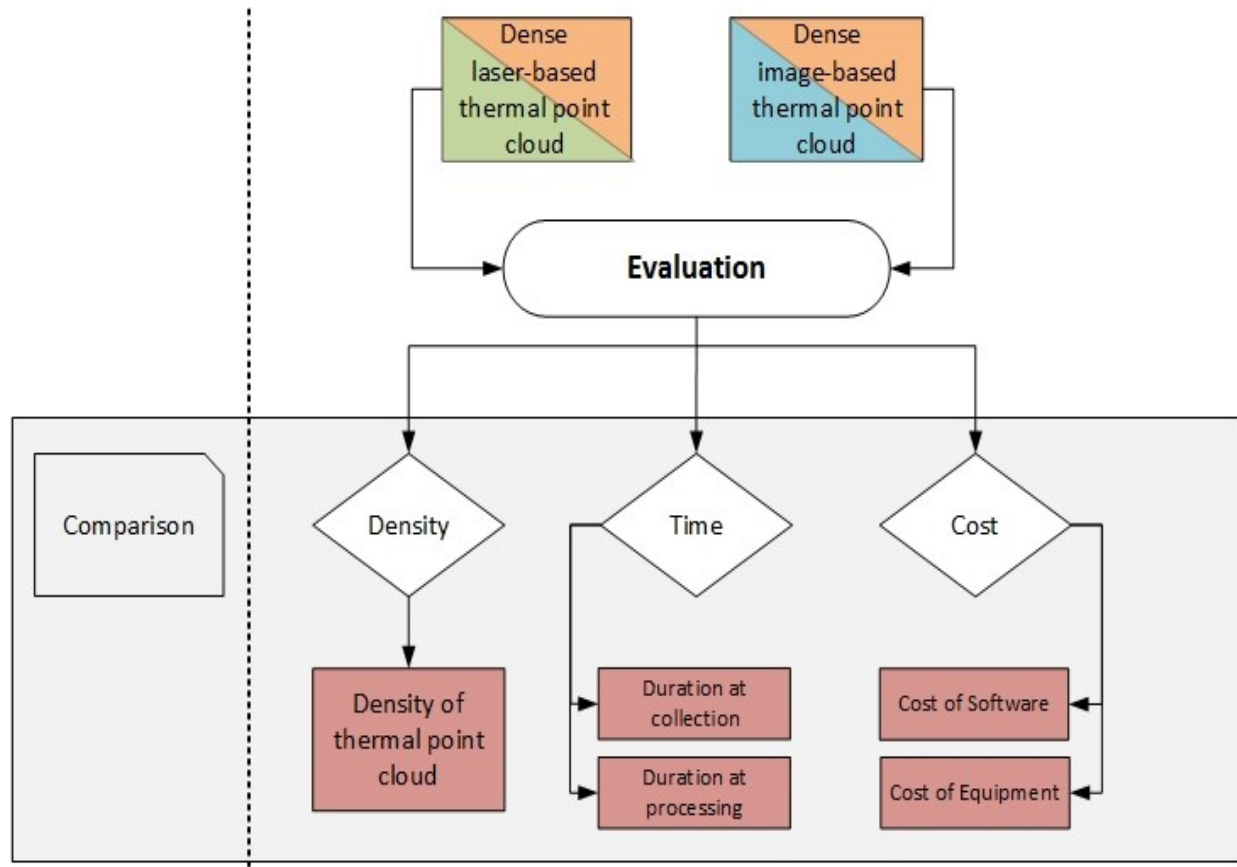


Figure 3-4: Flowchart for output models comparison and evaluation

3.3.1. Density-Based Evaluation

The Dense point cloud can be referred to the high number of 3D points in a given region of the point cloud model. Thus, dense point clouds have a larger total number of 3D points when compared to another sparse model. Dense point cloud models can show a high level of details which in turn will lead to a more accurate analysis and more precise decisions. Previous researchers used only laser-based point cloud models to guarantee a dense output model. In this research, the total number of 3D points will be evaluated and compared using both techniques of remote sensing, laser scanning (laser-based thermal model as the experimental design) and photogrammetry (image-based thermal model as the proposed methodology).

3.3.2. Time-Based Evaluation

Time is a vital factor for any proposed approach. Thus, time will be recorded for each stage using both techniques of spatial modeling. Including, time needed for data collection and later data processing. After, time comparison will be held to evaluate the results.

3.3.3. Cost-Based Evaluation

On the other hand, the cost is another crucial factor in evaluating the efficacy of any proposed technique. Thus, the cost of using different equipment and software will be recorded based on official statements and web pages of the responsible companies. Also, related operator cost of data collection and processing will be included. At the end, a cost-based comparison for each technique will be performed.

CHAPTER 4: IMPLEMENTATION AND RESULTS

This chapter is an application of the proposed methodology in chapter 3. To do so, three different environments will be studied. As a part of this task, methodology implementation and results of the three case studies will be presented below.

4.1. Implementation

In order to accomplish the main objective of this research, the experimental setup is required in terms of localizing case study environments, identifying the needed equipment for data collection and required software for data processing.

4.1.1. Environments

Three different case studies were defined to test the suggested approach. Case study I (Figure 4-1), is a Green line-subway tunnel segment located in the city of Montreal, Canada. While case study II is a gymnasium located at the athlete complex building of Concordia University's Loyola campus, Montreal, Canada (see Figure 4-2). Finally, case study III is a confined lab office located in the second basement-S2 floor of Concordia University's EV building (see Figure 4-3).

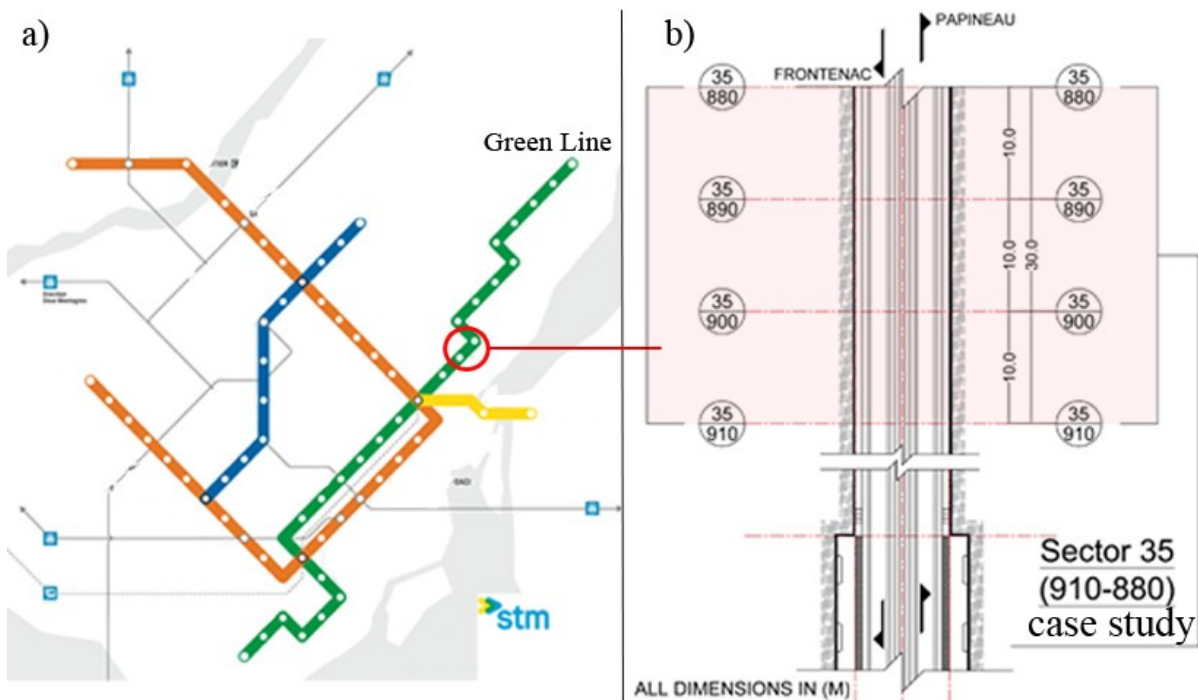


Figure 4-1: (a) Map for Montreal Subway(stm, 2016),(b) Schematic Plan for the tunnel testing environment

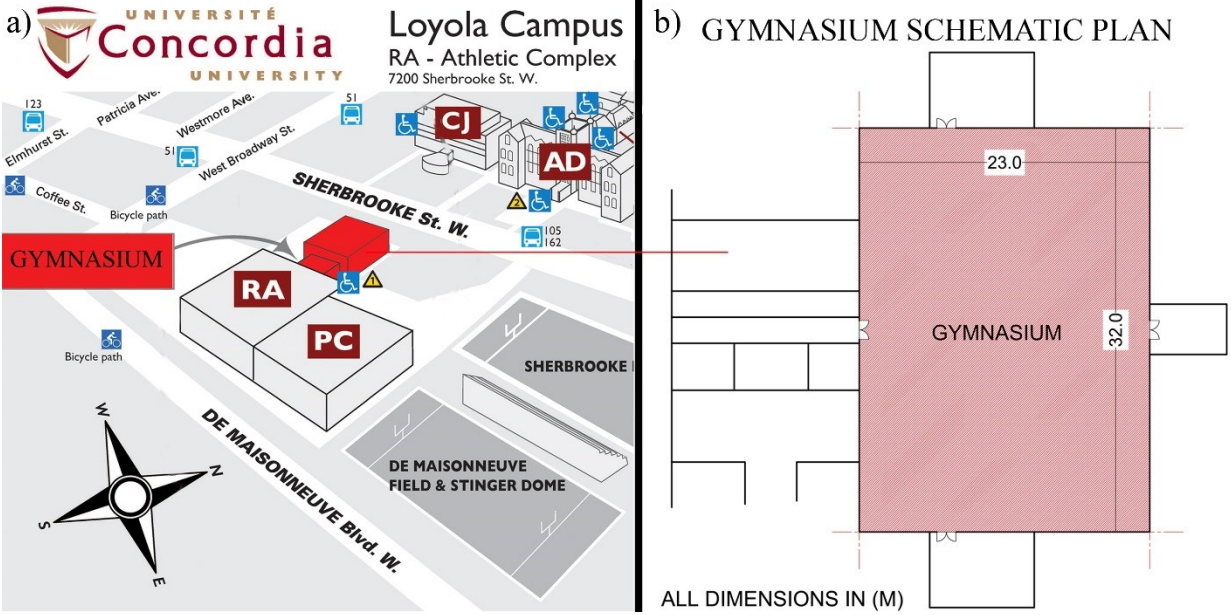


Figure 4-2: (a) Gymnasium building located in Loyola Campus (Concordia University, 2016), (b) Gymnasium schematic plan

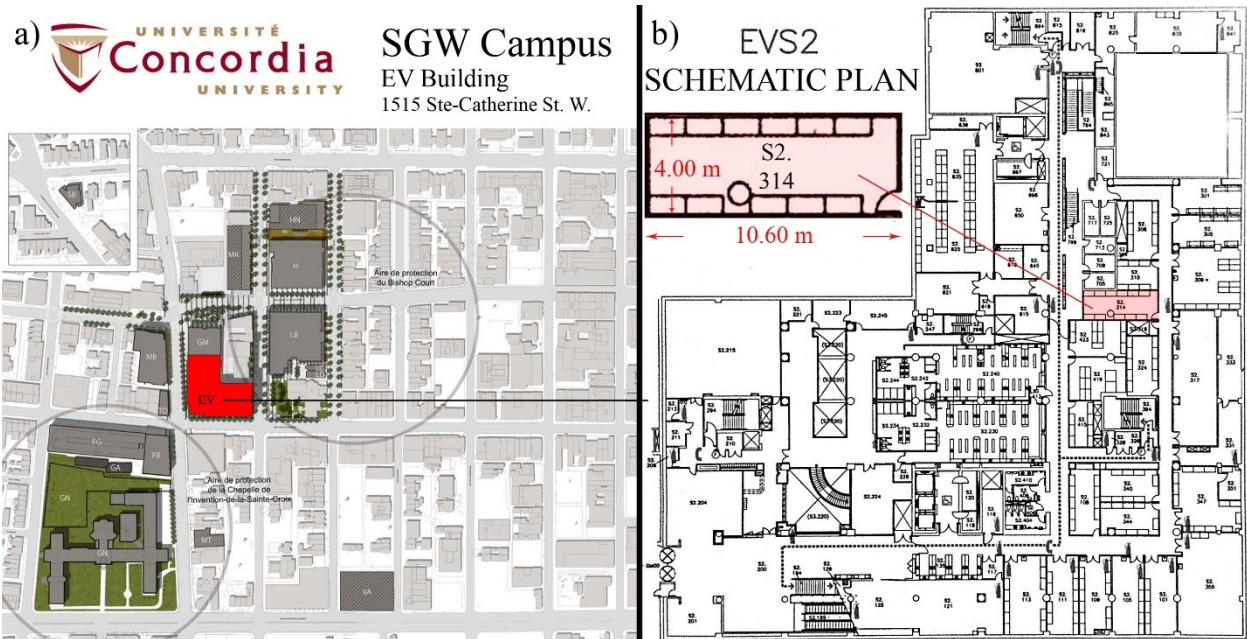


Figure 4-3: (a) EV building located in SGW Campus (Concordia University, 2012), (b) Lab office schematic plan

Reconstructing 3D thermal models can be affected by the surrounding environment characteristics. Thus, the three selected environments are referred to different and several variables. First, the subway tunnel segment environment is a challenging task with its cylindrical geometry, dark lighting conditions, and the rough material textures such as concrete (Figure 4-4).

On the other hand, the gymnasium environment is a rectangular-based geometry with a high ceiling, artificial lighting conditions and a reflective texturing such as metal and wood flooring (see Figure 4-5). Finally, a small confined lab office has a rectangular box geometry with a low ceiling of 3m height. Thus, the place is so narrow for data collection. Also, the test occurred with dark conditions. Lastly, the walls painted in stucco are uniform in color and reflective in texture. Consequently, this environment has a low number of features when compared to environments of case studies I and II (see Figure 4-6). As a result, the proposed methodology will be tested within unlike environments of different variables such as the geometry of surroundings, materials, and lighting conditions.



Figure 4-4: Images showing subway tunnel testing environment

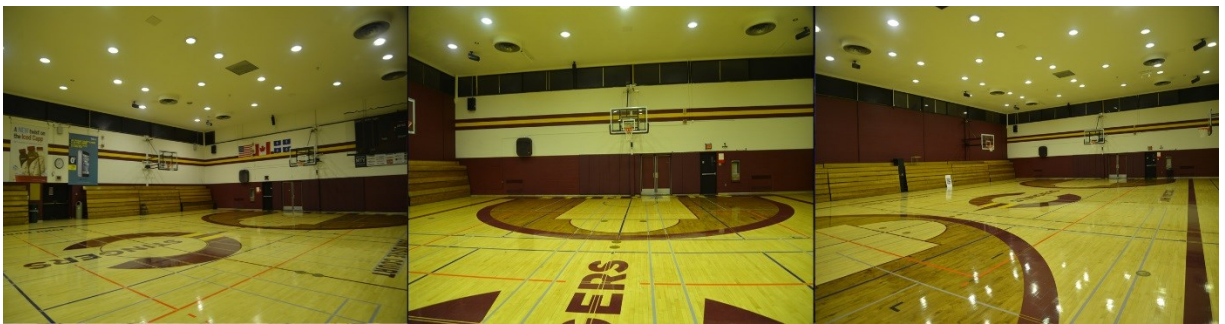


Figure 4-5: Images showing gymnasium testing environment

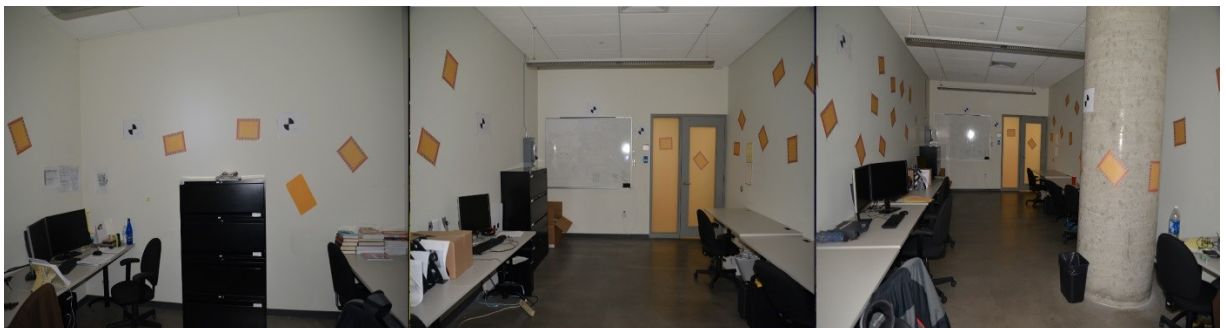


Figure 4-6: Images showing lab office testing environment

4.1.2. Hardware

This section will review the different equipment being used in executing different case studies and data collection. To do so, used equipment can be grouped into several categories as follow:

Equipment used for spatial modeling:

The proposed method suggested modeling spatial information through Digital Imagery system, while the experiment design relies on laser scanners on collecting accurate spatial information for later comparison. Thus, the proposed technique in generating an image-based point cloud was achieved using a visible camera “*Nikon Digital SLR Camera D600*” (see Figure 4-7). Following is a review of the technical specifications (see Table 4-1)



Figure 4-7: Nikon Digital SLR Camera D600 (Nikon, 2016)

Table 4-1: Technical data of the visible camera (Nikon, 2016)

<i>Camera</i>	<i>Nikon Digital SLR Camera D600, with a 35mm lens</i>
Image Sensor	35.9 x 24.0 mm CMOS sensor (Nikon FX format)
Image Size (pixels)	FX format (36x24): (6,016 x 4,016 pixels)
Weight	850 g
Storage	Micro SD card
LCD monitor	3.2 in.
View angle	170°

On the other hand, in the experimental design, a laser scanner “*Faro Focus 3D x 130*” was used to generate laser-based point clouds for all built environments under study (see Figure 4-8). The laser scanner was used to scan and collect 3D point clouds of an environment by applying different scans of multiple positions which cover a whole scene. To do so, reference targets including spherical and checkerboard (see Figure 4-9) were deployed in all testing environments before collecting data. This could help effectively in scans registration and alignment.



Figure 4-8: Faro Focus 3D x 130 (Faro Technologies Inc., 2011)



Figure 4-9: Deploying laser scanner and reference targets

Table 4-2: Technical data of the laser scanner (Faro Technologies Inc., 2014)

<i>Laser Scanner</i>	<i>Faro Focus 3D x 130</i>
Range (m)	0.6 - 130
Measurement speed (pts/sec)	122,000 - 976,000
Ranging error 2 (mm)	±2mm
Field of view (vertical/horizontal)	300° / 360°
Laser class	Laser class 1
Data storage	SD, SDHC™, SDXC™
Scanner control	<ul style="list-style-type: none"> • Touchscreen display • WLAN with a laptop/smartphone
Battery life	4.5 hours
Weight	5.2 kg
Size (mm)	240 x 200 x 100

According to the technical specification mentioned in (Table 4-2), the concept behind the name of this laser scanner is its maximum range which can scan up to (130 m). While a range of measurement speed is dependent on the settings being used. The accuracy of the laser scanner is measured in few millimeters with a ranging error that is defined as a systematic measurement error at around 10m and 25m (Faro Technologies Inc., 2014). The field of view FOV can nearly cover a whole horizontal scene angle, while it covers only 300° vertically leaving a circle hole directly below the position of a laser scanner. To avoid this, multiple scans of different positions can fill the missing parts of 3D point clouds. Also, this laser scanner is classified as a first class safe laser when using normally within any condition (Faro Technologies Inc., 2014). The different characteristics of storage and control are relatively considered flexible and user-friendly. Finally, a battery life is very efficient for multiple tasks which require long periods of time for scanning and surveying. Adding to this, it is a smaller equipment in size and much light in weight when compared to the old laser scanners. All of this have made this laser scanner an ultra-portable equipment that allows much faster scans with a more precise measurement.

Equipment used for Infrared thermography:

To accomplish the objective of Infrared thermography, a UAS-based thermal imagery system was used. Thus, a *Dji Matrice100 equipped with a Zenmuse XT* infrared camera was deployed in each of the case studies for thermal data collection. Following is a review of the technical specification of the different parts forming the UAS-based thermal imagery system. Main components defining this system are shown in (Figure 4-10) and include:

- [1] DJI Matrice100 aircraft. Its diagonal wheelbase measures 650 mm with a total weight (including battery) of 2431 g and can reach a maximum takeoff weight of 3600 g. While the maximum speed ranges from 17 m/s to 22 m/s and can stay in the air up to 28 minutes (DJI, 2016).
- [2] 3-axis gimbal that connects the infrared camera to the aircraft body and is responsible for orienting the camera direction.
- [3] FLIR Zenmuse XT infrared camera.
- [4] Ground control station used to control both the aircraft and the camera sensing. It consists of both parts: a remote controller (RC) and a smartphone device. Both RC and a smartphone are connected together via a Micro USB port.



Figure 4-10: UAS-based Thermal Imagery System: DJI Matrice100 equipped with Zenmuse XT Camera (DJI and FLIR, 2016)

[1] DJI Matrice100 aircraft

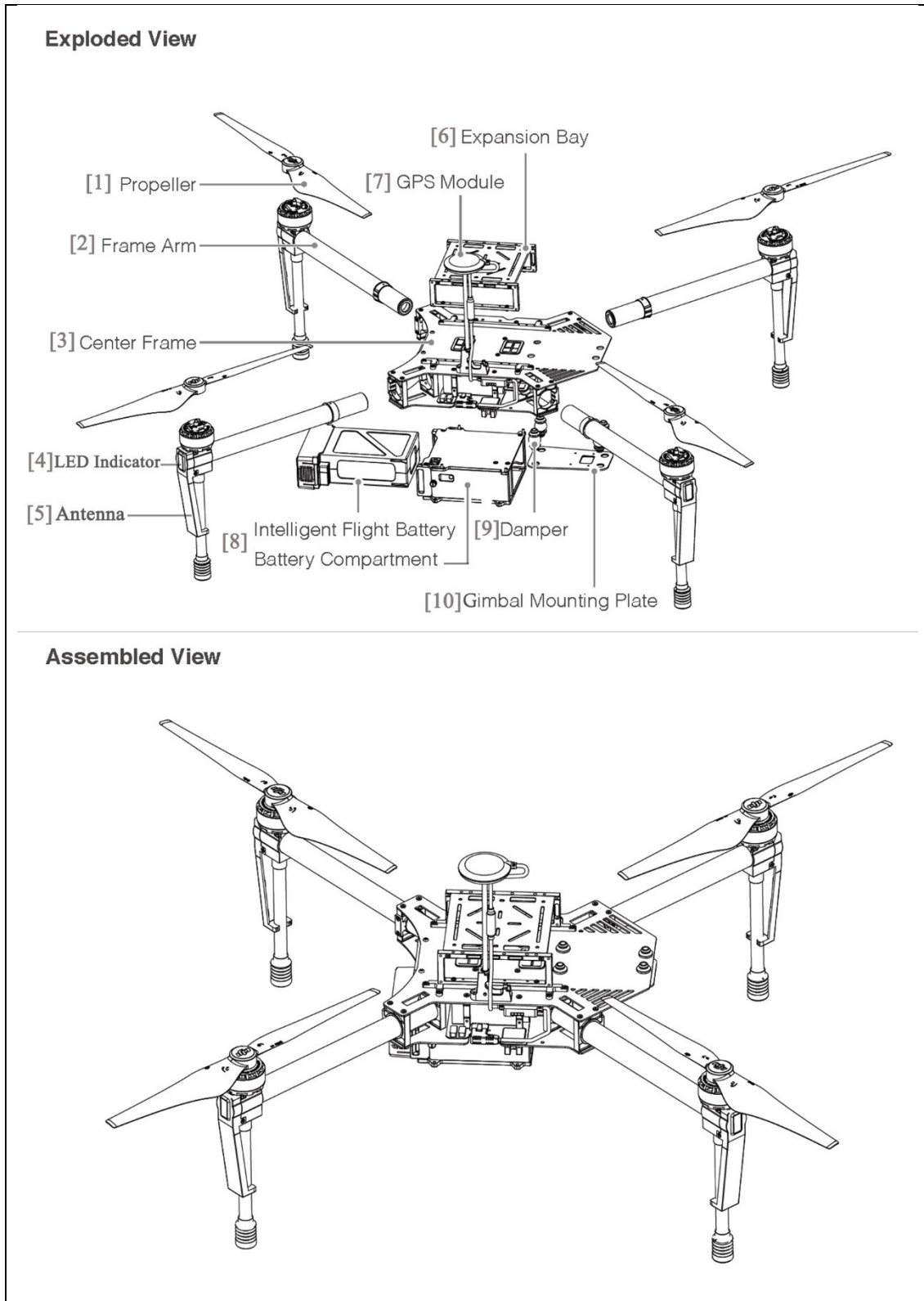


Figure 4-11: Components of the DJI Matrice100 (DJI, 2016)

Following is a detailed review for each of the mentioned parts shaping this system. To start with the DJI Matrice100 aircraft technical specifications as shown in Table 4-3. The aircraft is composed of several components as shown in Figure 4-11. Main components include (DJI, 2016):

- [1] Propellers: Four propellers with their motors are used for take-off. Adjacent propellers have different rotation directions. In which, the upper right and the lower left propellers rotate anticlockwise while the other two propellers rotate clockwise (see Figure 4-12-a).
- [2] Frame arms: Four frame arms that connect the motors/ propellers with the center frame using connecting cables (see Figure 4-12-b).
- [3] Center Frame: The main body of the aircraft that contains the flight controller, ESCs, and a battery compartment (see Figure 4-12-c).
- [4] LED indicators: Which can alert the operator about the aircraft's status.
- [5] Antennas: These antennas are the responsible for linking the aircraft body with the ground control station.
- [6] Expansion Bay: Used to extend the center frame by positioning it either at the top or at the bottom of a center frame (see Figure 4-12-d).
- [7] GPS module: Used to pinpoint a location of the aircraft, while an extension rod can be used to separate the GPS module from interfering with the center frame power board (see Figure 4-12-e).
- [8] TB48D Intelligent flight battery fixed into a battery compartment. Each battery has a capacity of 5700 mAh and a voltage of 22.8 which can hold up to 28 minutes of airtime. Also, four LED indicators are found on each battery that can detect the battery status.
- [9] Damper: Four dampers that connect the gimbal mounting plate with the center frame. These dampers can absorb the vibrations and assure high stability for a gimbal (see Figure 4-12-f).
- [10] Gimbal mounting plate: which is connected to the center frame using dampers. It has 10-pin and 8-pin ports that will connect the gimbal lock on its bottom using gimbal cables (see Figure 4-12-g).

Table 4-3: Technical specifications of the DJI Matrice100 aircraft (DJI, 2016)

<i>Air Craft</i>	<i>DJI Matrice100</i>
Weight (Battery and Propellers included)	2431 g
Dimensions (Wheelbase)	650 x 650 mm
Maximum Speed	22 m/s
Maximum Flight Time	28 m
Battery (TB48D)	5700 mAh – 22.8 V

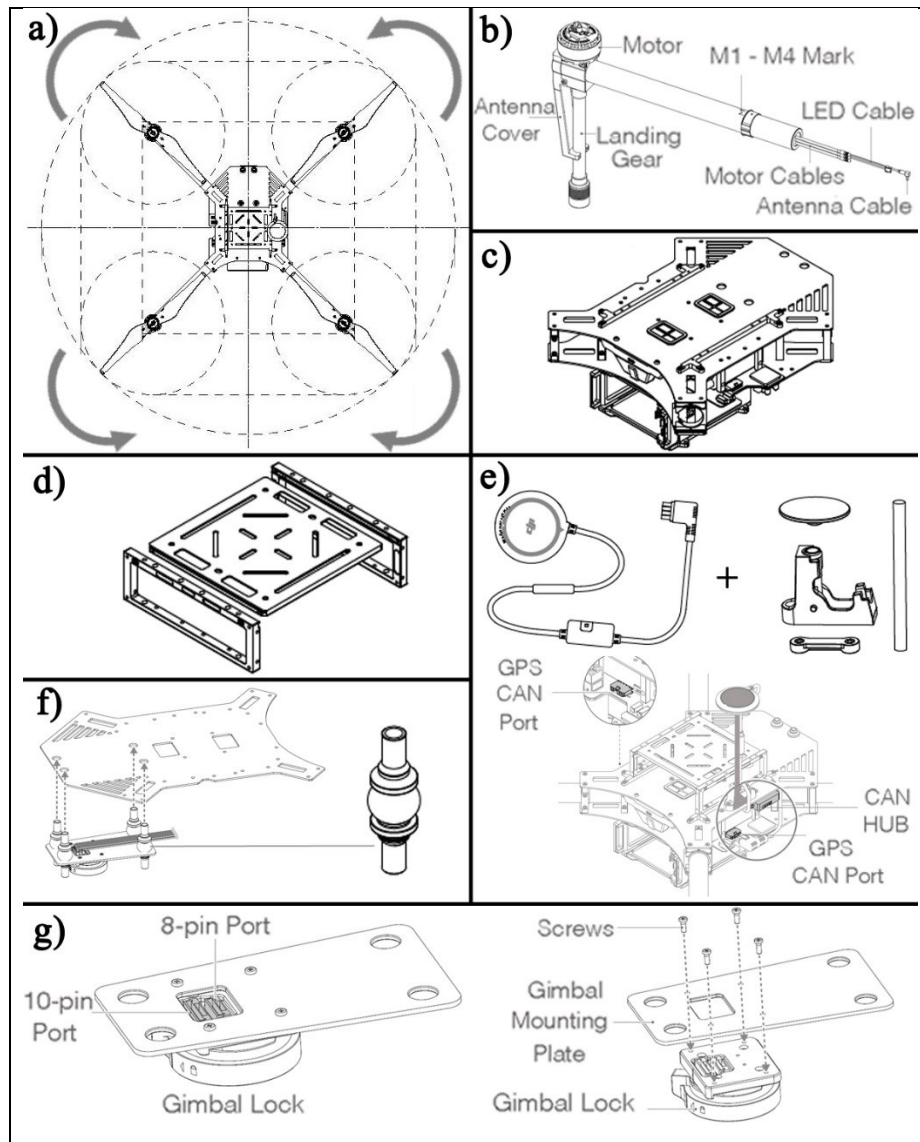


Figure 4-12: Detailed DJI Matrice100 components (DJI, 2016); (a) Propellers, (b) Frame Arm, (c) Center Frame, (d) Expansion Bay, (e) GPS module, (f) Damper, and (g) Gimbal mounting plate

[2] 3-Axis gimbal

While the gimbal profile offers a stable platform for the camera due to the 3-axis stabilization (pitch, roll, and yaw). Also, the gimbal can tilt the camera vertically by 120° and rotate horizontally by $+320^\circ$ to -320° (see Figure 4-13).

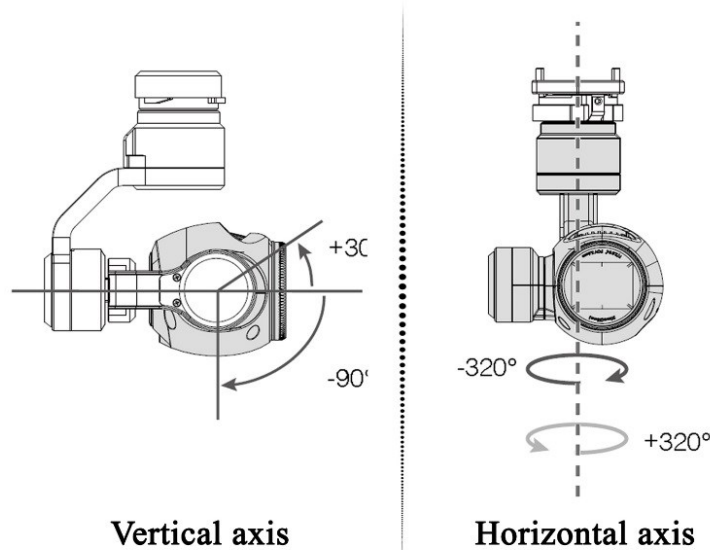


Figure 4-13: Gimbal profile (DJI, 2016)

[3] FLIR Zenmuse XT infrared camera

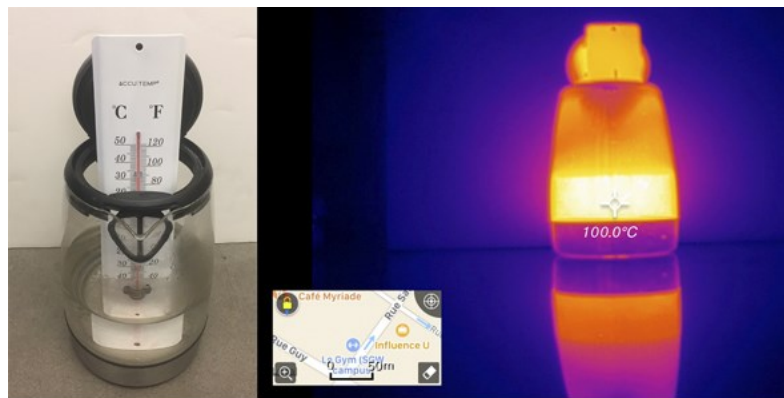
The UAS-based thermal imagery system has a high defined infrared camera mounted to the aircraft (Table 4-4). Thus, the matrice100 is equipped with an *FLIR Zenmuse XT* infrared camera sensing that shows a live streaming to the DJI GO smartphone application.

Table 4-4: Technical data of the infrared camera (DJI and FLIR, 2016)

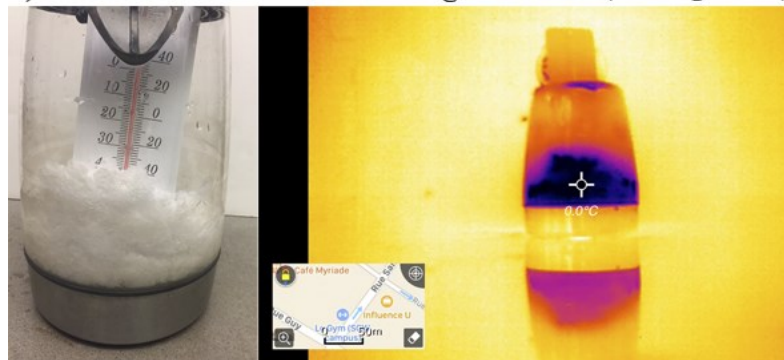
Camera	<i>FLIR Zenmuse XT@MATRICE 100</i>
Dimensions	103 x 74 x 102 mm
Weight	270 g
Temperature range	-40o to +550o C
Detector	640 x 512 UFPA
Spectral range	7.5-13.5 μm
Storage	Micro SD card: 32 GB
Image frequency	30 Hz

Infrared camera precision test

Flir Zenmuse XT infrared camera is a high-defined camera that can spot pixel temperature precisely. Thus, this infrared sensor has the ability to provide high-sensitivity infrared scans at 640/30fps with accurate temperature readings that can reach 0.08°C (Heliguy, 2017). Also, the used infrared sensor in this research is a brand new camera with a factory calibration using the 12-point inspection and calibration program. Technically, temperature references are used for calibration annually (FLIR Systems, 2017). In addition, the thermal precision test was acquired for the infrared camera to validate thermal readings. To do so, a simple test using thermometer was conducted. Specifically, an accurate temperature metal thermometer with dimensions of 29.2 cm was used to read the temperature at two conditions (Boiling water at 100°C and frozen ice at 0°C). In parallel, the Flir Zenmuse XT camera was used to capture thermal images at both conditions and spot the exact pixel temperature at each condition. In Figure 4-14, the captured thermal images showed an accurate temperature reading reflecting an accurate infrared sensor with correct thermal readings.



a) Thermometer and a thermal image at 100°C (Boiling water)



b) Thermometer and a thermal image at 0°C (Ice)

Figure 4-14: Thermal precision test at 100° and 0°C

[4] Ground control station

The ground control station consists of two parts; the remote controller (Figure 4-15) and the smartphone device. The remote controller can control both the aircraft and camera at the same time. For example, shutter buttons are used for capturing images and recording videos. Also, gimbal dials are used to control the orientation of a camera. On the other hand, a smartphone device is connected to the remote controller by a micro USB port (see Figure 4-16). A smartphone device can operate the DJI Go application for live video streaming, adjusting camera settings (resolution, color pallets, shutter speed, etc.), playback the captured images and videos, and show the status of the whole system (aircraft, camera, and the remote controller).

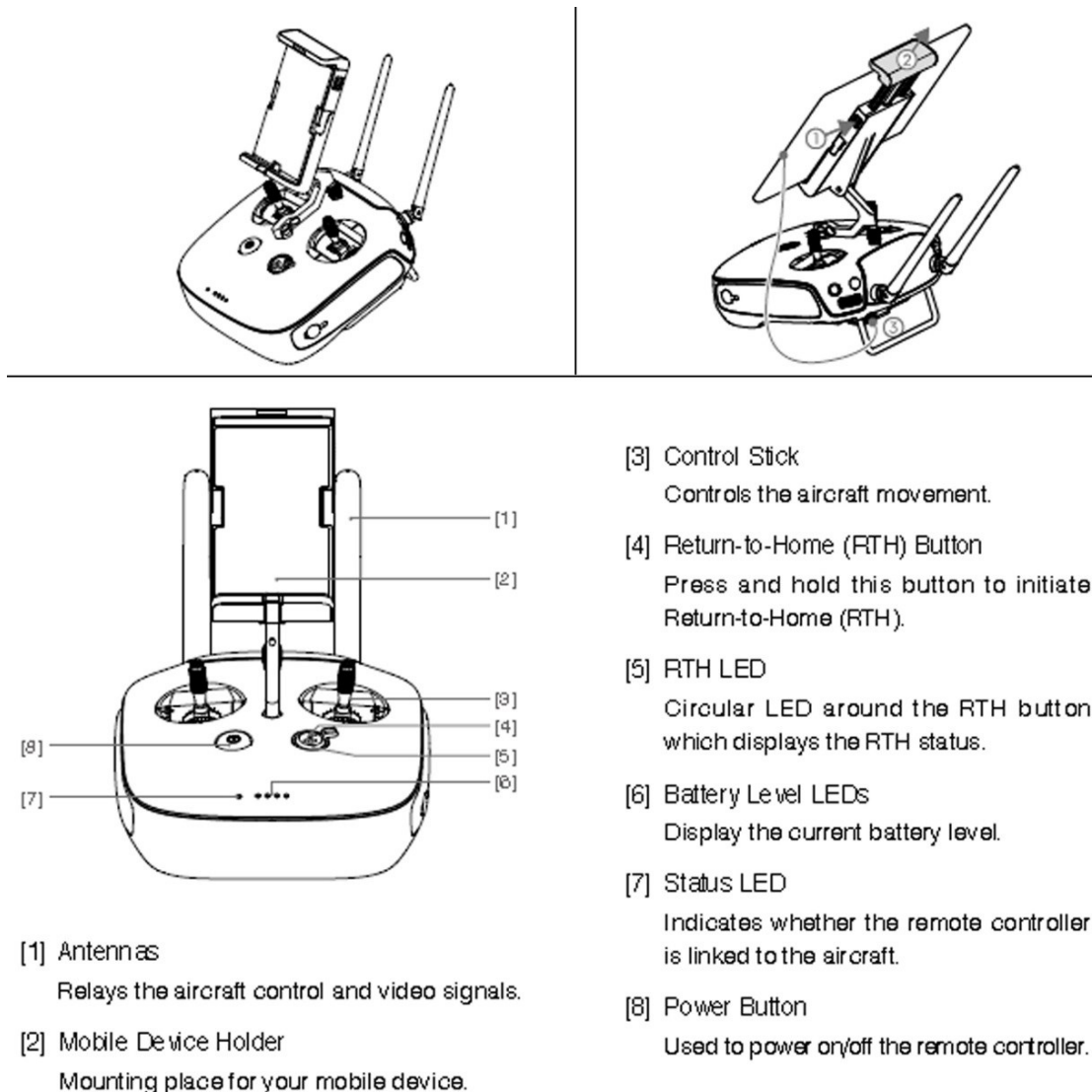


Figure 4-15: Components of remote controller (DJI, 2016)

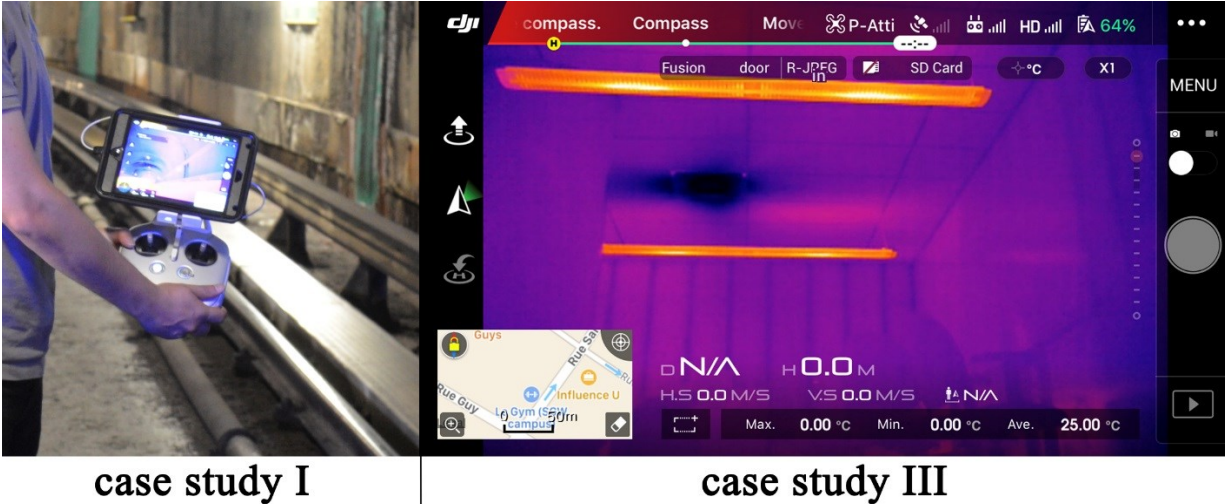


Figure 4-16: Ground control station in the case studies

Equipment used for data processing:

In order to process the collected data and reconstruct the proposed models, *Dell Precision Tower T5810* was used. This machine was used in modeling and generating both the image-based and laser-based point cloud models. Also, it was used in thermal data processing and mapping. Finally, it was used to generate, filter, and evaluate the output models of thermal-based point cloud models. Technically, (Table 4-5) shows the detailed specifications of this tower machine being used in this thesis.

Table 4-5: Technical specifications of the used tower machine

<i>Machine</i>	<i>Dell Precision Tower T5810</i>
Processor	Intel Xeon E5162 v3 (4C, 3.5GHz, 10M, 140W)
Memory (RAM)	16GB (4x4GB) 2133MHz DDR4
Storage	360 GB SATA Class 20 Solid State Drive (SSD)
Graphics	AMD FirePro W2100 2GB
Operating system	Windows 7 Professional (64-bit)

4.1.3. Software

This section will review the different software being used in different data processing tasks and 3D modeling. To do so, used software can be grouped into two main categories that are as follow:

Software used for spatial modeling:

To start with generating an image-based point cloud, the used software was *Autodesk Recap 360*. As shown in (Figure 4-17) Autodesk Recap 360 is a free image processing software which relies on running sfm algorithm in the generation of image-based point cloud models. To do so, a set of multiple overlapping images are needed to be imported into a cloud-based software. After, an automated process of feature extraction, detection and matching will take place leading to the reconstruction of the 3D point cloud model. However, manual registration and scaling can be applied to enhance the results and speed up the process. On the other hand, laser scans require multiple scans at different positions. To combine all scans into one model of one common coordinate systems, *Trimble Realworks* software (Figure 4-18) was used for registration and aligning multiple scans together. This could be accomplished by matching same reference targets and tags in different scans. Finally, output models were filtered from all unwanted points.

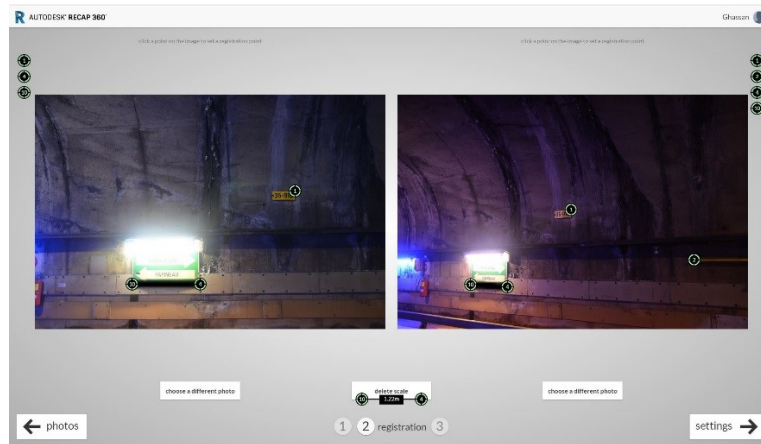


Figure 4-17: Image-based point cloud generation using Autodesk Recap 360 software

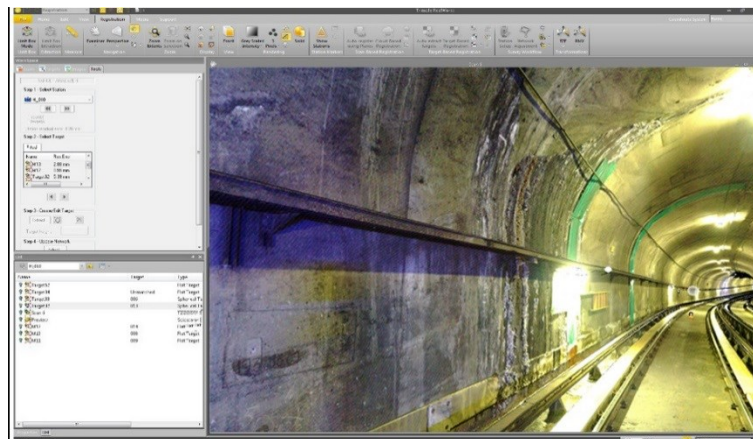


Figure 4-18: Laser-based point cloud generation using Trimble RealWorks software

Software used for infrared thermography:

In parallel, each set of overlapping thermal images were grouped together for image stitching. In this step, a commercial software *FLIR Tools Plus* (Figure 4-19) was used to create large radiometric panoramic images that cover a large surface area with an accurate temperature representation. Technically, the main concept behind this technique can be referred to feature extraction and matching. Detectable key features can be a point of interest which is different than its neighboring points such as corners and edges. So, exactly overlapped regions can be identified and matched. After, a visual correction validates the previous matches and acquire multiple images a unified coordinate system and image characteristics. Lastly, a radiometric correction takes place that overlay the color variation between the overlapping regions using linear transition method. Finally, accurate radiometric panoramic images were mapped to the dense 3D point cloud model using the free trial version of *3dreshaper 2016 MRI* software. (Figure 4-20).

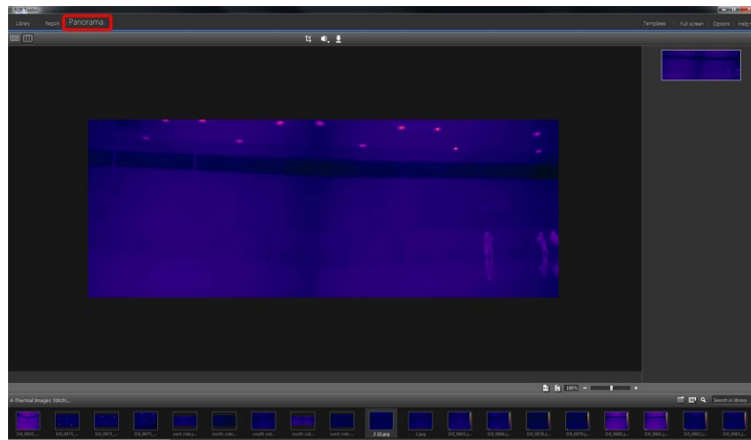


Figure 4-19: Radiometric panorama and image stitching using FLIR Tools Plus software

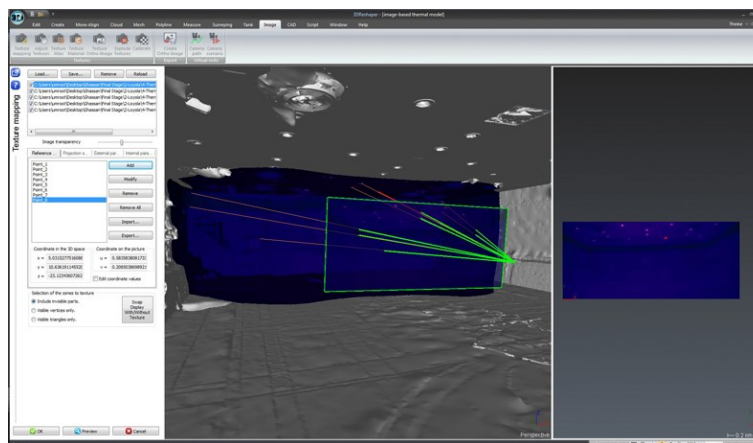


Figure 4-20: Thermal mapping using 3dreshaper software

4.2. Case Studies

In order to test the approach which was proposed in the methodology chapter. Figure 4-21, shows the flowchart and the task sequence in performing the different experiments. This flowchart will summarize all stages in order, the number of cases studies, used hardware, software, and finally the final outputs of each approach.

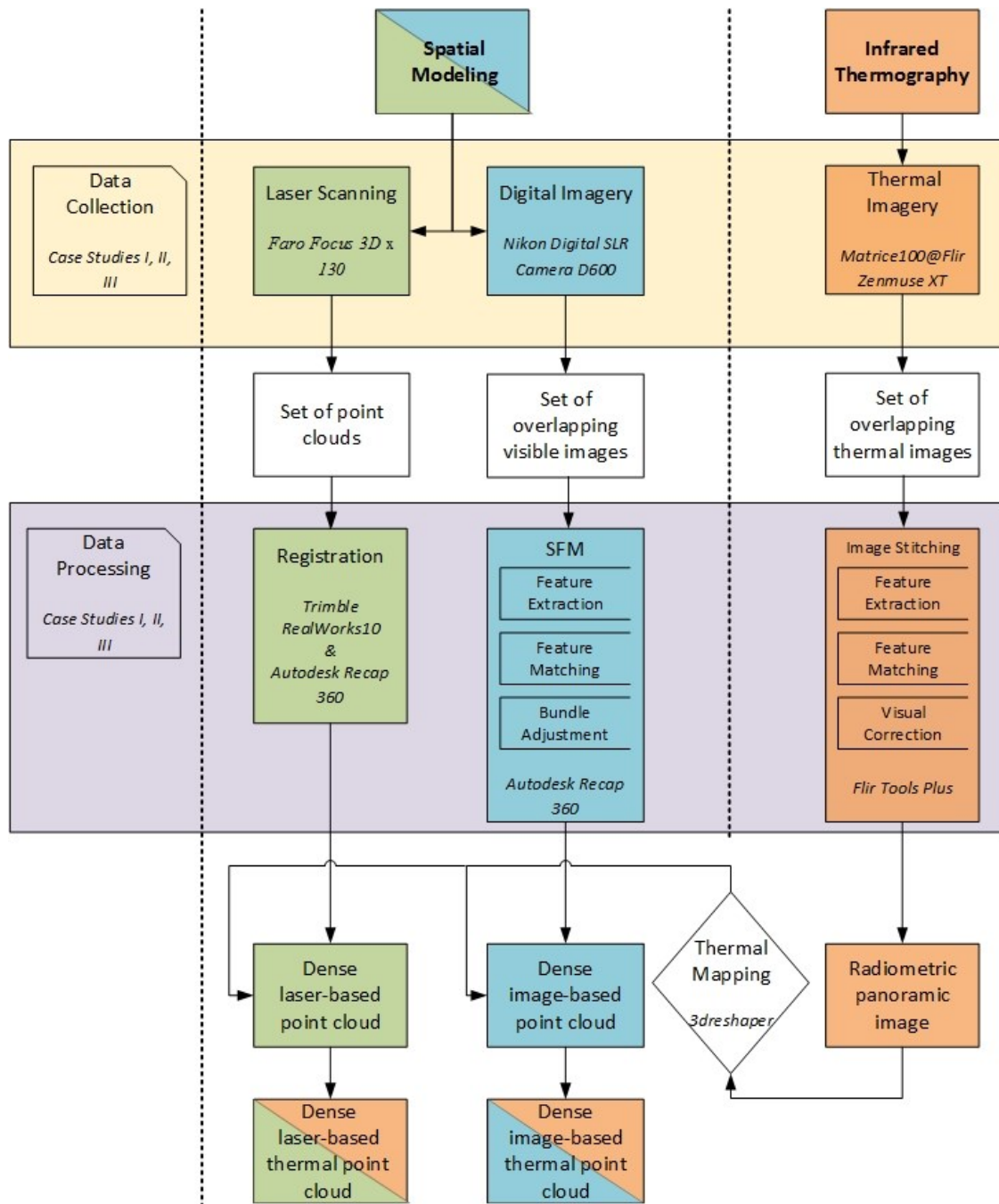


Figure 4-21: Flowchart of the followed research work in all case studies

4.2.1. Case Study I – Subway Tunnel Segment

Spatial Modeling

[1] Point Cloud Generation Using Digital Imagery:

Data Collection

In order to reconstruct an image-based 3D point cloud model for the subway tunnel segment environment, a set of overlapping images of the indoor environment were collected. To do so, a visible camera *Nikon Digital SLR Camera D600* was used for image acquisition with an overlap of 80% or more between consecutive images. Data acquisition started at night (2:00 am), and images were taken from different angles and positions at a maximum resolution of 6016 x 4016 pixels. Collecting images at high resolution can assure the generated model to be a high dense point cloud. Also, images were taken with a camera lens of focal length equal to 35 mm. This helped of capturing a full horizontal scene of an environment. With the fact of dark lighting conditions within the tunnel environment; the camera flash light was used while capturing photos. Images were collected back and forth and at high details. Finally, 157 photos were collected for the 30 m tunnel segment case study. Figure 4-22, shows a sample of the visible images collected from the subway tunnel segment in the city of Montreal, Canada. Data collection took place at the night of September ninth just after the closing of the subway service.



Figure 4-22: Sample of the images collected from the subway tunnel testing environment

Data Processing

After data collection, captured images were subjected to a manual filtration process. Where all blurry and unwanted images that include moving objects were removed from the collected set. For example in Figure 4-23, a sample of the blurry images that were removed in the filtration process. Accordingly, (Table 4-6) summarizes the output of the data collection stage. After completing the filtration of the total 157 collected images, the lasting set of overlapping images (148 images) were ready for processing and registration. Thus, the filtered images were uploaded into a cloud-based software for image processing (*Autodesk ReCap 360*) for an automated reconstruction process of 3D point clouds. To achieve the designated output, the software undergoes three main steps. First, the software identifies, extract and match common feature points in images. While this step can be done automatically, it was advised to correct and suggest some common feature points manually to assure a more accurate model and speed up the registration process (see Figure 4-24). Consequently, 13 feature points were assigned manually over 28 different images. Second, images were listed in order then the position and orientation of each image were calculated. Lastly, extracted feature points of known location and orientation were matched together in a process known as triangulation. As a result of these steps, a 3D point cloud model of the studied case study was reconstructed. But, a filtration process was needed to remove any unwanted points. These unwanted points could be far points out of the model. Also, the scale of the model was revised by using a known dimension from the environment. A built-in tag of the subway tunnel was previously measured manually using a measuring tape. Then, this measurement was used in scaling the reconstructed output as shown in (Figure 4-25-b). While (Figure 4-25-a) shows the exact distance in the resulted point cloud model. Finally, an image-based point cloud model of the subway tunnel segment was reconstructed (see Figure 4-26). In summary, the visible point clouds were orthogonally projected to form an orthogonal image (Figure 4-27). In which, it represents an adequate layout with direct metric measurements using a graphic scale to measure distances and areas.

Table 4-6: summary of data collection for the subway tunnel segment image-based point cloud

No. of images before filtration	No. of images after filtration	No. of images registered	Image resolution (pixels)	Focal length (mm)
157	148	146	6016 x 4016	35



Figure 4-23: Examples of the removed blurry images

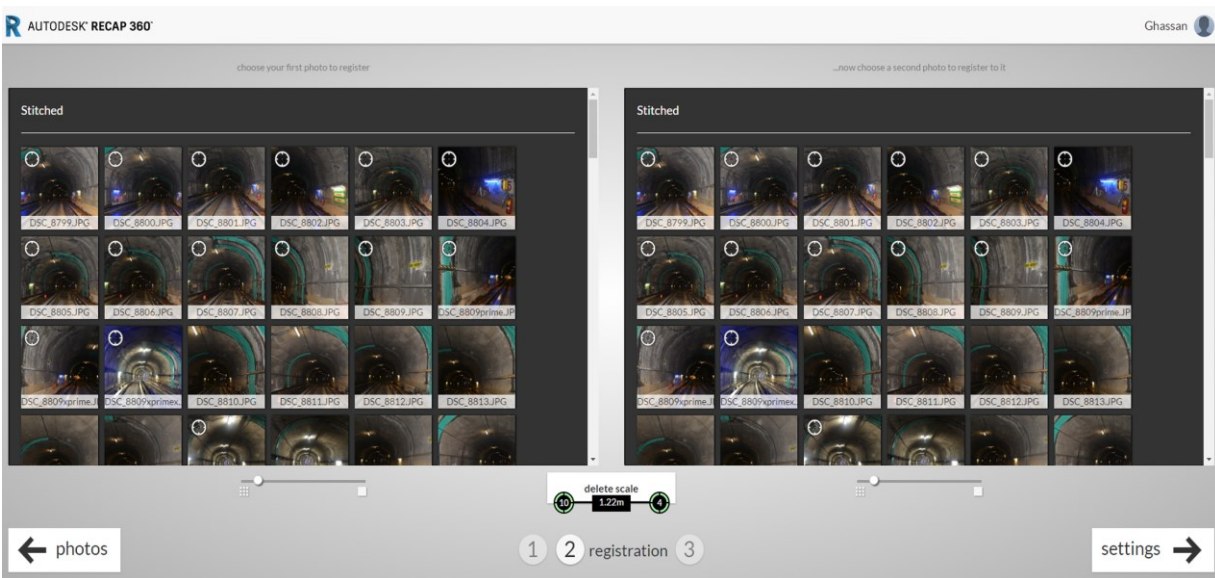


Figure 4-24: Manual registration of images in Autodesk Recap 360

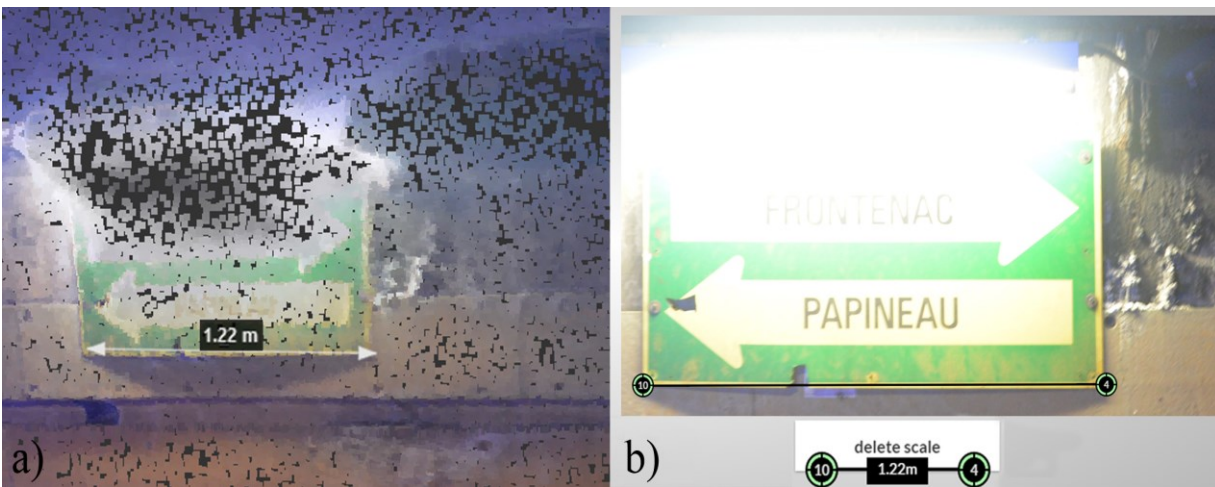


Figure 4-25: Scaling: (a) a measurement from the generated point cloud model, and (b) a known real measurement while data processing

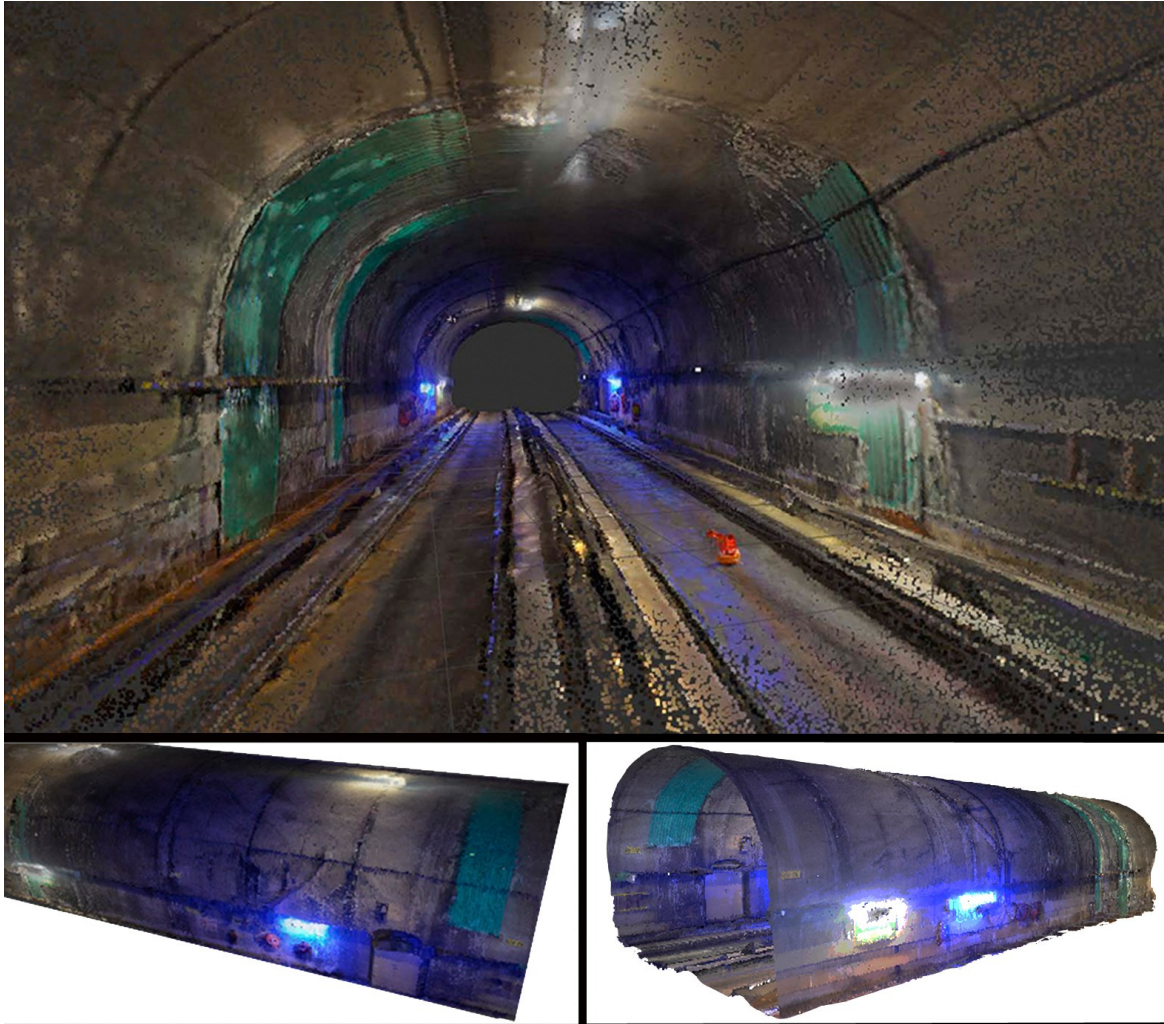


Figure 4-26: 3D image-based point cloud Model of the Subway tunnel segment

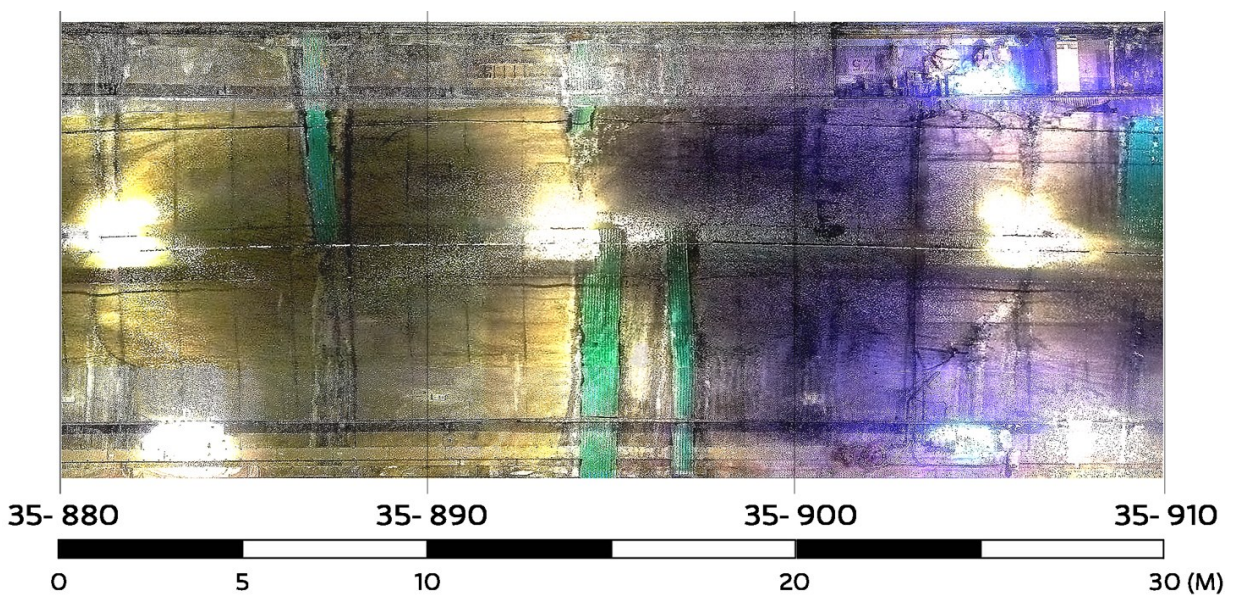


Figure 4-27: As-is image-based ortho-photo for the subway tunnel segment environment

[2] Point Cloud Generation Using Laser Scanning:

Data Collection

For the generation of a laser-based point cloud model of the subway tunnel segment, a *Faro Focus3D X 130* laser scanner was deployed in site for scanning. However, multiple scans of different positions were required in order to cover the whole scene of the environment. Multiple scans at different positions are considered vital in the generation of a complete point cloud model. Thus, reference spherical targets were placed for later registration. Registering different scans includes the alignment of multiple scans into one model of a common coordinate system. Usually, three reference targets of different elevations are considered enough for scan registration. But for the subway tunnel segment, the curved cylindrical geometry of the environment requires five spherical targets to be deployed at different intended locations and elevations (see Figure 4-28). After, the laser scanner was fixed to a tripod at the first position for scanning (Figure 4-29). Next, the settings were adjusted corresponding to the appropriate condition of an indoor surrounding, dark lighting conditions, and with high resolution (see Figure 4-30). After the scanning of the first position was complete, collected data were saved on the SD card and checked manually before moving to the second location. Then, both laser scanner and tripod were moved to the second position which was planned previously. Similarly, a second scan was completed and checked manually. Finally, the two successful scans were considered enough to cover the whole scene of the surrounding as shown in Figure 4-31.



Figure 4-28: Five spherical targets deployed in the subway tunnel environment



Figure 4-29: Images while laser scanning the subway tunnel testing environment



Figure 4-30: Adjusting settings for scanning (similar in all case studies)

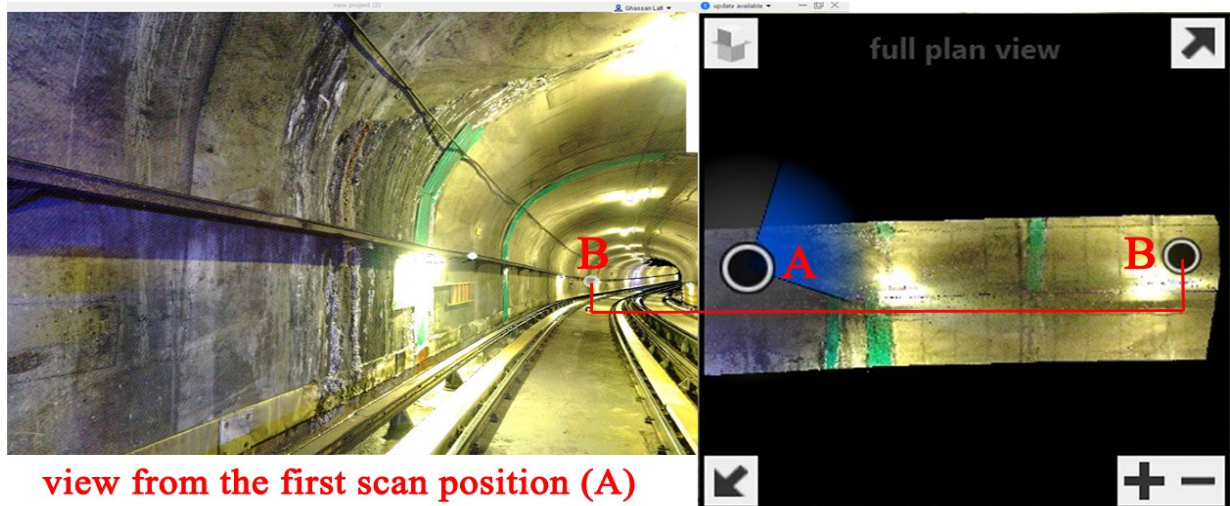


Figure 4-31: Scanning positions in the subway tunnel environment

Data Processing

In order to process the scanned data, multiple scans of the subway tunnel were imported from the SD card into (*Trimble Realworks 10*) software then exported into a compatible extension (.pts). Next, all exported scans were imported into (*Autodesk ReCap 360*) for automatic registration (Figure 4-32). Registration is the alignment of multiple scans together into one model of common coordinates using previously deployed reference targets. Figure 4-33 shows the report of registering the two scans of the subway tunnel. Registration was successful with a 100% accuracy which was measured in mm. Finally, the laser-based point cloud model of the subway tunnel segment was reconstructed (Figure 4-34). In summary, laser-based point clouds were orthogonally projected to form an orthogonal image (see Figure 4-35). In which, it represents an adequate layout with direct metric measurements using a graphic scale to measure distances and areas.

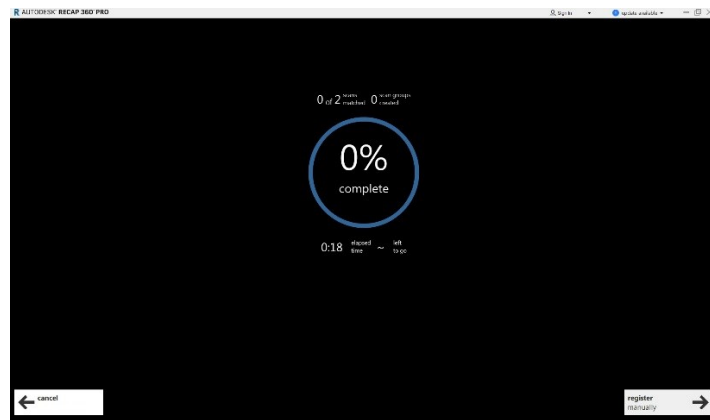


Figure 4-32: Automatic registration of scans using Autodesk Recap 360

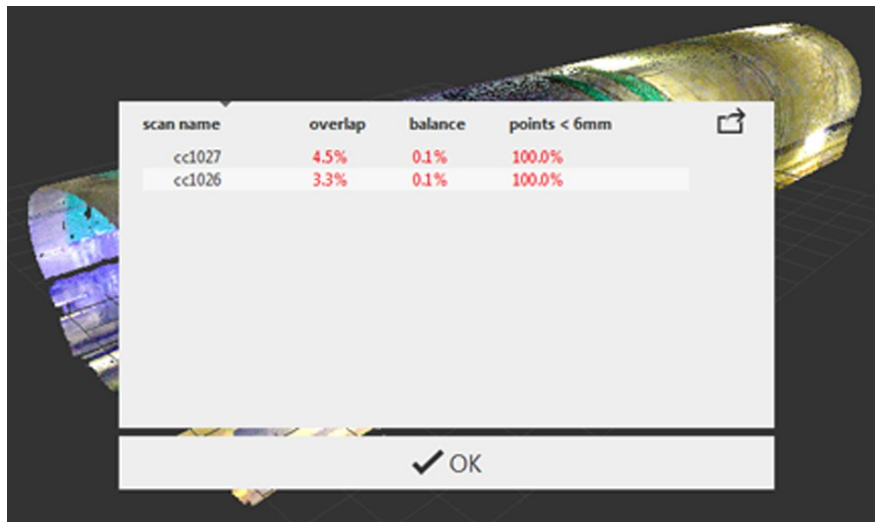


Figure 4-33: Scan registration report

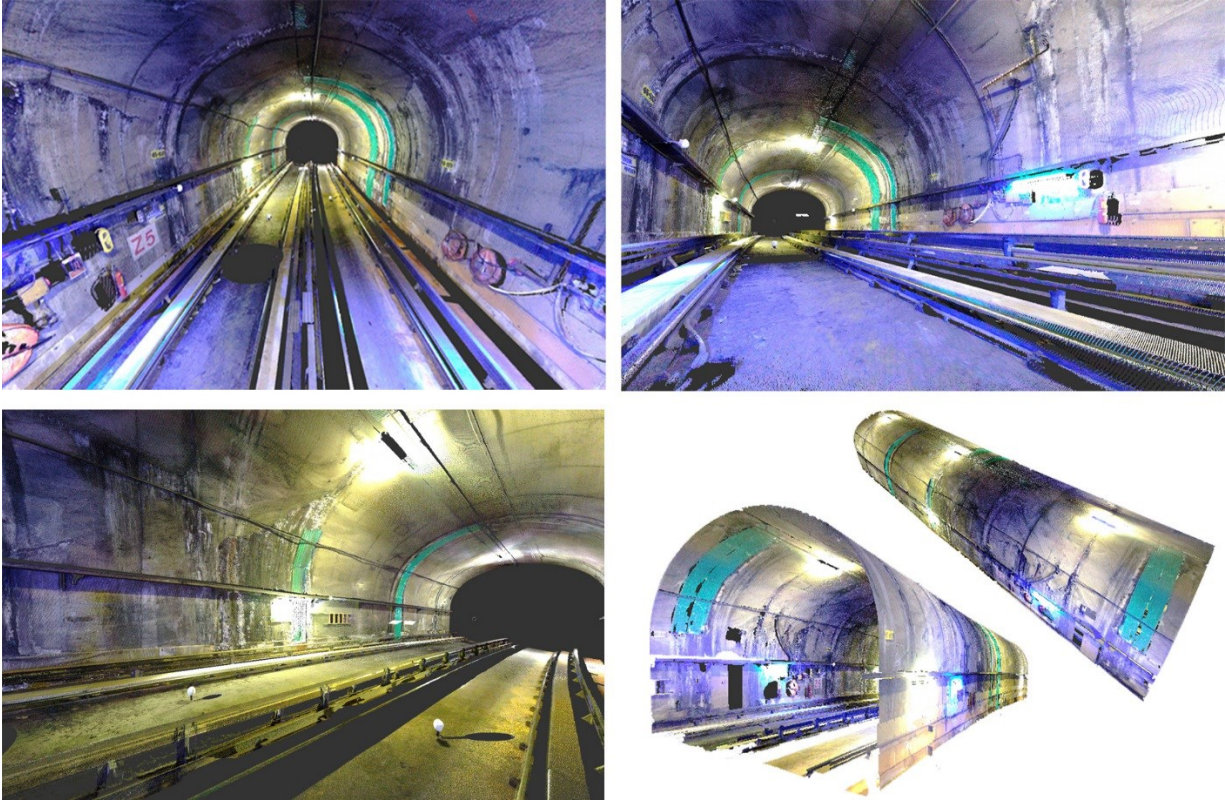


Figure 4-34: 3D Laser-based point cloud Model of the Subway tunnel segment

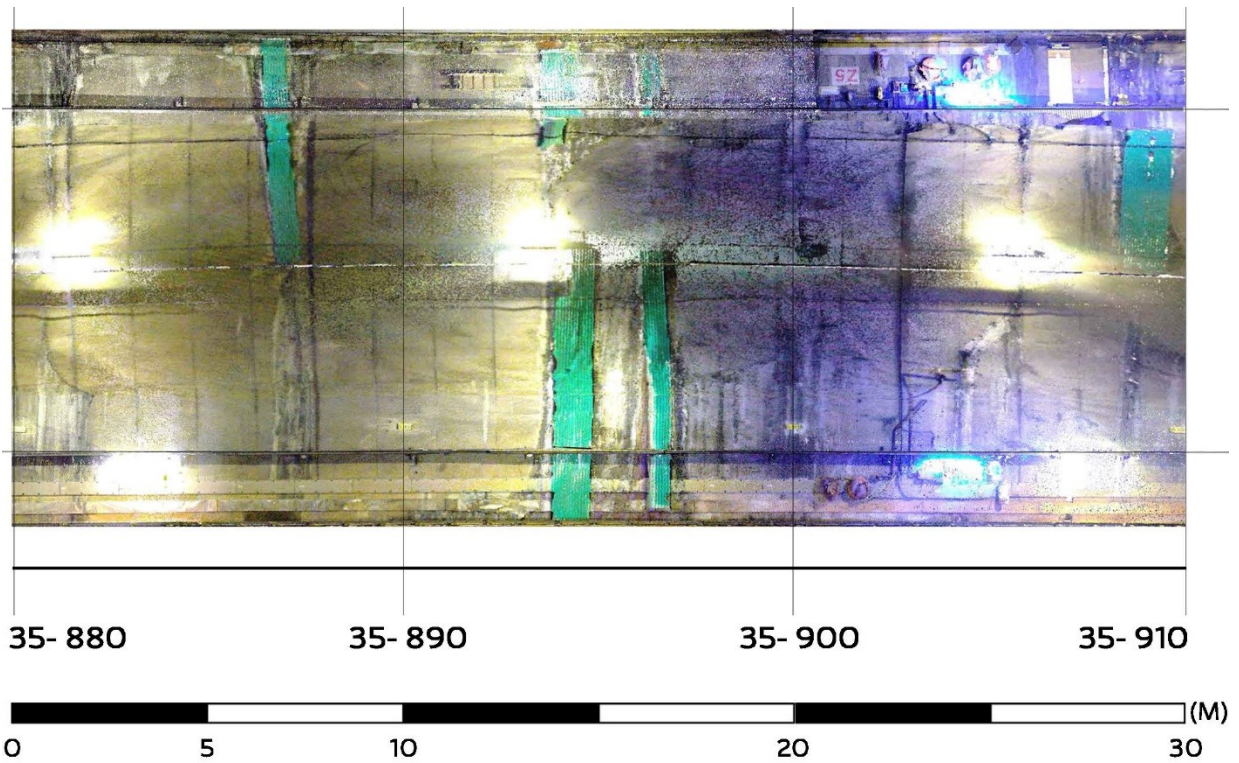


Figure 4-35: As-is laser-based ortho-photo for the subway tunnel segment environment

Infrared Thermography

Data Collection

In order to generate a 3D thermal point cloud model for the subway tunnel segment environment, a set of overlapping thermal images of the indoor environment were collected. To do so, a UAS-based thermal imagery system was deployed in the site at night after (2:00 am). Data collection took place at the night of September ninth, just after the closing of the subway service. To start, light torches were added at the site to work as thermal reference targets (see Figure 4-36). Consequently, an infrared camera *Flir Zenmuse XT* mounted on *Matrice100* drone was used for thermal image acquisition. First, the UAS was launched, the infrared camera was linked to the remote controller. Then both the aircraft and the thermal camera were calibrated, and the settings were adjusted. The IR resolution was set to its maximum of 640 x 512 pixels. Following, the UAS was directed through a straight pathway and images were captured in a modular manner with a consistent distance from the facing plane surfaces. This process was repeated back and forth for several times until the collection of the whole scene of an environment was completed. The aim of modular capturing manner is to minimize the temperature variation between images. Captured images were viewed and altered automatically using the live-streaming feature and the DJI Go application. Collected images were directly checked in site and more images were captured when needed. Also, an overlap of 50% or more was preserved between consecutive images as shown in Figure 4-37.

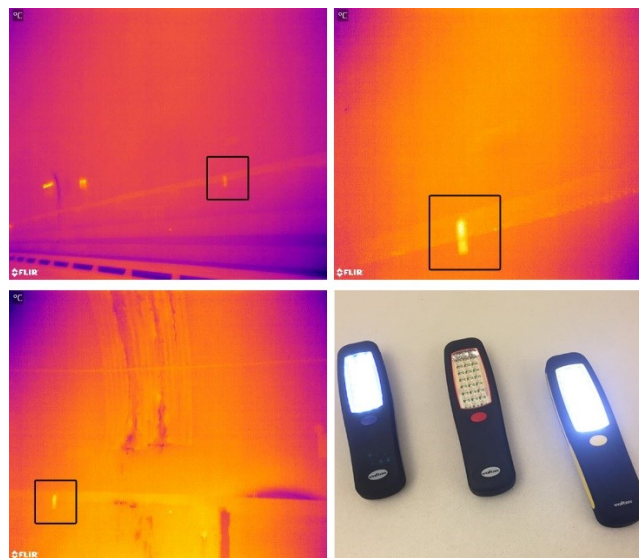


Figure 4-36: Sample of the light torches used as thermal targets



Figure 4-37: Sample of overlapping thermal images collected from the subway tunnel environment

Data Processing

Starting with data processing, a set of overlapping thermal images were chosen which were the best fit to this experiment. Table 4-7 summarizes the data collection stage, where 19 images were grouped together for image stitching. In this step, two commercial software (*FLIR Tools Plus* and *IRT stitch*) were used to create large radiometric panoramic images that cover a large surface area with an accurate temperature representation. Technically, the main concept behind this technique can be referred to feature extraction and matching. Detectable key features can be a point of interest which is different than its neighboring points such as corners and edges (see Figure 4-38). So, exactly overlapped regions can be identified and matched. After, a visual correction validates the previous matches and acquire multiple images a unified coordinate system and image characteristics. Lastly, a radiometric correction takes place that overlay the color variation between the overlapping regions using linear transition method. In summary, accurate radiometric panoramic images were created which solved the thermal variation problem encountered by previous researchers (see Figure 4-39). Finally, panoramic images were mapped to both image-based and laser-based 3D point clouds via control points such as vertices and corners using 3dreshaper software. (Figure 4-40) shows the final filtered as-is 3D thermal point cloud models that represent both spatial and infrared information of the tunnel segment. In summary, thermal point clouds were orthogonally projected to form an image-based ortho-thermal image (Figure 4-41) and a laser-based ortho-thermal image (Figure 4-42). Both ortho-thermal photos represent an adequate layout with direct thermal and metric measurements. First, a temperature scale can identify the hot and cold areas depending on the color visualization and a graphic scale can be used to measure distances and areas.

Table 4-7: summary of thermal data collection for subway tunnel segment

Number of thermal images processed	Number of images registered	Image resolution (pixels)	Focal length (mm)
19	14	640 x 512	13

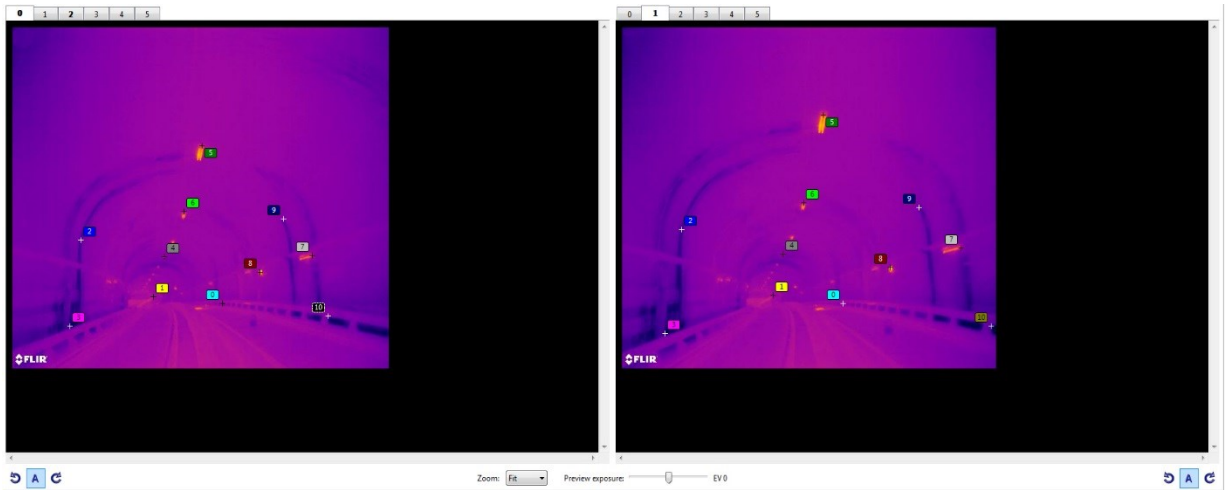


Figure 4-38: A sample for feature extraction and matching

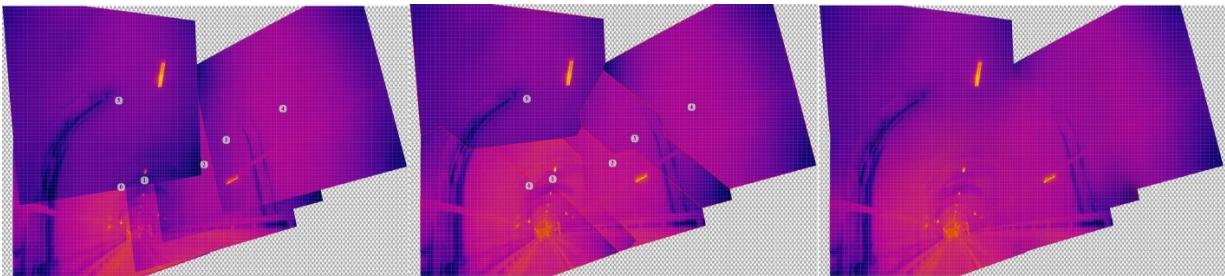
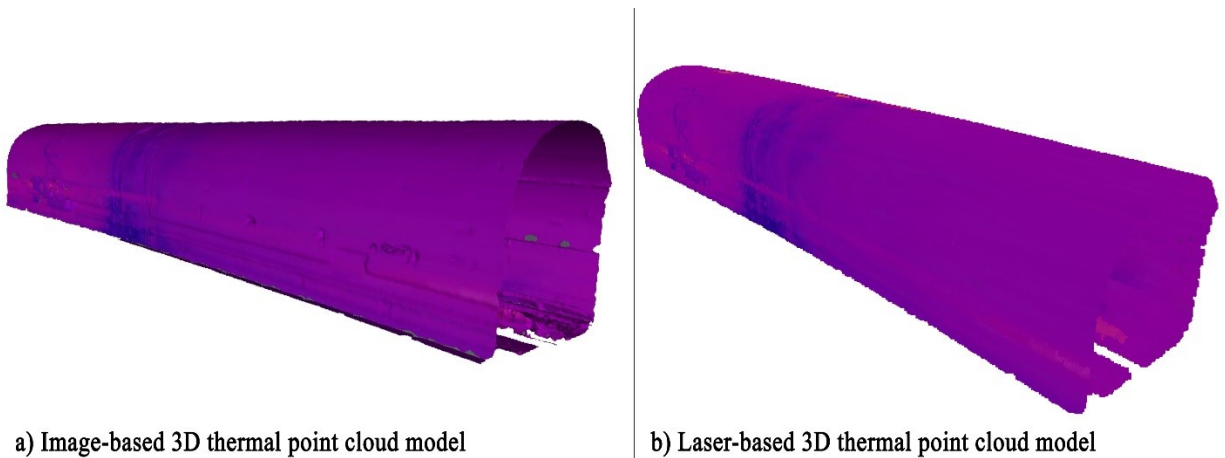


Figure 4-39: A sample for thermal image stitching



a) Image-based 3D thermal point cloud model

b) Laser-based 3D thermal point cloud model

Figure 4-40: As-is 3D Thermal Model of the Subway tunnel segment; a) Image-based 3D thermal model, and b) Laser-based thermal model

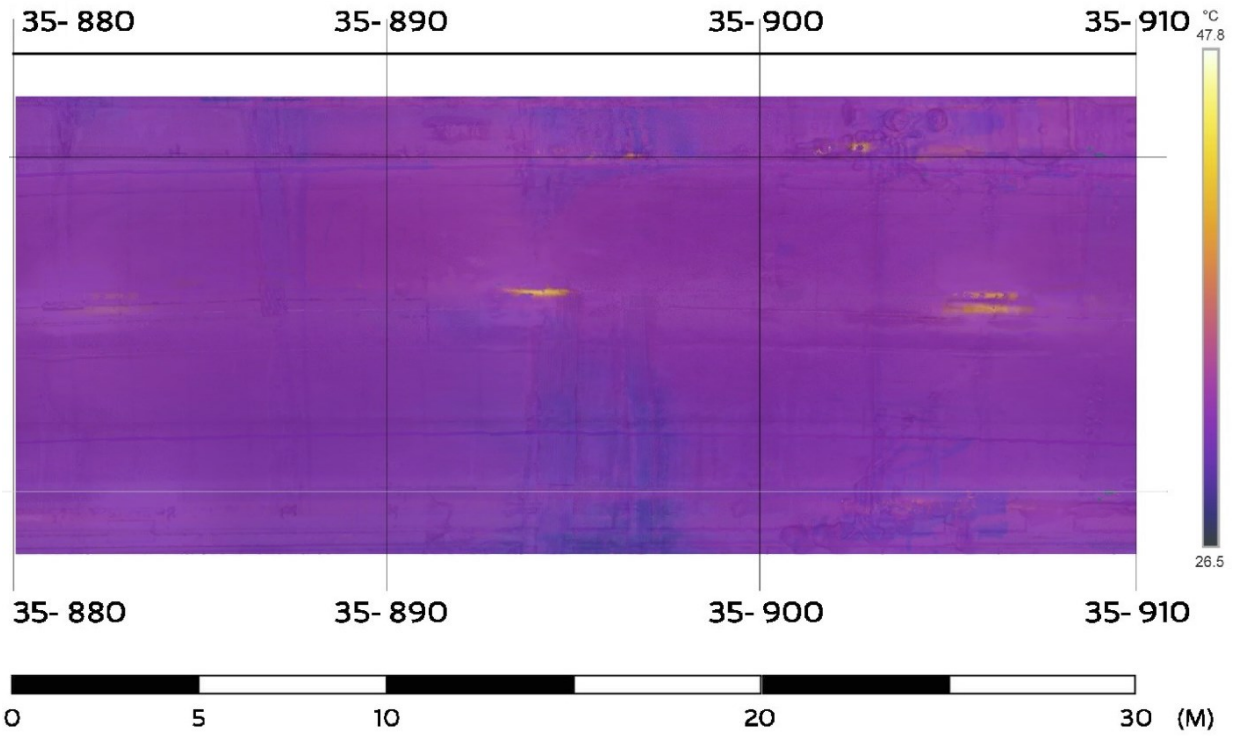


Figure 4-41: As-is image-based thermal ortho-photo for the subway tunnel segment environment

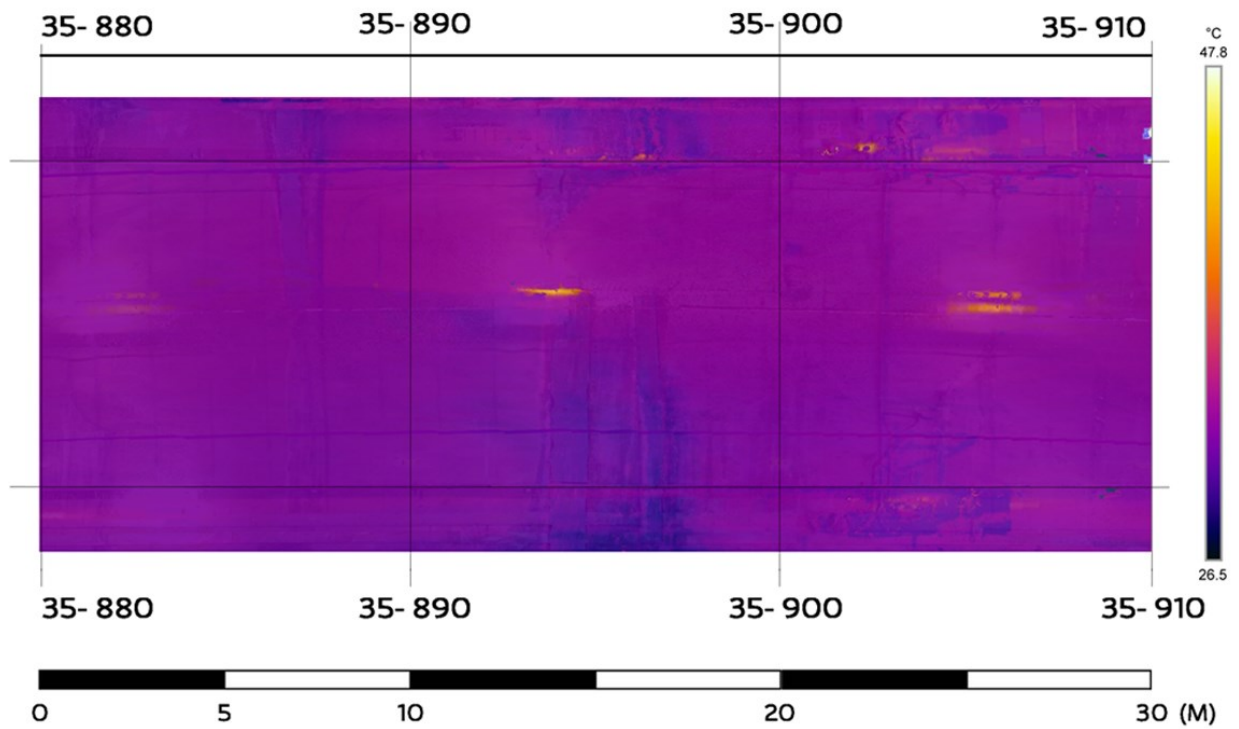


Figure 4-42: As-is laser-based thermal ortho-photo for the subway tunnel segment environment

Evaluation

Density evaluation

First, dense point cloud models are referred to the high number of 3D points in a given region of a reconstructed model. Thus, dense point cloud models have a large total number of 3D points that can reach millions of points. Dense point cloud models can show a high level of details which in turn will result in a more accurate analysis and precise decision making. Following is the recorded total number of points in all 3D point cloud models (Table 4-8).

Table 4-8: Density evaluation of the subway tunnel environment

	Total Number of 3D points
3D image-based point cloud	1,497,606
Image-based 3D thermal point cloud	(Before filtration): 1,497,606
	(After filtration): 1,272,326
3D laser-based point cloud	37,386,416
Laser-based 3D thermal point cloud	37,386,416

Time-based evaluation

Moreover, the time of each stage was recorded including the time needed for data collection and data processing for both image-based modelings (Table 4-9) and laser-based modeling (Table 4-10). Technically, the duration of setting up an environment include the needed time for deploying an equipment, adjusting the required settings and setting up targets such as; light torches for thermal thermography, spherical targets for laser scanning, and measuring a built-in tag for later image-based model scaling. While time needed for capturing images and scanning were also documented. Next, the filtration process for both visible and thermal images included the removal of any unwanted data. Generating point clouds using a cloud-based software and scans registration were also recorded. On the other hand, the duration of thermal images stitching and mapping was noted. In summary, the total time required for image-based modeling is much greater with respect to that of laser-based modeling. However, image-based modeling can still be considered as efficient since more than 20 hr were processed on a cloud-based software. So, the net total average time for image-based modeling excluding the cloud-based processing is only 2 hr and 27 min.

Table 4-9: Time-based evaluation for image-based 3D thermal point clouds generation

			Digital Imagery	Thermal Imagery
Data	Setting Up environment		7 min	16 min
Collection	Image acquisition		20 min	49 min
Average total duration for Data Collection			27 min	1 hr. and 5 min
Data Processing	Filtration		15 min	15 min
	Point cloud generation	Manual registration	35 min	-
		Cloud processing	20 hr. and 51 min	-
	Image stitching		-	25 min
	Mapping and filtration		-	35 min
Average total duration for Data Processing			21 hr. and 40 min	1 hr. and 15 min
Average total duration for 3D image-based point cloud generation			22 hr. and 07 min	2 hr. and 20 min
Average total duration for image-based 3D thermal point cloud generation			24 hr. and 27 min	

Table 4-10: Time-based evaluation for laser-based and 3D thermal point clouds generation

		Laser Scanning	Thermal Imagery
Data	Setting Up environment	15 min	16 min
Collection	Two laser Scans /Image acquisition	50 min	49 min
Average total duration for Data Collection		1 hr. and 5 min	1 hr. and 5 min
Data Processing	Filtration	-	15 min
	registration	2 hr.	-
	Image stitching	-	25 min
	Mapping and filtration	-	35 min
Average total duration for Data Processing		2 hr.	1 hr. and 15 min
Average total duration for 3D image-based point cloud generation		3 hr. and 05 min	2 hr. and 20 min
Average total duration for image-based 3D thermal point cloud generation		5 hr. and 25 min	

Cost-based evaluation

On the other hand, the cost of using different equipment and software was recorded based on official statements and companies web pages. Also, the operator cost related to data collection and processing was estimated at (20\$/hour). Taking on the consideration that the cloud-based processing require no manpower, the operator cost was calculated by multiplying the hourly rate and the needed time of data collection and processing excluding the cloud-based processing duration. Therefore, Table 4-11 shows the cost needed to generate image-based thermal models while Table 4-12, reflects the cost of laser-based thermal modeling.

Table 4-11: Cost-based evaluation for image-based 3D thermal point cloud generation

	Digital Imagery	Thermal imagery system
Equipment cost (\$)	1,900 ¹	19,000 ³
Software cost (\$)	300 ²	295 ⁴ ; 3,800 ⁵
Operator cost (\$)	20\$ x 2.25 = 45	20\$ x 2.25 = 45
Total Cost	2,245	23,140
	25,385 \$	

Table 4-12: Cost-based evaluation for Laser-based and 3D thermal point clouds generation

	Laser Scanning	Thermal imagery system
Equipment cost (\$)	54,775 ⁶	19,000
Software cost (\$)	9,625 ⁷	295; 3,800
Operator cost (\$)	20\$ x 3.17 = 64	20\$ x 2.25 = 45
Total Cost	64,464	23,140
	87,604 \$	

¹ A digital camera *Nikon Digital SLR Camera D600* (Nikon, 2016). ² Autodesk Recap 360 software with a 300 \$/ year, (Autodesk, 2016). ³ *Matrice100@zenmuse XT* with iPad, Acquired from an official invoice from (Safety express Ltd, 2016). ⁴ *FLIR Tools Plus*, Acquired from an official invoice from (Safety express Ltd, 2016). ⁵ 3dReshaper software. Retrieved from (RPLS.Network, 2016). ⁶ *Faro Focus 3D X130* laser scanner with a package including targets and a tripod. Acquired from an official invoice from (Cansel Survey Equipment Ltd., 2015). ⁷ *Trimble RealWorks 10*. Acquired from (Cansel Survey Equipment Ltd., 2015).

4.2.2. Case Study II – Gymnasium at Loyola Campus

Spatial Modeling

[1] Point Cloud Generation Using Digital Imagery:

Data Collection

Similarly as in case study I, visible images was collected for an indoor Gymnasium environment at Loyola Campus in the city of Montreal, Canada. With the fact that this environment is different than that of case study I by means of a) a rectangular symmetric geometry, b) artificial lighting conditions, and c) reflective textures like hardwood. Thus, two checkerboards of known dimensions were positioned in the environment prior to image acquisition for later registration and scaling (see Figure 4-43). Accordingly, images were collected from different angles and locations preserving an overlapping of 80% between consecutive images as shown in (Figure 4-44).



Figure 4-43: Checkerboards as reference targets in the Gymnasium environment

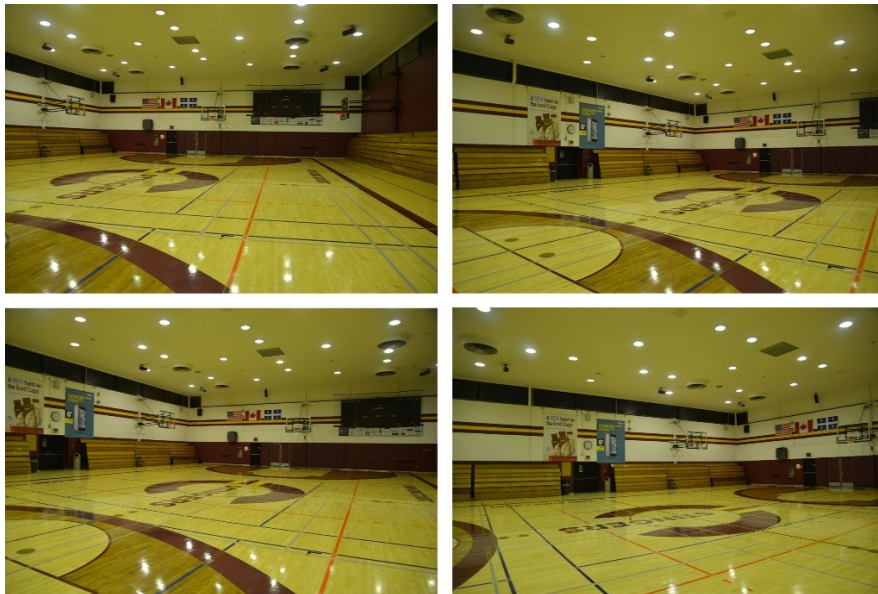


Figure 4-44: Sample of overlapping images collected from the gymnasium testing environment

Data Processing

Next, the collected data were filtered and all blurry images, unwanted images that contain moving objects were removed. The summary of data collection is reviewed in (Table 4-13), in which the 120 filtered images were uploaded into (*Autodesk ReCap 360*) software. First, some images were registered manually and the model was scaled using known dimensions of checkerboards. Consequently, an automated process resulted in the reconstruction of a 3D point cloud model for the gymnasium testing environment. After, the generated model was filtered from any unwanted points. Finally, an image-based point cloud model of the gymnasium testing environment was reconstructed (see Figure 4-45). In summary, the visible point clouds were orthogonally projected to form an orthogonal image (Figure 4-46). In which, it represents an adequate layout with direct metric measurements using a graphic scale to measure distances.

Table 4-13: summary of data collection for Gymnasium environment

No. of images before filtration	No. of images after filtration	No. of images registered	Image resolution (pixels)	Focal length (mm)
146	120	120	6016 x 4016	35

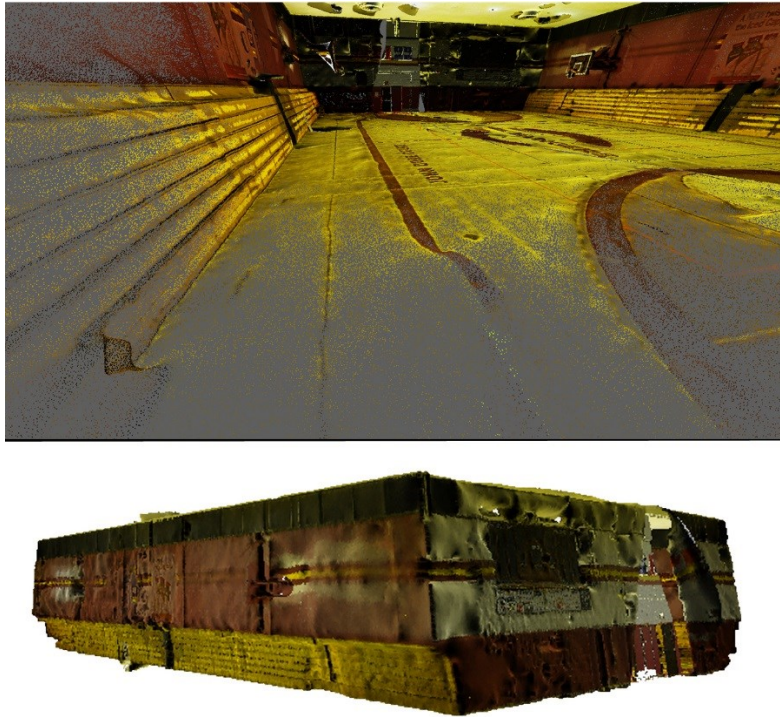


Figure 4-45: 3D image-based point cloud model of the gymnasium testing environment

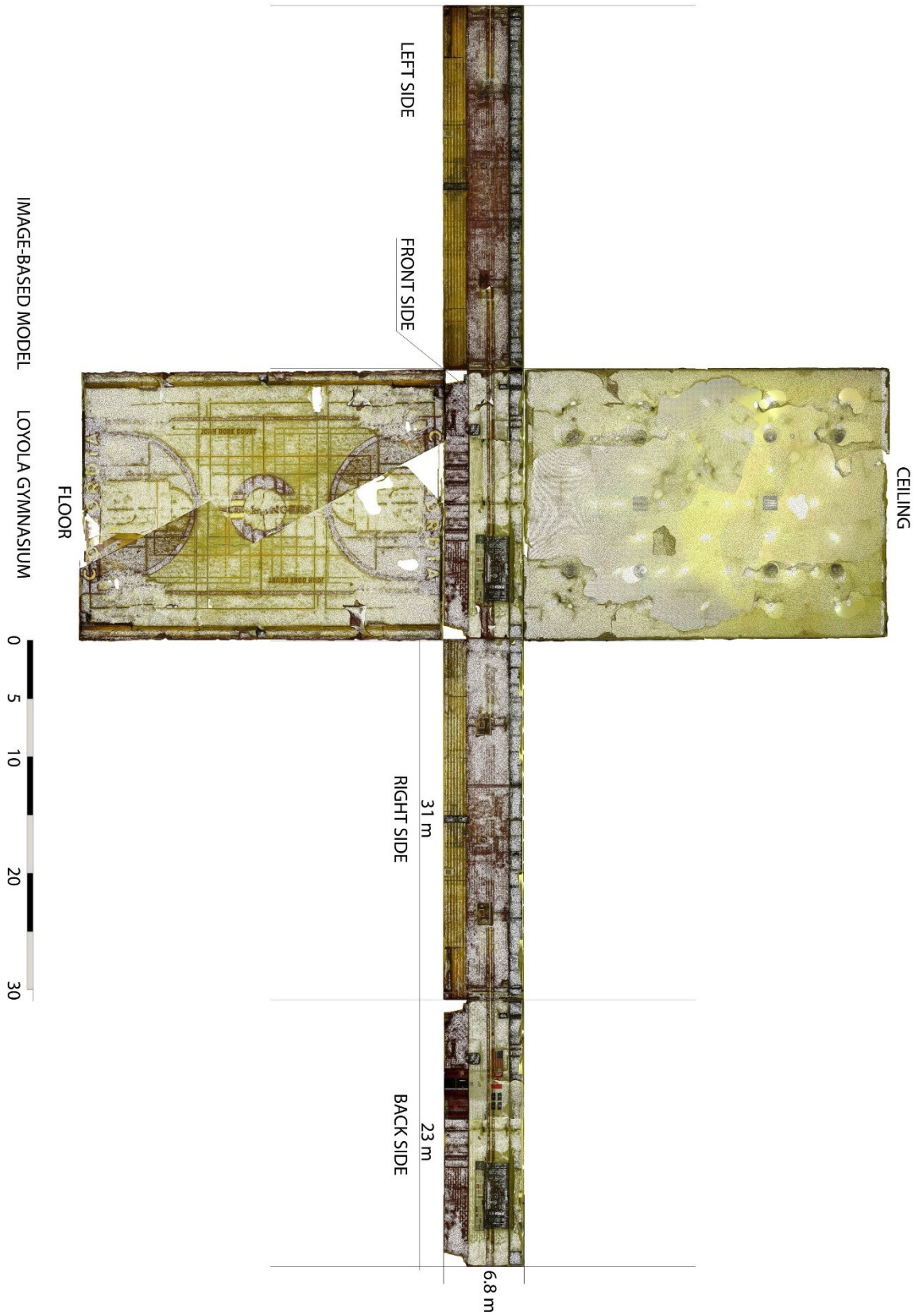


Figure 4-46: As-is image-based ortho-photo of the gymnasium testing environment

[2] Point Cloud Generation Using Laser Scanning:

Data Collection

Similar as case study I, a *Faro Focus3D X 130* laser scanner was deployed in the testing environment for scanning. First, five spherical targets and two checkerboards were added to the testing environment at different locations. Next, three scans were applied to cover the wide inner surrounding of the gymnasium. The respective positions of the three scans are presented in Figure 4-47, these scans were enough to capture the whole environment.

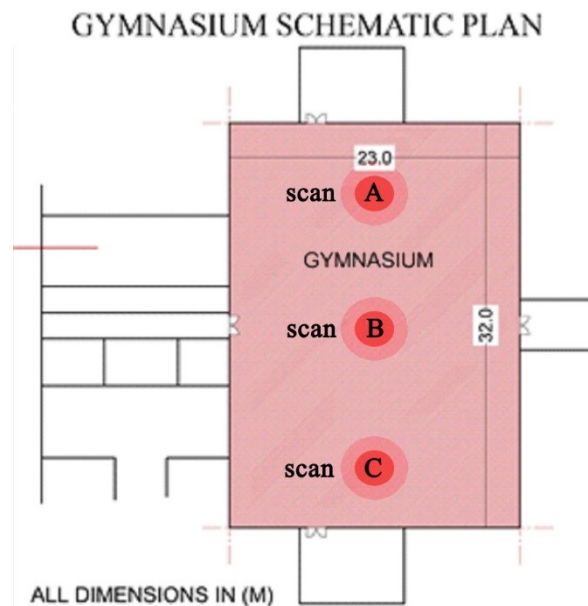


Figure 4-47: The scanning positions used in gymnasium testing environment.

Data Processing

In the processing stage, multiple scanned data of the gymnasium testing environment were imported from the SD card into (*Trimble Realworks 10*) software then exported into a compatible extension (.pts). Then, all exported scans were imported into (*Autodesk ReCap 360*) for later alignment into one model of a common coordinate system. This process is known as scans registration. Next, registration was successful with a 100% accuracy with a mm unit of measurement. Finally, the laser-based point cloud model of the gymnasium testing environment was reconstructed (Figure 4-48). In summary, laser-based point clouds were orthogonally projected to form an orthogonal image (Figure 4-49). In which, it represents an adequate layout with direct metric measurements using a graphic scale to measure distances and areas.

Table 4-14: Laser scanning summary for the gymnasium testing environment

Number of scans	Number of spherical spheres used	Number of checkboard targets
3	5	2

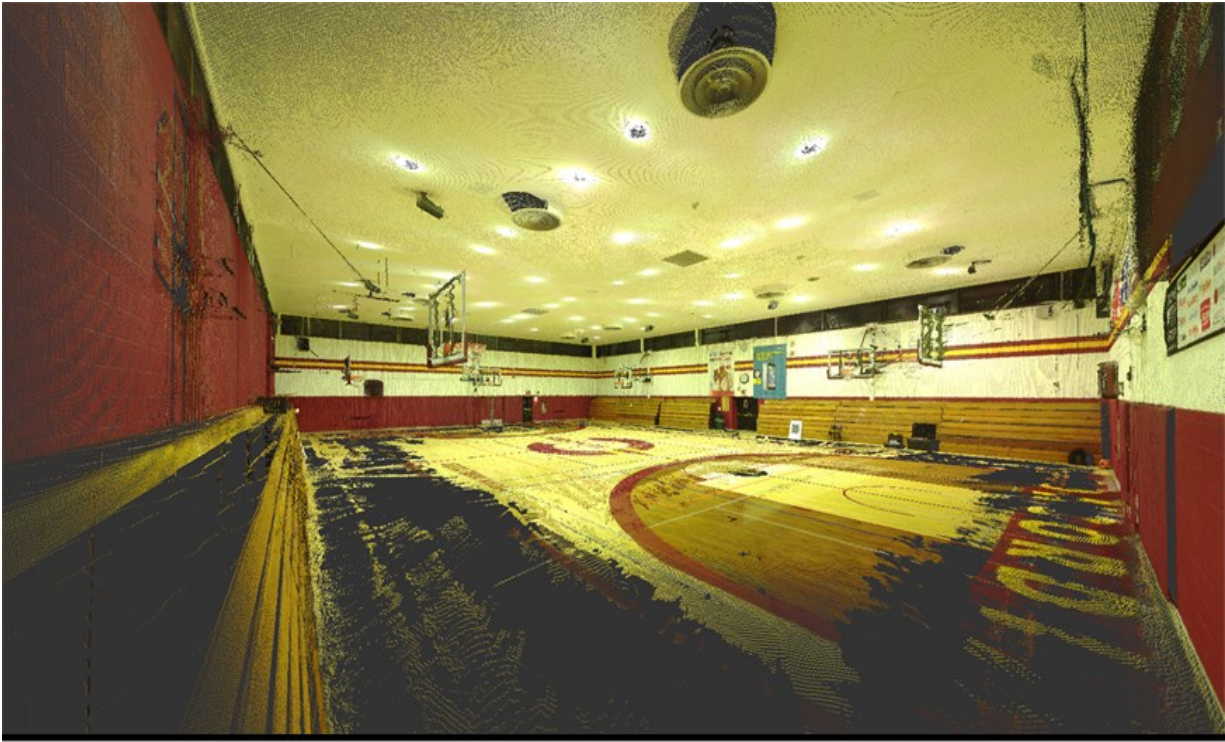


Figure 4-48: 3D Laser-based point cloud Model of the gymnasium testing environment

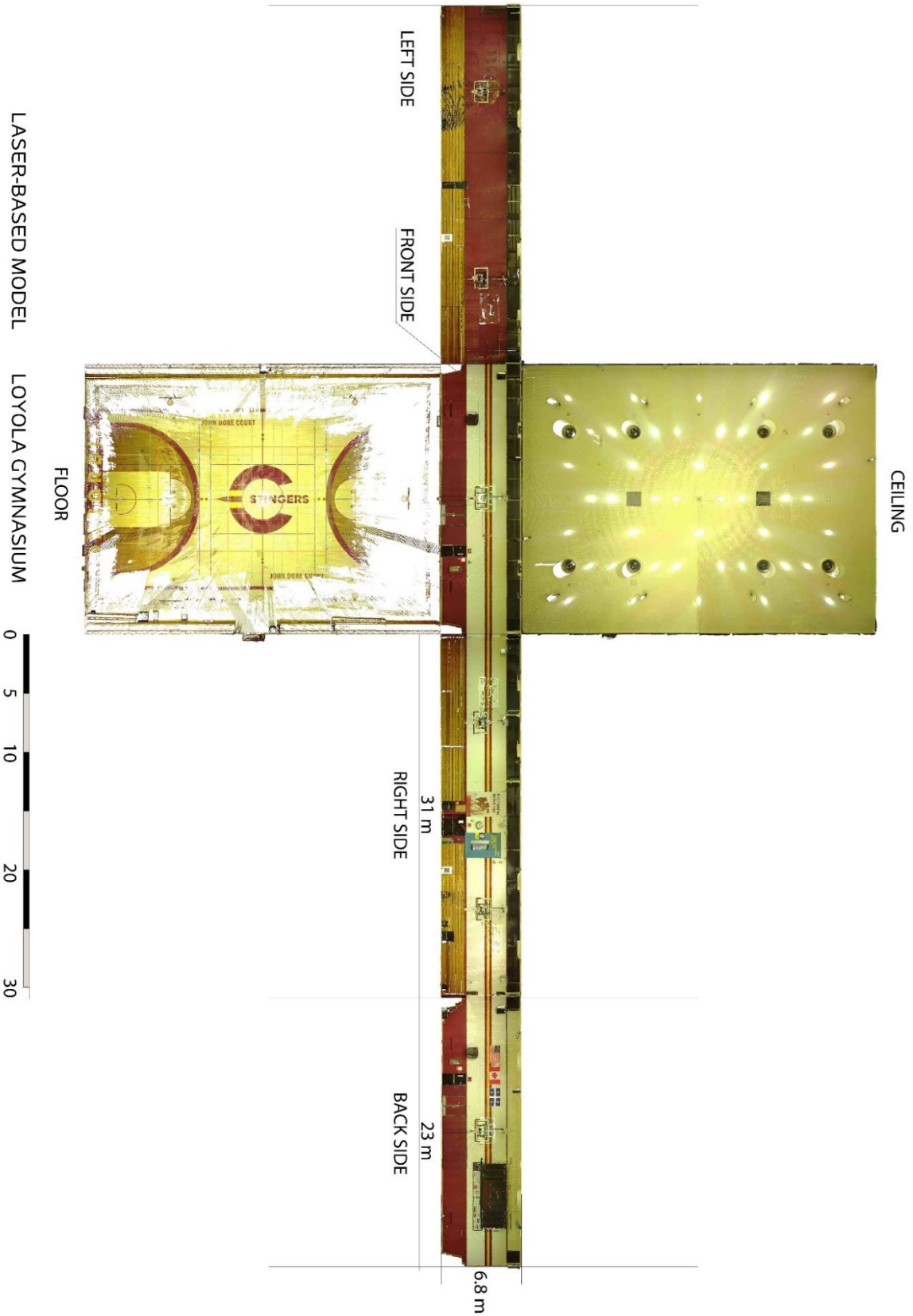


Figure 4-49: As-is laser-based ortho-photo of the gymnasium testing environment

Infrared Thermography

Data Collection

Similar to the case study I, the UAS-based thermal imagery system was used for infrared thermography task. Accordingly, an infrared sensing camera *Flir Zenmuse XT* mounted on *Matrice100* drone was used for thermal image acquisition. To start, the UAS was launched and the infrared camera sensing was connected remotely to the remote controller. Then both the aircraft and the camera were calibrated, and the settings were adjusted. With the highest resolution of 640 x 512 pixels, images were captured in a modular manner with a consistent distance from the facing plane surfaces. This process was repeated for several times until the collection of the whole scene of an environment was completed. Collecting thermal images with a consistent distance from the facing plane would minimize the temperature variation between images. Using the live streaming feature via DJI Go application, images were viewed and revised directly in site and more images were captured when needed. Also, an overlap of 50% or more was preserved between consecutive images as shown in Figure 4-50.



Figure 4-50: Sample of overlapping thermal images collected from the gymnasium environment

Data Processing

Starting with the filtration of the collected thermal images, only – were chosen for stitching. The filtered images were uploaded to *FLIR Tools Plus* software for image stitching. Then, features were extracted and matched between images similar to the process in the case study I (see Figure 4-38). Accordingly, final output was the generation of large radiometric panoramic images as explained before in case study I, (see Figure 4-39). Finally, panoramic images were mapped to both image-based and laser-based 3D point clouds via control points such as vertices and corners using 3dreshaper software.

As a result, (Figure 4-51-a) represents the final filtered as-is image-based 3D thermal point cloud model. While (Figure 4-51-b), shows the final as-is laser-based 3D thermal point cloud model. These as-is 3D thermal point cloud models represent both spatial and infrared information of the gymnasium testing environment. In summary, thermal point clouds were orthogonally projected to form an image-based ortho-thermal image (Figure 4-52) and a laser-based ortho-thermal image (Figure 4-53). Both ortho-thermal photos represent an adequate layout with direct thermal and metric measurements. First, a temperature scale can identify the hot and cold areas depending on the color visualization and a graphic scale can be used to measure distances and areas.

Table 4-15: summary of thermal data collection for gymnasium testing segment

Number of thermal images processed	Number of images registered	Image resolution (pixels)	Focal length (mm)
23	20	640 x 512	13

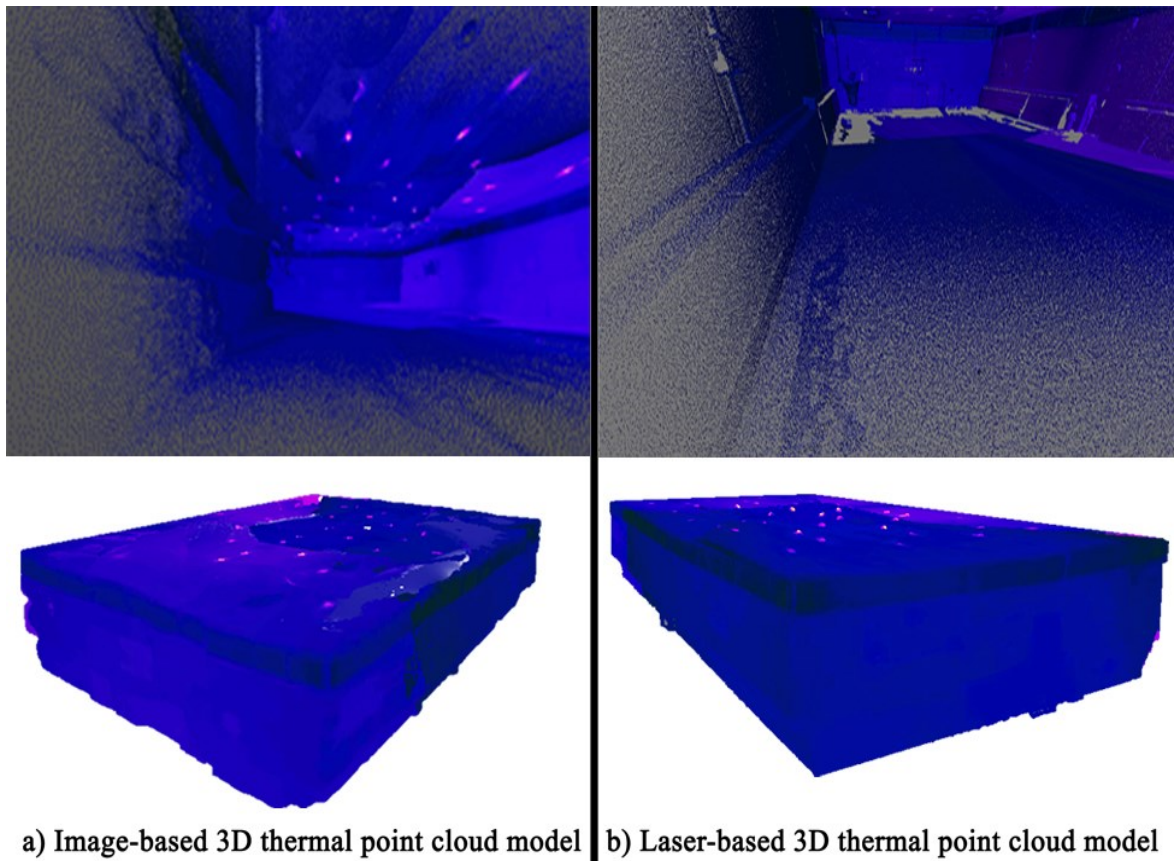


Figure 4-51: As-is 3D Thermal Model of the gymnasium testing environment; a) Image-based 3D thermal model, and b) Laser-based thermal model

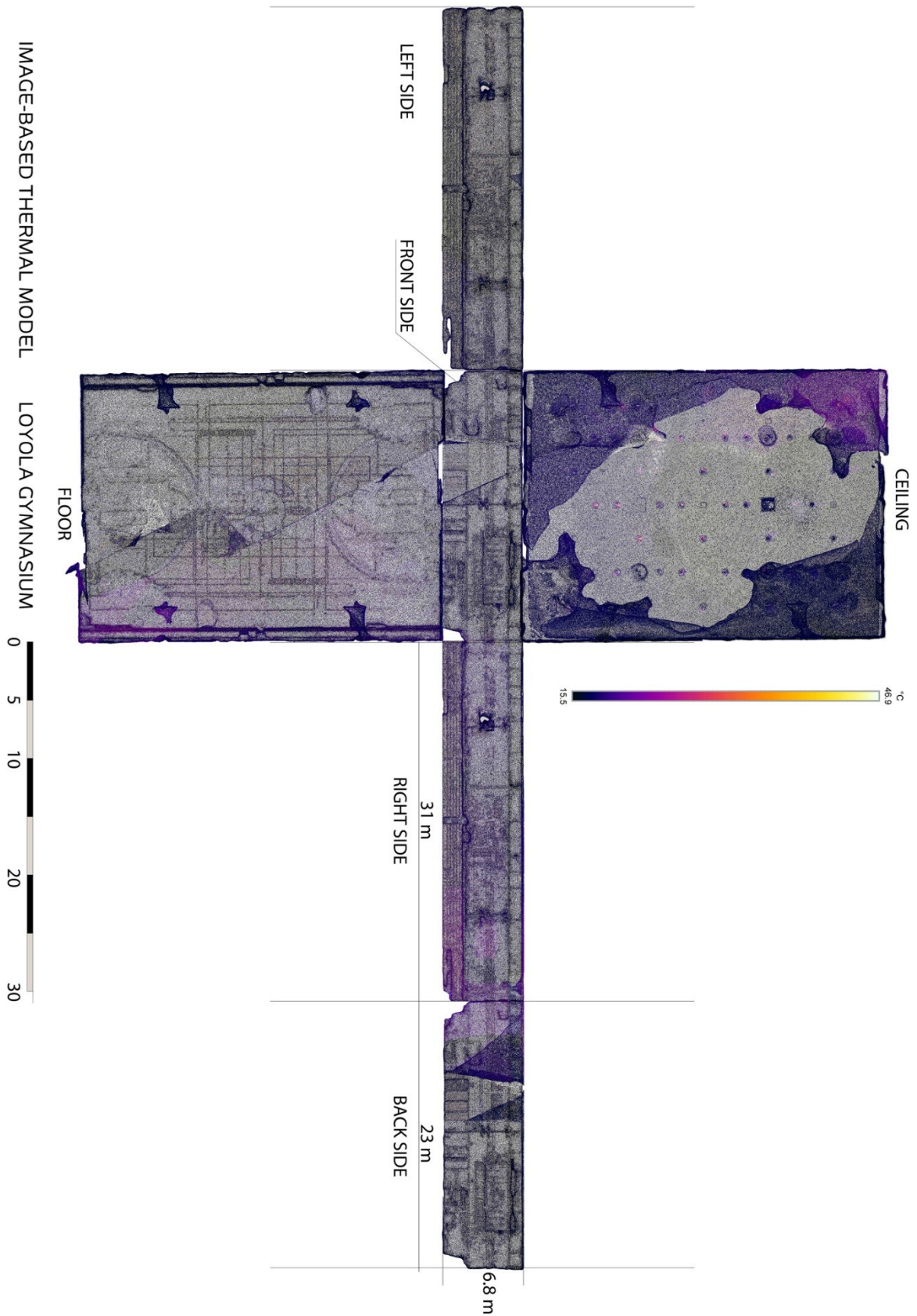


Figure 4-52: As-is image-based thermal ortho-photo for the gymnasium testing environment

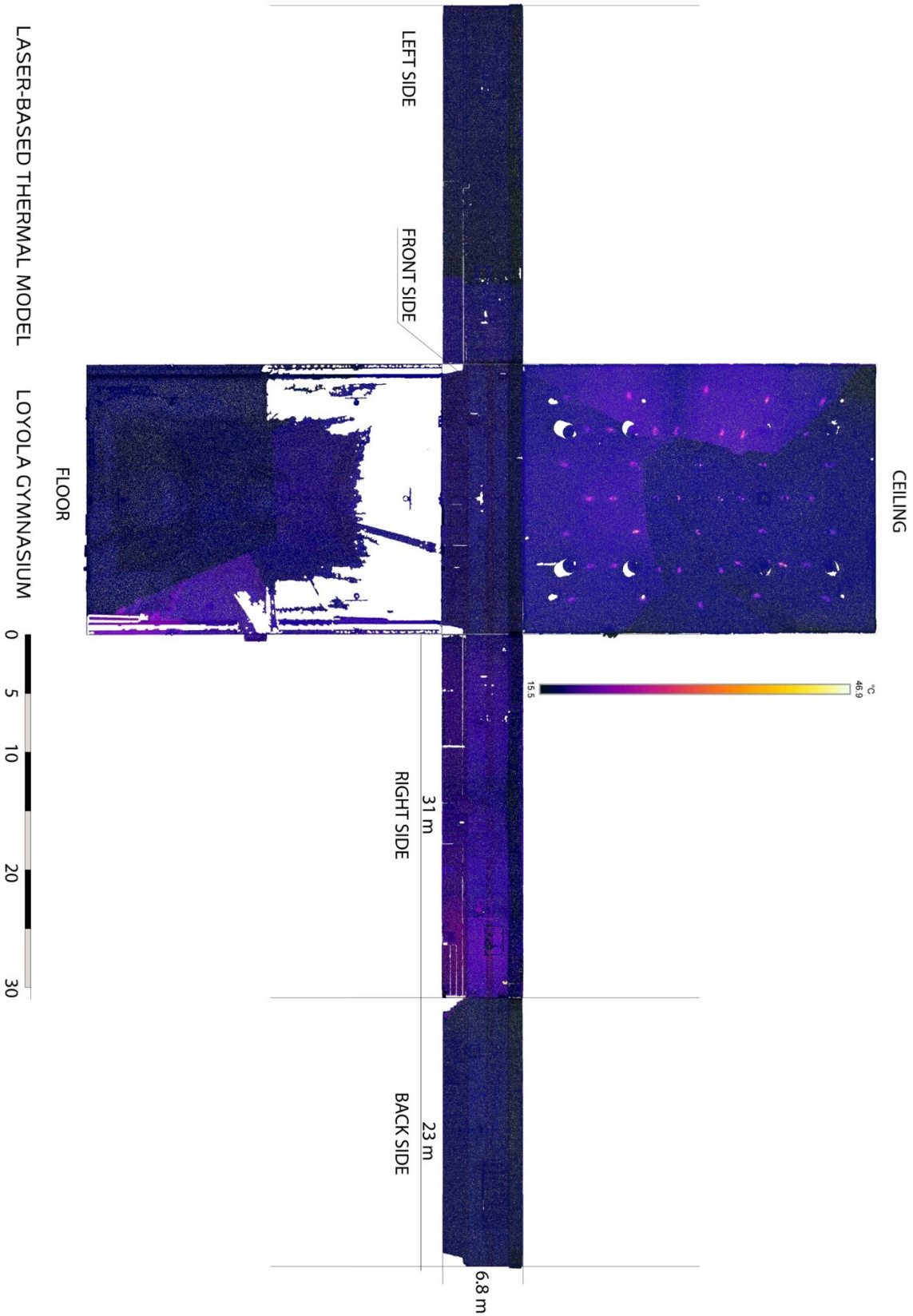


Figure 4-53: As-is laser-based thermal ortho-photo for the gymnasium testing environment

Evaluation

Density evaluation

Similarly, as in case study I, the density of all point cloud models were recorded as shown in the following Table 4-16.

Table 4-16: Density evaluation of the gymnasium testing environment

	Total Number of 3D points
3D image-based point cloud	1,519,514
Image-based 3D thermal point cloud	(Before filtration): 1,519,514
	(After filtration): 1,349,977
3D laser-based point cloud	46,456,181
Laser-based 3D thermal point cloud	46,456,181

Time-based evaluation

Table 4-17: Time-based evaluation for image-based 3D thermal point clouds generation

			Digital Imagery	Thermal Imagery
Data	Setting Up environment		5 min	10 min
Collection	Image acquisition		10 min	30 min
Average total duration for Data Collection			15 min	40 min
Data Processing	Filtration		15 min	15 min
	Point cloud generation	Manual registration	40 min	-
		Cloud processing	16 hr. and 10 min	-
	Image stitching		-	30 min
	Mapping and filtration		-	55 min
Average total duration for Data Processing			17 hr. and 05 min	1 hr. and 40 min
Average total duration for 3D image-based point cloud generation			17 hr. and 20 min	2 hr. and 20 min
Average total duration for image-based 3D thermal point cloud generation			19 hr. and 40 min	

Table 4-18: Time-based evaluation for laser-based and 3D thermal point clouds generation

		Laser Scanning	Thermal Imagery
Data Collection	Setting Up environment	15 min	10 min
	Three laser Scans /Image acquisition	1 hr	30 min
Average total duration for Data Collection		1 hr. and 15 min	40 min
Data Processing	Filtration	-	15 min
	registration	2 hr.	-
	Image stitching	-	30 min
	Mapping and filtration	-	55 min
Average total duration for Data Processing		2 hr.	1 hr. and 40 min
Average total duration for 3D image-based point cloud generation		3 hr. and 15 min	2 hr. and 20 min
Average total duration for image-based 3D thermal point cloud generation		5 hr. and 35 min	

Moreover, the required duration to accomplish each stage was recorded as shown in Table 4-17 and Table 4-18 respectively.

Cost-based evaluation

Finally, the cost was evaluated and reviewed in case study I. Thus, (Table 4-19) shows the summary of the required cost for each technique.

Table 4-19: Cost-based evaluation

		Cost (\$)
image-based visible and thermal 3D point clouds generation	Digital Imagery	2,225
	Thermal imagery system	23,140
	Total Cost (\$)	25,365 \$
Laser-based visible and thermal 3D point clouds generation	Laser scanning	64,467
	Thermal imagery system	23,140
	Total Cost (\$)	87,607 \$

4.2.3. Case Study III – Lab Office in EV Building

Spatial Modeling

[1] Point Cloud Generation Using Digital Imagery:

Data Collection

Similarly, as previous case studies I and II, visible images were collected for the lab office testing environment at EV building of Concordia University. Technically, a small confined office room with small geometrical dimensions of (4m x 10.2 m) was studied in dark conditions. Also, the stucco walls of this room is a reflective texture material with a uniform white color. This could lower the efficiency of image-base modeling, so visual markers and reference targets were attached to the walls in order to increase the number of features and improve the quality of the reconstructed 3D point cloud model. As shown in (Figure 4-54), several visual markers were added to the walls randomly. Also, reference targets of known dimensions were added for later manual registration and scaling. Accordingly, images were collected using the camera flashlight at different locations and angles preserving a minimum overlapping of 80% between consecutive images as shown in (Figure 4-55).



Figure 4-54: Visual markers attached to the walls of the lab office testing environment

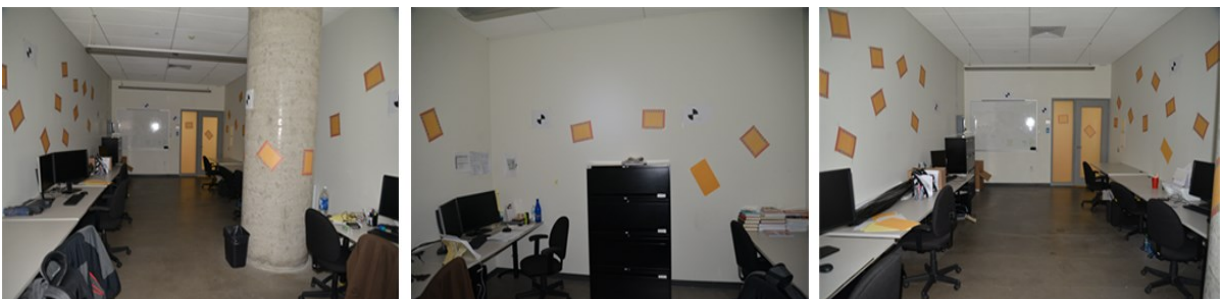


Figure 4-55: Sample of overlapping images collected from the lab office testing environment

Data Processing

After unwanted images were filtered and removed so 136 images were uploaded into (*Autodesk ReCap 360*) software. First, some images were registered manually and the model was scaled using known dimensions of reference targets. Consequently, an automated process resulted in the reconstruction of a 3D point cloud model for the lab office testing environment. Finally, an image-based point cloud model of the lab office testing environment was reconstructed and the visible point clouds were orthogonally projected to form an orthogonal image (Figure 4-56). Also, the summary of data collection is reviewed in the following (Table 4-20).

Table 4-20: summary of data collection for the lab office testing environment

No. of visual markers and reference targets	No. of images before filtration	No. of images after filtration	No. of images registered	Image resolution (pixels)	Focal length (mm)
57	138	136	136	6016 x 4016	35

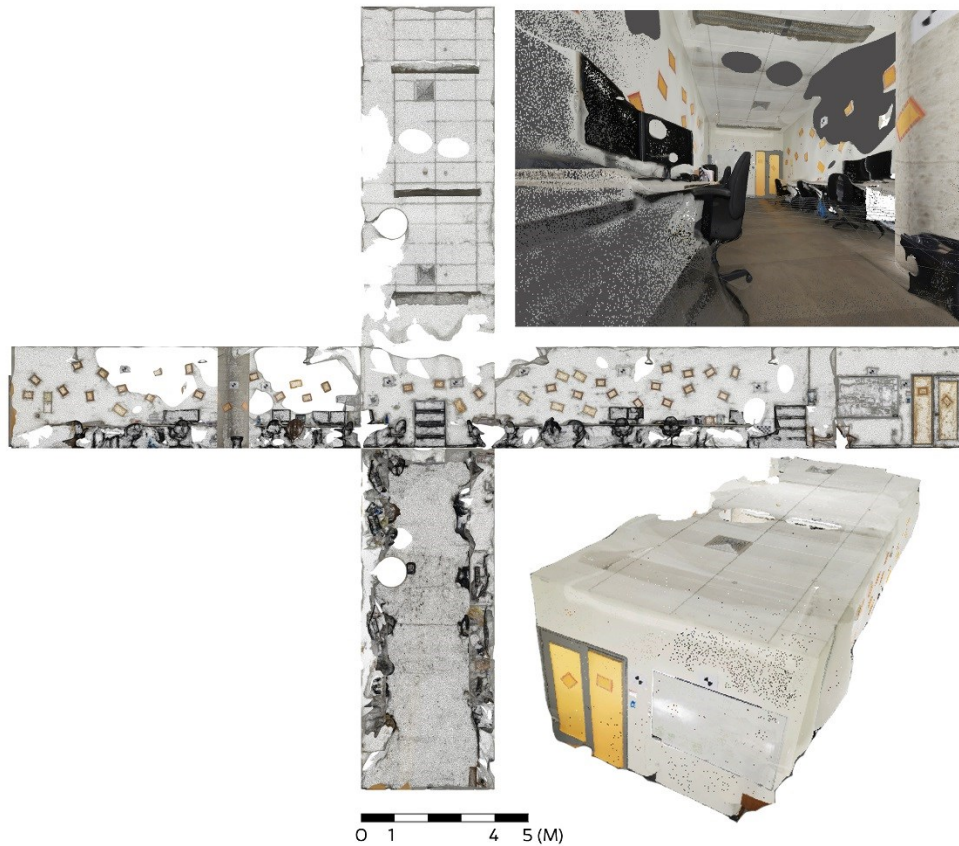


Figure 4-56: 3D image-based point cloud model of the lab office testing environment

[2] Point Cloud Generation Using Laser Scanning:

Data Collection

Likewise, previous case studies I and II, a *Faro Focus3D X 130* laser scanner was deployed in the lab office testing environment for scanning and five spherical targets were localized at different locations. Next, two scans were conducted in gray color settings most compatible to dark conditions. The corresponding two scan positions were enough to capture the whole environment (see Figure 4-57), while (Table 4-21) summarizes data collection stage for laser scanning.

Table 4-21: Laser scanning summary for the lab office testing environment

Number of scans	Number of spherical spheres used	Number of reference targets
2	5	8

Data Processing

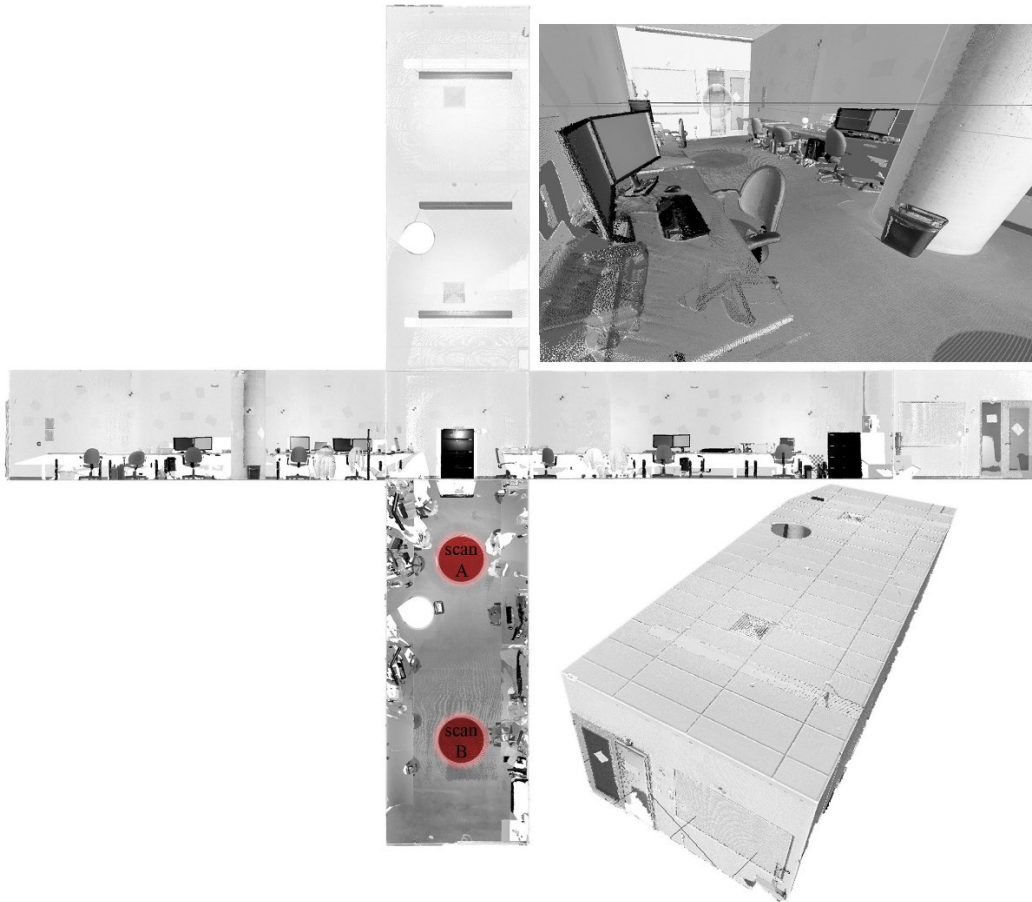


Figure 4-57: 3D laser-based point cloud model of the lab office testing environment

In data processing stage, two scans of the lab office testing environment were uploaded from the SD card into (*Trimble Realworks 10*) software then exported into a compatible extension (.pts) and then registered using (*Autodesk ReCap 360*). Finally, a laser-based point cloud model of the lab office testing environment was reconstructed and the visible point clouds were orthogonally projected to form an orthogonal image (Figure 4-57).

Infrared Thermography

Data Collection

Similar to case studies I and II, an infrared sensing camera *Flir Zenmuse XT* mounted on *Matrice100* drone was used for thermal image acquisition. To start, both the aircraft and the infrared camera sensing was launched, calibrated and connected to the remote controller. Then, settings were adjusted and the black and white color palate were chosen for this experiment. Image acquisition was performed remotely and in a modular manner with a consistent distance from the facing plane surfaces as discussed before. This process was repeated for several times until the collection of the whole scene of an environment was completed. Also, an overlap of 50% or more was preserved between consecutive images. (Figure 4-58) is a sample of thermal data collection stage. And data processing was similar to previous discussions, results are shown in (Figure 4-59).

Table 4-22: summary of thermal data collection for the lab office testing segment

Number of thermal images processed	Number of images registered	Image resolution (pixels)	Focal length (mm)
20	18	640 x 512	13

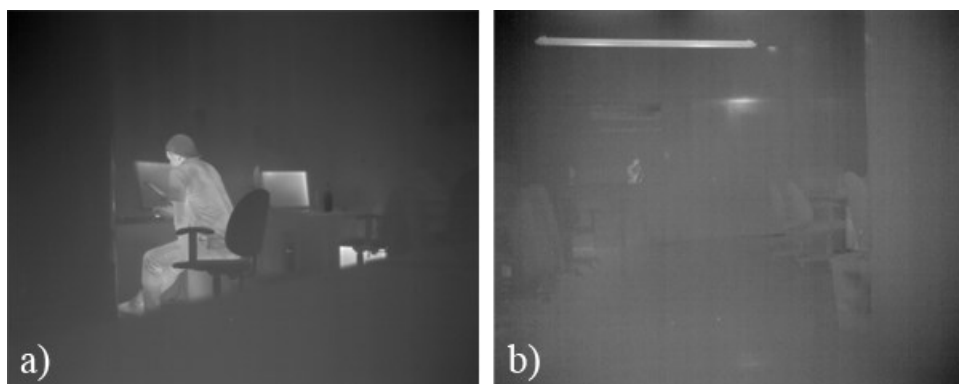


Figure 4-58: Thermal data collection in lab office testing environment; a) capturing images remotely, and b) sample of the collected thermal images

Data Processing

a)

°C
29.2

19.5

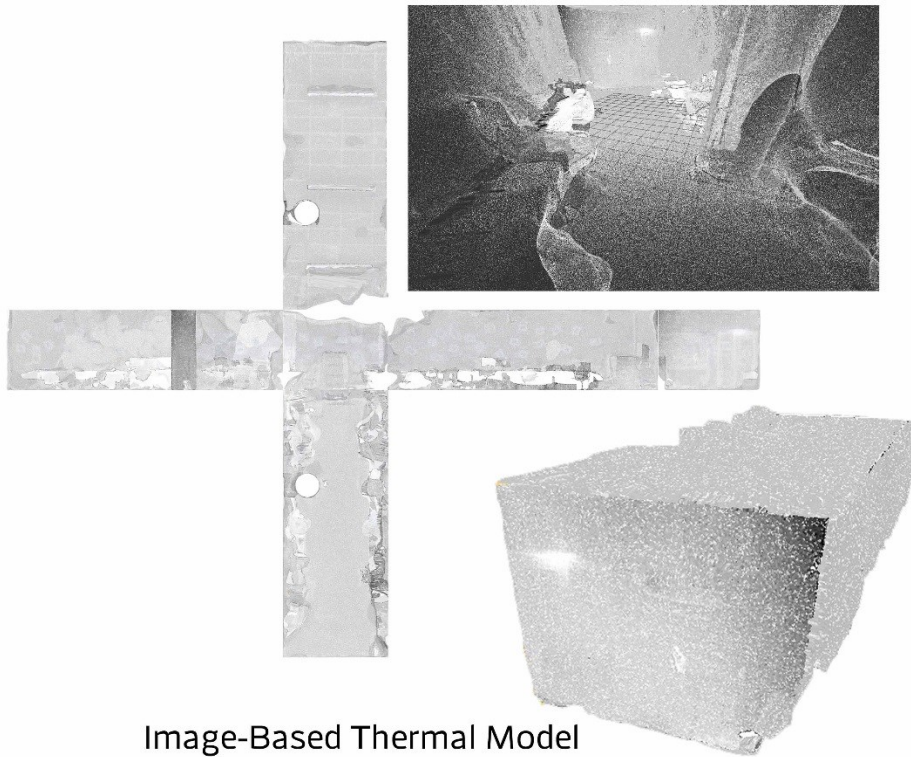
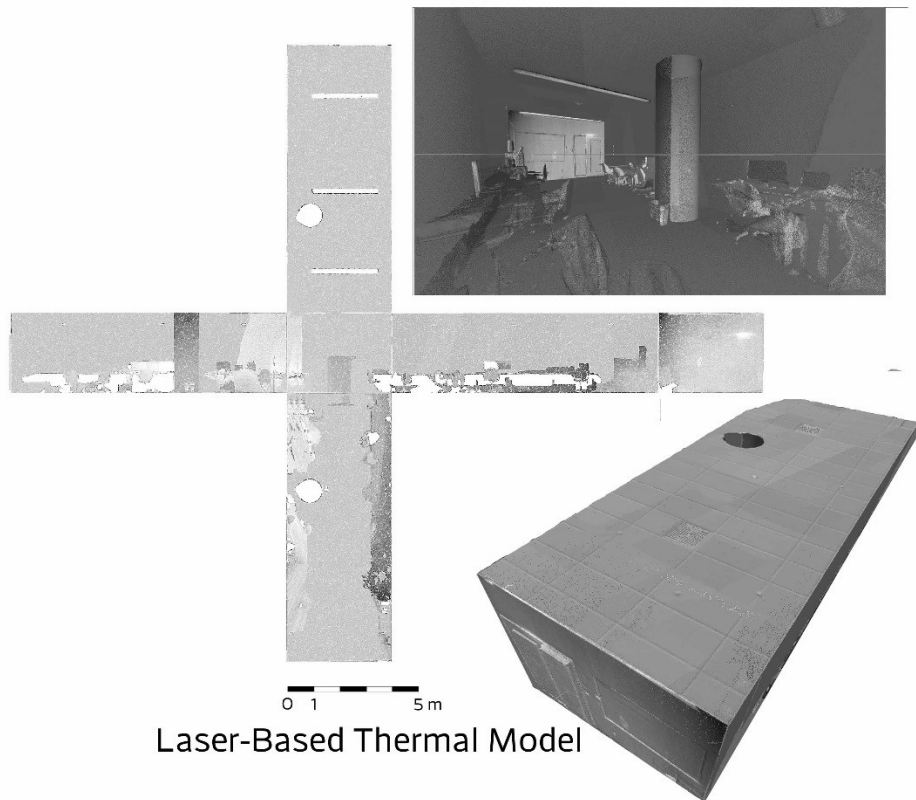


Image-Based Thermal Model

b)

°C
29.2

19.5



Laser-Based Thermal Model

Figure 4-59: (a) Image-based 3D thermal point cloud model of the lab office testing environment, and (b) laser-based 3D thermal point cloud model of the lab office testing environment

Evaluation

Density evaluation

Similarly, as in case studies I and II, the density of all point cloud models for case study III was recorded as shown in the following (Table 4-23).

Table 4-23: Density evaluation of the lab office testing environment

	Total Number of 3D points
3D image-based point cloud	7,000,342
Image-based 3D thermal point cloud	(Before filtration): 7,000,342
	(After filtration): 6,938,941
3D laser-based point cloud	11,742,896
Laser-based 3D thermal point cloud	11,742,896

Time-based evaluation

Table 4-24: Time-based evaluation for image-based 3D thermal point clouds generation

			Digital Imagery	Thermal Imagery
Data	Setting Up environment		30 min (visual markers)	10 min
Collection	Image acquisition		10 min	15 min
Average total duration for Data Collection			40 min	25 min
Data Processing	Filtration		15 min	15 min
	Point cloud generation	Manual registration	30 min	-
		Cloud processing	21 hr and 30 min	-
	Image stitching		-	30 min
	Mapping and filtration		-	45 min
Average total duration for Data Processing			22 hr and 15 min	1 hr and 30 min
Average total duration for 3D image-based point cloud generation			22 hr and 55 min	1 hr and 55 min
Average total duration for image-based 3D thermal point cloud generation			24 hr and 50 min	

Table 4-25: Time-based evaluation for laser-based and 3D thermal point clouds generation

		Laser Scanning	Thermal Imagery
Data Collection	Setting Up environment	15 min	10 min
	Two laser Scans /Image acquisition	30 min	15 min
Average total duration for Data Collection		45 min	25 min
Data Processing	Filtration	-	15 min
	registration	1 hr.	-
	Image stitching	-	30 min
	Mapping and filtration	-	45 min
Average total duration for Data Processing		1 hr.	1 hr. and 30 min
Average total duration for 3D image-based point cloud generation		1 hr. and 45 min	1 hr. and 55 min
Average total duration for image-based 3D thermal point cloud generation		3 hr. and 40 min	

Moreover, the required durations to accomplish each stage for the lab office testing environment were recorded as shown in (Table 4-24) and (Table 4-25) respectively.

Cost-based evaluation

Finally, the cost was evaluated and reviewed in both case studies I and II. Thus, (Table 4-26) shows the summary of the required cost for each technique.

Table 4-26: Cost-based evaluation

		Cost (\$)
image-based visible and thermal 3D point clouds generation	Digital Imagery	2,229
	Thermal imagery system	23,134
	Total Cost (\$)	25,363 \$
Laser-based visible and thermal 3D point clouds generation	Laser scanning	64,422
	Thermal imagery system	23,134
	Total Cost (\$)	87,556 \$

4.3. Discussion and Remarks

4.3.1. Output models Comparison

Density-based evaluation:

Starting with the term “density” within 3D point cloud modeling, it is directly related to the number of reconstructed spatial 3D points. Thus, the density of 3D thermal points is heavily dependent on the generated 3D visible spatial points. Theoretically, a total number of 3D thermal points must be similar to its respective spatial model. Technically, this is the case for laser-based point clouds and laser-based thermal point clouds. However, it is different for image-based thermal point clouds since the generated models are filtered after mapping. The filtration process is a must for image-based point clouds since edges and far corners are not consistent and need to be cleaned which is not the case for laser-based models that have a very accurate 3D point clouds. As a result, a filtered image-based thermal point cloud model will have a lower number of 3D points than its corresponding visible image-based point cloud model. This is presented clearly in the density-based summary of all models shown in Table 4-27.

In summary, Figure 4-60 can reflect that laser-based thermal point clouds are much higher in density when compared to those of image-based point clouds. Still, these values vary from one case study to another. Starting with case study I, the total number of laser-based 3D points is approximately (x 25) higher than that of image-based 3D points. However, both models showed the complete and accurate generation of planes and surfaces even when applied in dark conditions and different (tunnel geometry) geometric shapes. On the other hand, case study II shows a higher number of laser-based thermal 3D points approximately to (x30) when compared to that of image-based thermal 3D points. However, the image-based 3D thermal model was able to generate more areas and show complete surfaces than that of a laser-based thermal model (see Figure 4-61). The reason behind this is that far distances from a laser scanner location are less chance to be scanned or have less dense points than areas which are closer to the laser scanner position. On the other hand, the image-based thermal model showed complete areas with sparse 3D point’s generation. Lastly, the lab office testing environment is considered as the smallest case study among all. Although, the laser-based 3D points are only (x1.67) more than that of image-based 3D points. But, image-based point cloud model showed incomplete areas and surfaces due to the reflective and uniform textures of stucco walls.

Table 4-27: Density evaluation summary of all case studies

Number of 3D points	Proposed methodology		Experimental Design	
	Image-based point cloud models		Laser-based point cloud models	
	Visible models	Thermal models	Visible models	Thermal models
Case study I	1,497,606	1,272,326	37,386,416	37,386,416
Case study II	1,519,514	1,349,977	46,456,181	46,456,181
Case study III	7,000,342	6,938,941	11,742,896	11,742,896

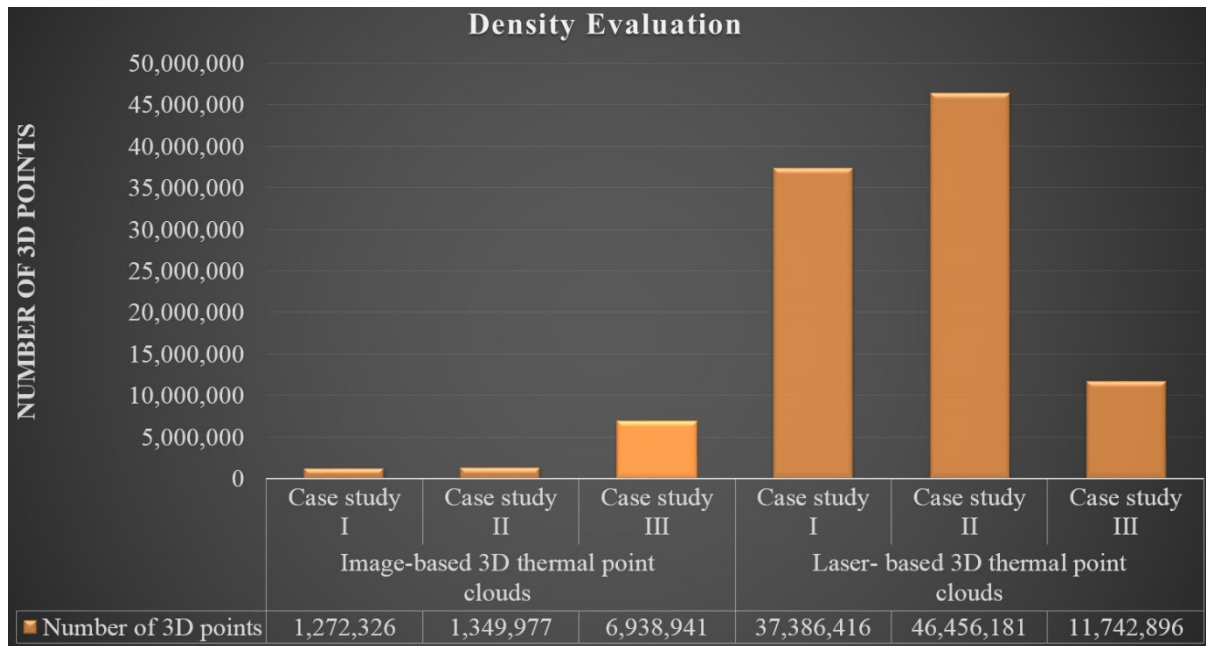


Figure 4-60: Density-based evaluation for all generated thermal models

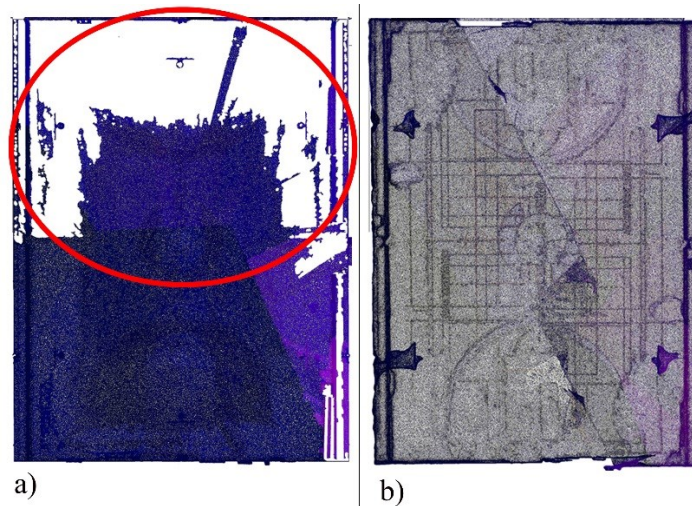


Figure 4-61: Sample for complete and incomplete surface generation of point clouds

Time-based evaluation:

While the needed duration of time for each stage was mentioned in the previous section, Table 4-28, summarizes the final duration of time for both the proposed methodology and the experimental design model. Theoretically, laser-based thermal molding shows faster process when compared to the overall time needed for image-based thermal modeling. But, this is not the case since the time needed must be related to the overall duration period spent by the operator to execute all processes. Thus, a realistic comparison would exclude the time needed for cloud processing since the process is not consuming the time of the operator who can continue his work normally. As a result, the proposed methodology of image-based thermal modeling shows faster process when compared to that of laser-based thermal modeling (see Figure 4-62).

Table 4-28: Time evaluation summary in all case studies

Time Needed	Proposed methodology		Experimental Design
	Image-based thermal point cloud models		Laser-based thermal point cloud models
	Including cloud processing	Excluding cloud processing	
Case study I	24 hr, 27 min	4 hr, 50 min	5 hr, 25 min
Case study II	19 hr, 40 min	3 hr, 20 min	5 hr, 35 min
Case study III	24 hr, 50 min	3 hr, 20 min	3 hr, 40 min

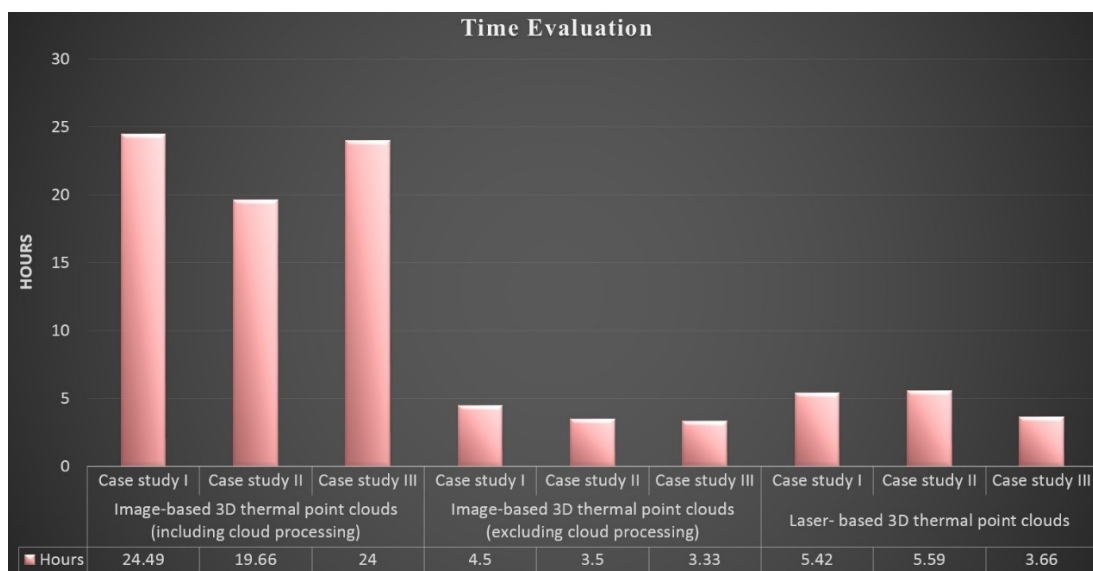


Figure 4-62: Time-Based evaluation for all generated thermal models

Cost-based evaluation:

Furthermore, the cost is considered as a crucial factor for the evaluation of any approach. Thus, the cost of all used equipment and software in this research were recorded and presented for all case studies. Also, the needed operator cost for data collection and processing was estimated. Although the proposed methodology can work with a standalone infrared camera sensing, this research used a modern thermal imagery method that included a UAS-based thermal imagery system. Consequently, Figure 4-63 shows that the cost of the proposed methodology is considered much affordable when compared to that of laser-based thermal modeling. Both, the standalone infrared camera sensing and the used UAS-based thermal imagery system are up to four times cheaper than laser-based thermal modeling system.

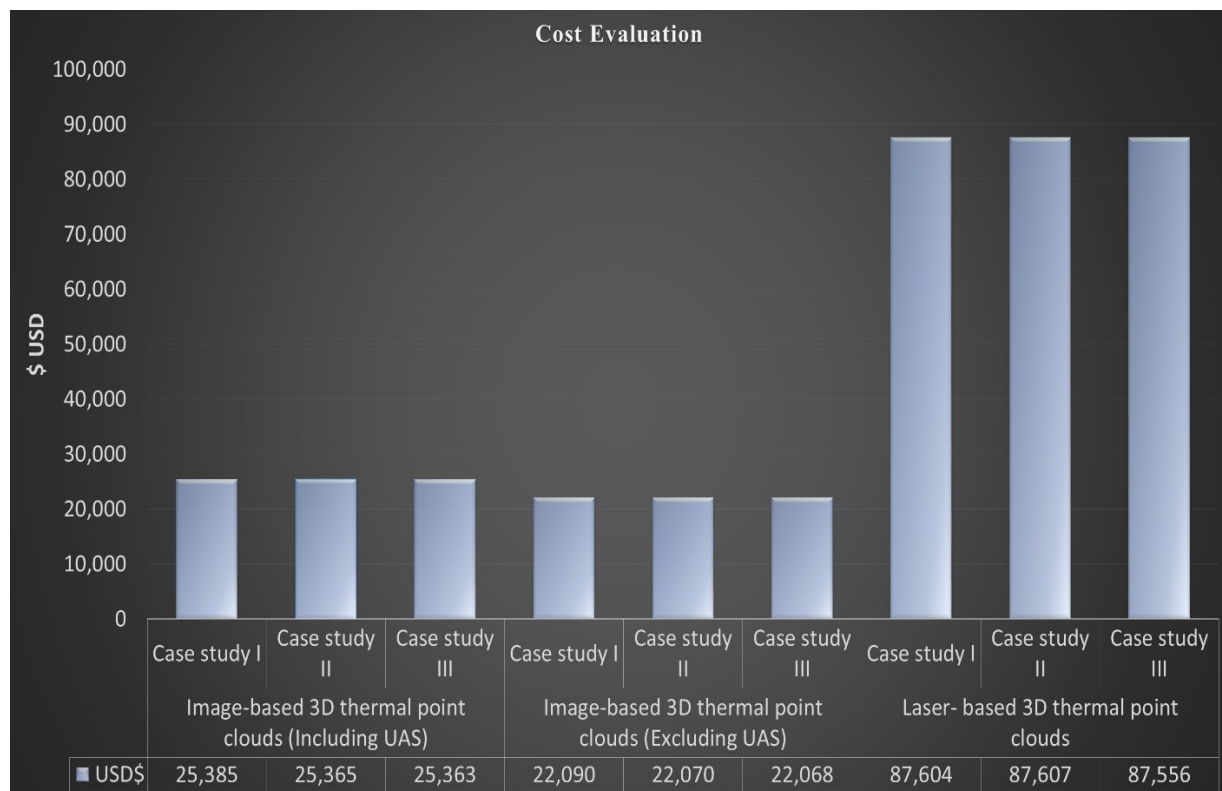


Figure 4-63: Average cost-based evaluation for generated thermal models

4.3.2. Remarks

Furthermore, the proposed methodology was also compared with respect to other existing methods in the 3D thermal modeling of indoor environments. Thus, all related studies including used systems, methods, and their results are shown below as follow (see Table 4-29):

Table 4-29: Differences between related existing studies and the proposed methodology

	(Ham & Golparvar-Fard, 2012)	(Borrmann et al., 2012)	(Oreifej et al., 2014)	Proposed Methodology
System used	EPAR (Figure 4-64-a)	Irma3D (Figure 4-64-b)	e-pack (see Figure 4-64-c)	Separate digital and IR imagery system (see Figure 4-64-d)
equipment used in Data collection	Handheld IR camera sensing with built-in digital camera	An IR camera sensing fixed on a 3D laser scanner	Five 2D laser scanners, two IR cameras, two optical camera sensors, orientation sensor, and a laptop	IR camera sensing and a digital camera sensing
Data processing methodology	Image fusion; 3D reconstruction using sfm	IR fusion to 3D laser-based point clouds	Reconstruction of 3D laser-based geometry; texturing point clouds using visible and IR images	3D visible reconstruction using sfm; Thermal image stitching; Thermal mapping
Testing environments	Buildings	Buildings	Buildings	Buildings and infrastructures
Advantages	Low cost of used equipment, low manpower; mobile,	Real-time data fusion, robotic mobile system, time-effective	Complete generation of both visible and thermal models; mobile	Complete visible and thermal models; cost and time effective, low manpower; very mobile (could be attached to UAS), camera sensors can be upgraded easily

Limitations	Very low model resolution, low model accuracy, and incomplete model generation, limited camera sensing upgrade (built-in system)	Cost-intensive system, and limited field of view (fov) related to fixed position of IR camera. Thus, reconstructed model is incomplete	Cost-intensive system, heavy and bulk system, system is carried on the back of the operator	Heavily dependent on the reconstructed 3D image-based point clouds
Models output	Figure 4-65-a	Figure 4-65-b	Figure 4-65-c	Figure 4-66



a) EPAR



b) Irma3D



c) e-pack

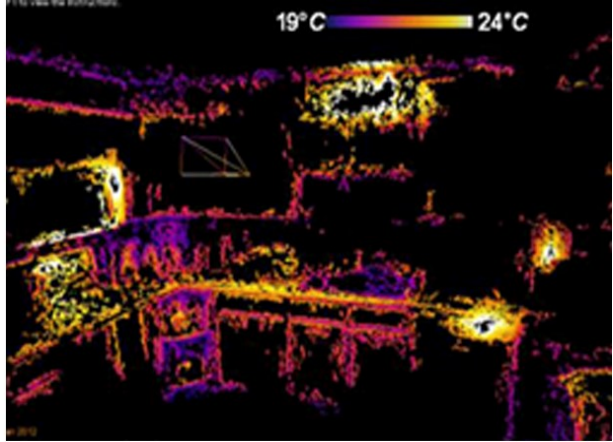


d) proposed methodology

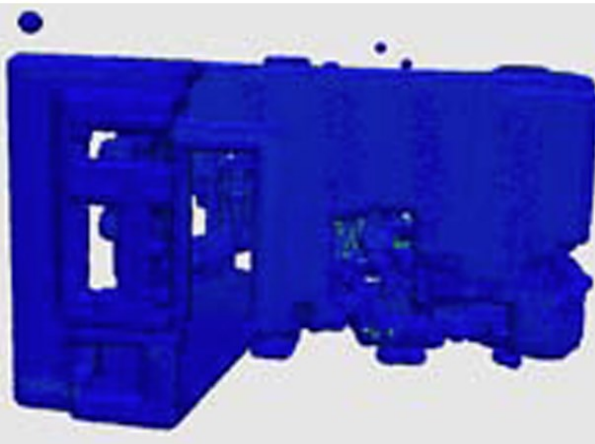
Figure 4-64: Used systems in existing studies and the proposed methodology



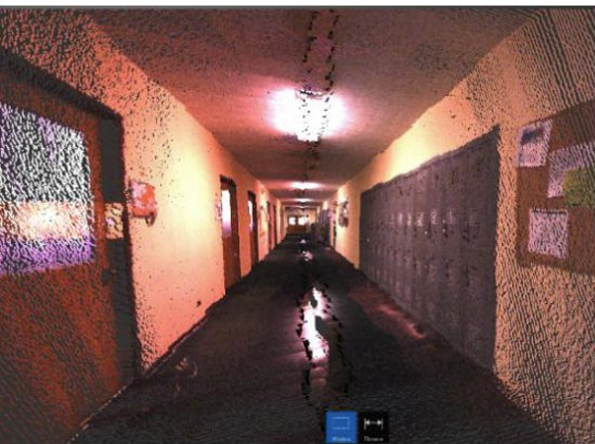
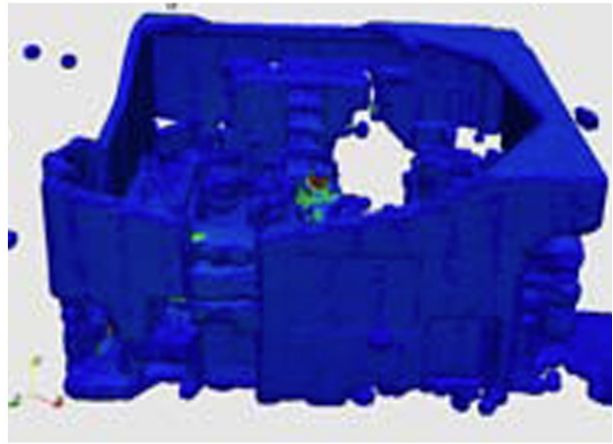
a) (Ham & Golparvar-Fard, 2012)
3D visible point cloud model



(Ham & Golparvar-Fard, 2012)
3D thermal point cloud model



b) (Borrmann et al., 2012), 3D thermal point cloud model



c) (Oreifej et al., 2014)
3D visible point cloud model



(Oreifej et al., 2014)
3D thermal point cloud model

Figure 4-65: Output models of related existing studies

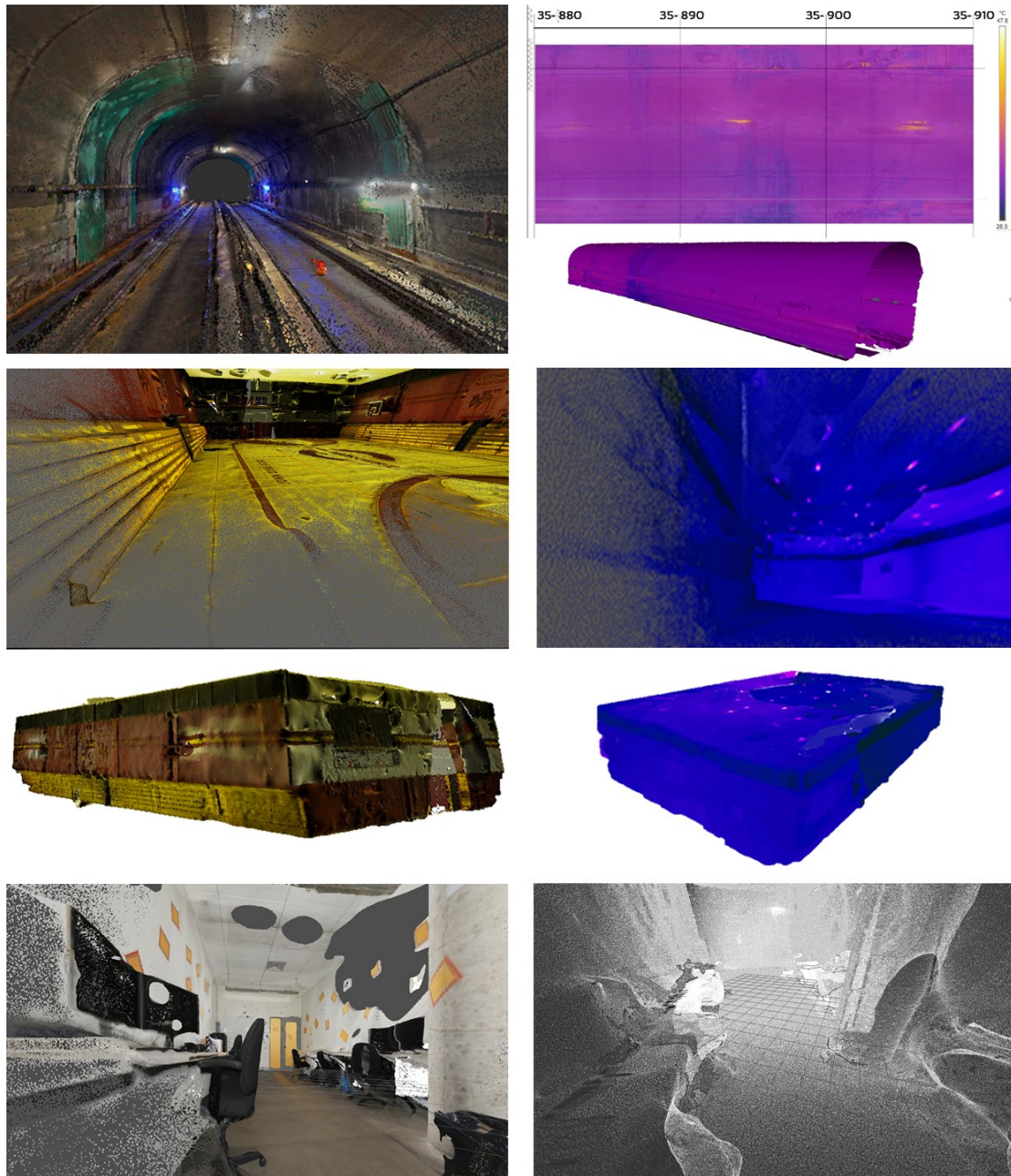


Figure 4-66: Output models of the proposed methodology

Finally, the output models were generated successfully even when using affordable equipment such as thermal and digital cameras only. Also, the resulted 3D thermal models were useful in detecting defects based on the thermal color variation. For example, the blue color in the projected thermal ortho-gram of the subway tunnel presented in Figure 4-66 reflects a water source leak. The respective blue color reflects the presence of colder area when compared to the neighboring areas. Thus, using thermal model was successful in identifying the water leakage.

Temperature color variation analysis

In order to verify the temperature reading accuracy, a temperature color variation analysis was conducted to compare color variation between input thermal images and 3D thermal output models. To do so, common sections between an input 2D thermal image and its respective thermal representation of the 3D thermal model were selected. Next, color variation analysis representing the temperature differences were recorded and compared. In Figure 4-67, an example for a random section selection between input 2D thermal images and output 3D thermal models. Next, color variation between two sections will be recorded and compared. Respectively, this process was performed at different sections randomly for the three case studies.

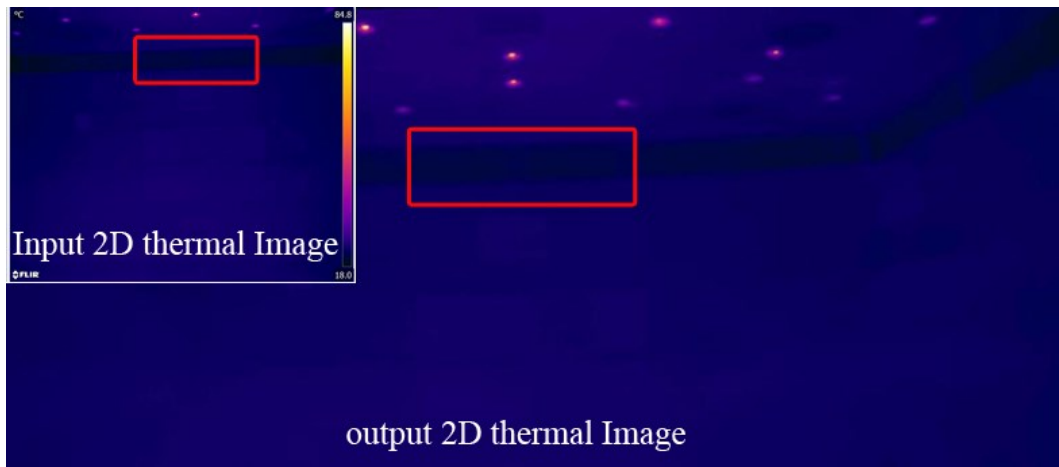


Figure 4-67: Section selection between 2D thermal input and 3D thermal output

In order to conduct a color variation comparison, the color value of each pixel must be recorded. Where, each pixel has a color value represented by a system known as RGB (Red, Green, and Blue). The level values for each of the R, G, and B colors can vary from 0 to 100 percent intensity. While each level is signified by a range of decimal numbers from 0 to 255 (different levels of each color). In Figure 4-68, two exact sections were recorded from a 2D thermal image input and its respective section in the output. The value distribution was recorded for each color and to the whole section. Respectively, the same number of pixels in both the input and the output showed a slight difference in color representation. The small difference in standard deviation between the input and the output can indicate a minimal variation in color visualization. Where the standard deviation reflects the value distribution around the average. Therefore, the output models have an accurate color visualization with respect to the input thermal images. Thus, the temperature representation using color differences in the 3D thermal models are also accurate.

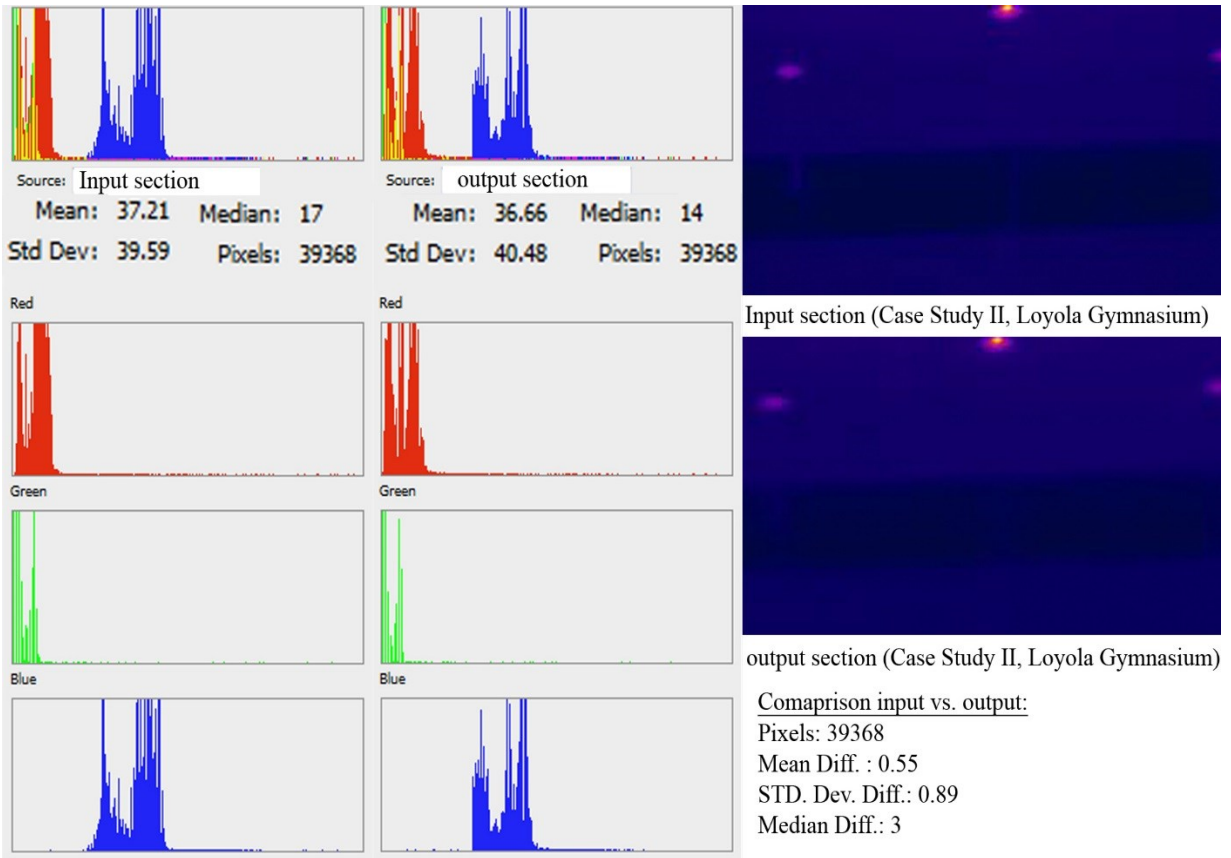


Figure 4-68: An example of color variation analysis

A set of different section comparison at different locations were applied and recorded in the below Table 4-30. Results in all case studies showed an accurate color visualization in the 3D thermal models when compared to the 2D thermal image inputs. Therefore, the temperature representation using color difference visualization is also accurate.

Table 4-30: Color variation analysis

	Section Comparison	Number of pixels	Mean	Median	Std. Deviation	Std. deviation difference
Case Study I	input	3478	95.39	127	64.91	0.13
	output	3478	94.63	128	64.78	
Case Study II	input	39368	37.21	17	39.59	0.89
	output	39368	36.66	14	40.48	
Case Study III	input	32480	94.96	97	21.22	0.83
	output	32480	91.41	93	20.39	

4.3.3. Limitations of the Proposed Methodology

In this section, all problems encountered while performing different experiments will be reviewed and discussed. Thus, all limitations concerning image-based 3D thermal modeling of indoor environments of buildings and infrastructures will be outlined. Technically, two main limitations were examined related to image-based spatial modeling and thermal images stitching.

Problems related to image-based spatial modeling:

Data collection within narrow spaces

Collecting both visual and thermal images for the confined lab office environment with very narrow and restricted space showed some difficulties. To start, the width of the lab office environment of 4 meters as shown in (Figure 4-69). Thus, covering a large area of the facing surface in just one image is almost impossible. In order to solve this problem and cover the whole facing surface, more images were required to be captured. This could add more processing time of the reconstructed 3D spatial model and more time in thermal stitching.

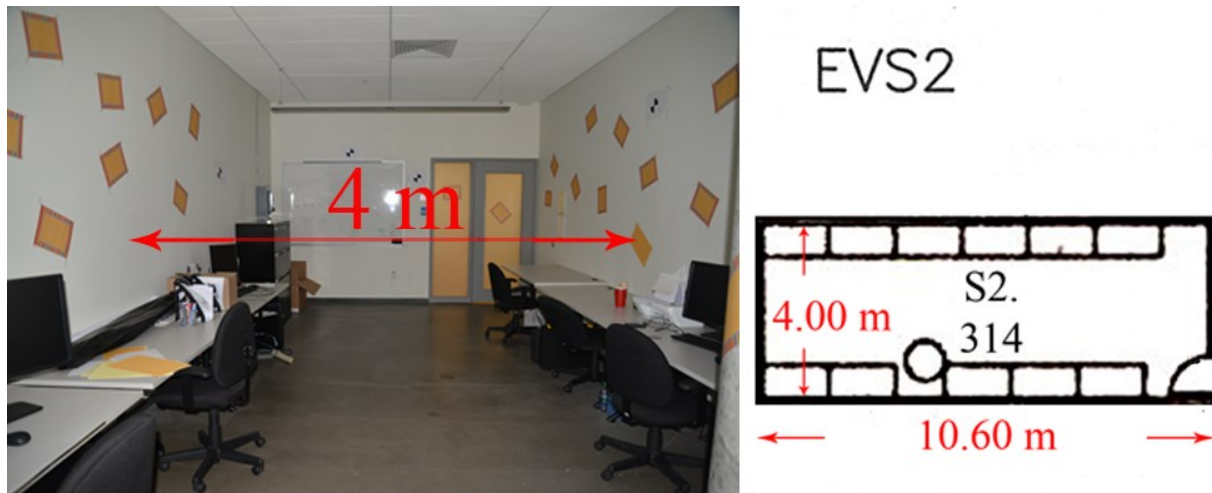


Figure 4-69: Narrow space dimension of the lab office testing environment

Modeling surfaces with a uniform texture

While modeling image-based 3D point clouds, only case study III (lab office) has shown incomplete modeling of surfaces with uniform texture as white stucco walls. On the other hand, visual markers were added to these walls in order to increase the number of features of a model as suggested by (Snavely et al., 2010). Still, results showed a deficiency in generating a complete and accurate model as shown in Figure 4-70.



Figure 4-70: Incomplete surface modeling of walls with uniform textures

Problems related to thermal mapping into incomplete surfaces:

Based on the abovementioned problem of incomplete surface modeling, thermal modeling as well should have the same limitation of missing parts of thermal information. But, this, in turn, would reflect a wrong indication of the collected data. As a result, a solution was by filling the big holes by a modeled wall in the same location of the as-is point cloud surface. Next, thermal information will be mapped to both generated spatial point clouds and a modeled wall. Accordingly, this would preserve a correct visualization of thermal information (see Figure 4-71). However, filled-based thermal surfaces were not considered as a generated 3D point clouds.

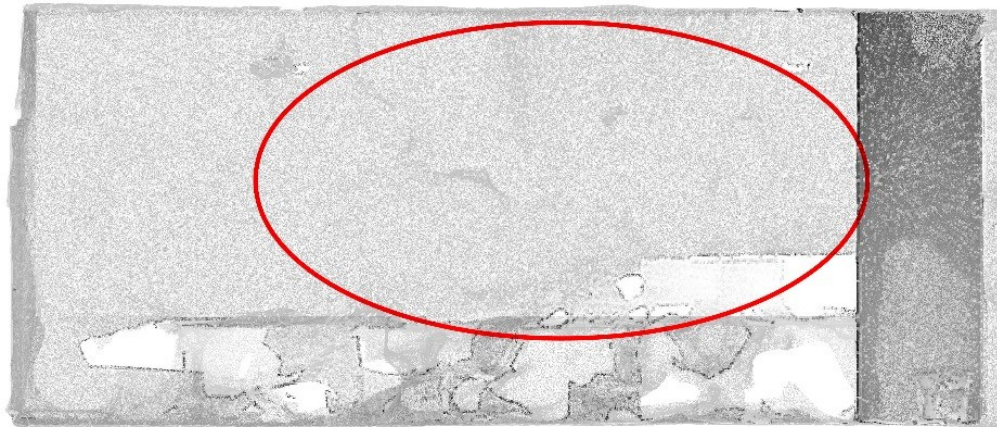


Figure 4-71: thermal modeling of incomplete surfaces

CHAPTER 5: CONCLUSION

Infrared thermography (IR) is a modern non-destructive technique that was implemented lately in applications related to several areas of the architecture, engineering, and construction (AEC) industries such as facility condition assessment, energy performance analysis, defect detection, etc.... However, current practices related to thermal inspection in the existing built environments are heavily dependent on the captured 2D IR images. However, researchers, engineers, and audits believe that relying on 2D IR images alone is an obsolete practice which is considered as error-prone, time-consuming, and cost-intensive (Giel & Issa, 2011; Qu, Coco, Rönnäng, & Sun, 2014). Moreover, depending on selective 2D IR images for analyzing and reporting require more effort for searching and authorization. All of this would end in adding more time and money to a project. On the other hand, industries related to AEC in North America are considered as the highest energy consumers. Yet, current energy performance analysis using IR relies mainly on analyzing and reporting 2D IR images. Which in turn will reflect a limited representation of the studied geometry. Therefore, these practices are considered as inaccurate and misleading since the collected data are missing most of the 3D as-built environment conditions. Although infrared thermography is a promising technology in AEC, related 2D IR practices were considered as time-consuming, and labor intensive (Azhar & Brown, 2009; Lagüela et al., 2012; Chao Wang, 2014).

Nowadays, infrared sensing and software related to thermal imaging were improved in a tremendous way. Consequently, modern researchers have suggested 3D thermal modeling techniques as a replacement for the still 2D IR images in documenting, analyzing, and reporting. However, existing studies in 3D thermal modeling have been mainly used in the reconstruction of exterior facades of buildings and generation of outdoor environments (Cho et al., 2015; Ham & Golparvar-Fard, 2012). Where, only a few researchers who tried to test 3D thermal modeling approach for indoor built environments (Borrmann et al., 2012; Oreifej et al., 2014). Yet, further studies need to be acquired to overcome 3D thermal modeling limitations such as the high cost, slow process, and the need of highly trained professionals. In summary, till the date of conducting this research, no one has tried to develop a 3D thermal modeling method for indoor built environments; which is affordable in terms of accuracy, cost, time and effort.

This chapter is a summary of the strategies, findings, and remarks that have been used in developing a 3D thermal modeling method. Where the first section will summarize the research objectives, proposed method, and results. Next, answers of the proposed questions in chapter one will be discussed and examined. Moreover, research contributions and possible implantation of the proposed methodology in field applications will be present. Finally, a conclusion section will provide a future research work suggestions and recommendations.

5.1. Summary

Based on the existing gap in the literature, the need for a new approach in the reconstructing of 3D thermal models of built environments was discussed and examined in this research. In specific, the proposed methodology suggested the use of 2D IR and visible images collected separately using both infrared and digital cameras respectively. To test this method, it was applied in three different case studies of different variables which are; the geometric shape of an environment, lighting conditions, and material textures. Thus, the first case study was conducted in a subway tunnel segment in the city of Montreal, Canada. While the second case study was applied in a gymnasium located at the athlete complex building of Concordia University's Loyola campus, Montreal, Canada. Finally, case study III was a confined lab office located in the second basement-S2 floor of Concordia University's EV building. Moreover, in order to evaluate the efficacy of the output models of the proposed methodology, they were compared to another 3D thermal point clouds which were developed by a laser scanner and an infrared camera. Finally, both the proposed model of image-based 3D thermal point clouds and the laser-based 3D thermal point clouds were evaluated in terms of density, time, and cost. After comparing the outputs of the proposed methodology, results have shown that;

(1) Even with less-dense point clouds, the proposed methodology can guarantee a high chance of complete surface generation in the point cloud models.

(2) The proposed methodology showed that it is more feasible in terms of time and cost over the results of the experimental design model.

(3) The proposed methodology can be a reliable method in replacing the 2D thermal inspection of facilities and performing energy performance analysis, especially for environments with large surfaces. Thus, helping engineers, audits, and inspectors in improving final decisions.

5.2. Concluding Remarks

This research has proposed the use of 2D IR and visible images collected separately by an infrared and digital camera respectively, to reconstruct image-based 3D spatial and thermal point cloud models of built environments. In the beginning of this research, three questions were asked as the hypothesis of this study. Following is the contributions examined from the whole study that can guide and answer the proposed questions.

- [1] Can 2D visible, and infrared images collected separately be used in the generation of as-is 3D thermal models of the built environments?

2D visible images collected by a digital camera were filtered and processed using sfm approach to generate 3D image-based point cloud models. On the other hand, 2D IR images collected separately using an infrared camera were filtered and stitched together to form large radiometric panorama image that covers a large surface area with an accurate temperature representation. Next, radiometric panorama images were mapped into the image-based point clouds to form an accurate image-based 3D thermal point cloud models. This can guarantee that 2D visible and infrared images that are collected separately can be used in the generation of as-is 3D thermal models of built environments.

- [2] If yes, are these models feasible enough to be implemented in the field? And, Why?

In order to test the efficiency of the generated models, they were compared to another 3D thermal point clouds which were developed by a laser scanner and an infrared camera. Results have shown that the output models of the proposed methodology have less-dense point clouds; yet, they succeeded in generating almost complete surface planes. Furthermore, results from the proposed methodology have shown that this method is more affordable by means of time and cost over the experimental design.

- [3] Can this method facilitate the replacement of 2D thermal inspection with 3D thermal models? And, How?

Several advantages can be achieved by reconstructing the proposed 3D thermal model of built environments. For example, complete 3D as-built documentation can be achieved within short durations compared to the missing data with a 2D thermal inspection that requires long

durations. Also, having 3D models will lead in turn to complete 2D documents and drawings that can be shared easily for the collaboration with other domains of the same interest. Finally, 3D models can be constructed easily and can be executed within reasonable durations for evaluating, monitoring, and controlling the condition of a facility.

This methodology can be applicable for all indoor built environments. For example, it can be used in (O&M) for defect detection and facility control and monitoring. It is also beneficial in energy performance analysis that can help in turn to simulate the energy efficiency of a facility. Therefore, it can help engineers, audits, and inspectors in improving final decisions and related retrofits.

5.3. Future Work

In the future, the proposed methodology could be tested in more environments with featureless surfaces in order to overcome problems related to thermal mapping to incomplete point cloud surfaces. Moreover, more studies could be applied to enhance data collection within narrow and restricted environments. For example, a modular grid system could be developed for image acquisition. Furthermore, UAS-based thermal imagery system was used in this research. Still, more studies are needed to test the feasibility of this system for 3D thermal modeling of built environments. For example, a digital camera can be mounted on a UAS along with the infrared camera. And both can collect images at the same time but separately. More case studies of different variables are in need to be tested. Consequently, multiple advantages could be achieved using this system that includes but not limited to; post-disaster modeling without endangering human life. Or in the modeling of dangerous and top secret places that require no staff to enter; for example, military bases and nuclear plants.

BIBLIOGRAPHY

- 3DReshaper. (2016). 3D Reshaper Technical specifications. Retrieved from www.3dreshaper.com
- Ahluwalia, S. S. (2008). A framework for efficient condition assessment of the building infrastructure. Retrieved from <https://uwspace.uwaterloo.ca/handle/10012/4093>
- Alba, M. I., Barazzetti, L., Scaioni, M., Rosina, E., & Previtali, M. (2011). Mapping Infrared Data on Terrestrial Laser Scanning 3D Models of Buildings. *Remote Sensing*, 3(12), 1847–1870.
- Amekudzi, A., & McNeil, S. (2008). Building condition assessment metrics: best practices. Retrieved from <http://ascelibrary.org/doi/pdf/10.1061/9780784409589.ch20>
- Andi. (2015). Cheerson CX10 Review. Retrieved January 7, 2017, from <http://www.gizchina.com/2015/01/16/cheerson-cx10-review/>
- Asdrubali, F., Baldinelli, G., & Bianchi, F. (2012). A quantitative methodology to evaluate thermal bridges in buildings. *Applied Energy*.
- Autodesk. (2016). ReCap 360 Pro subscription. Retrieved January 4, 2017, from <http://www.autodesk.com/store/products/recap-360-pro?term=1year&support=basic>
- Azhar, S., & Brown, J. (2009). BIM for sustainability analyses. *International Journal of Construction Education and Research*, 5(4), 276–292.
- Barreira, E., & Freitas, V. (2005). Importance of thermography in the study of ETICS finishing coatings degradation due to algae and mildew growth.
- Barreira, E., & Freitas, V. de. (2007). Evaluation of building materials using infrared thermography. *Construction and Building Materials*.

- Ben. (2015). An Overview of Military Drones. Retrieved January 7, 2017, from <http://www.droneuav.co.uk/military-drones/an-overview-of-military-drones/>
- Bhatla, A., Choe, S. S. Y., Fierro, O., & Leite, F. (2012). Evaluation of accuracy of as-built 3D modeling from photos taken by handheld digital cameras. *Automation in Construction*, 28, 116–127.
- BIBUS. (2016). ZCorp ZScanner® 700. Retrieved January 7, 2017, from <http://www.bibus.sk/en/products-solutions/e-manufacturing/3d-scanners/zcorp-zscannerr-700/>
- Binda, L., Cantini, L., & Cucci, M. (2011). Thermovision: Applications in Conservation Field to Detect Hidden Characteristics of Building Structures. In *Masonry Conf., Minneapolis, USA* (pp. 1–12).
- Borrmann, D., Elseberg, J., & Nüchter, A. (2013). Thermal 3D mapping of building façades. *Intelligent Autonomous Systems 12*.
- Borrmann, D., Nüchter, A., DJakulovi'c, M., Maurovi'c, I., Petrovi'c, I., Osmankovi'c, D., & Velagi'c, J. (2012). The Project ThermalMapper-Thermal 3D Mapping of Indoor Environments for Saving Energy, 31–38.
- Cansel Survey Equipment Ltd. (2015). official invoice. Retrieved January 4, 2017, from <https://www.cansel.ca/>
- Cho, Y. K. Y., Ham, Y., & Golpavar-Fard, M. (2015). 3D as-is building energy modeling and diagnostics: A review of the state-of-the-art. *Advanced Engineering Informatics*, 29(2), 184–195.

- Chouinard, L., & Andersen, G. (1996). Ranking models used for condition assessment of civil infrastructure systems. *Journal of Infrastructure*.
- Colomina, I., & Molina, P. (2014). Unmanned aerial systems for photogrammetry and remote sensing: A review. *ISPRS Journal of Photogrammetry and Remote*.
- Concordia University. (2012). *Université Concordia, Plan directeur*.
- Concordia University. (2016). *Loyola Campus RA - Athletic Complex*. Retrieved from http://www.concordia.ca/content/dam/concordia/services/recreation/docs/RA_Map_2.pdf
- dji. (2016). Phantom 3 Professional Aircraft. Retrieved January 7, 2017, from <http://www.dji.com/phantom-3-pro/aircraft#sub-feature>
- Dji. (2014). DJI released its new Spreading Wings S1000 octocopter drone. Retrieved January 7, 2017, from <http://www.dji.com/newsroom/news/dji-released-its-new-spreading-wings-s1000-octocopter-platform>
- DJI. (2016). *DJI Matrice 100 Technical Sheet*. Retrieved from https://dl.djicdn.com/downloads/dev/Matrice/en/M100_In_the_Box_en_160304.pdf
- DJI and FLIR. (2016). DJI Matrice Zenmuse XT. Retrieved December 28, 2016, from <http://www.dji.com/zenmuse-xt?site=developer>
- Eisenbeiß, H. (2009). UAV Photogrammetry. (*Unpublished PhD Dissertation*)., (University of Technology Dresden, Zurich, Switzerland.).
- Elhassan, W., Nejad, P., Daliri, F., & Zhu, Z. (2015). 3D Modeling of Building Indoor Environments with Handheld Camera and Unmanned Aerial Vehicle – A Case Study. In *15th Annual International Conference on Construction Applications of Virtual Reality*.

- Enerdata. (2016). Global Energy Statistical Yearbook 2016. Retrieved from <https://yearbook.enerdata.net/>
- Essess. (2016). Essess. Retrieved January 7, 2017, from <http://www.essess.com/about/about-us/>
- Eweda, A., Zayed, T., & Alkass, S. (2013). Space-Based Condition Assessment Model for Buildings: Case Study of Educational Buildings. *Journal of Performance of*
- Faro Technologies Inc. (2011). *FARO ® Laser Scanner Focus 3D X 130 Technical Sheet*.
- Faro Technologies Inc. (2014). FARO Focus3D X 130: Technical sheet. Retrieved December 28, 2016, from <http://www.faro.com/en-us/products/3d-surveying/faro-focus3d/overview#main>
- Farrag, S., Yehia, S., & Qaddoumi, N. (2015). Investigation of Mix-Variation Effect on Defect-Detection Ability Using Infrared Thermography as a Nondestructive Evaluation Technique. *Journal of Bridge Engineering*, 4015055.
- FLIR. (2013). *FLIR Thermal Imaging Cameras*. Retrieved from http://www.flir.com/uploadedFiles/Thermography_USA/Products/Product_Literature/flir-automation-brochure.pdf
- FLIR. (2014a). FLIR thermal imaging cameras for predictive maintenance. Retrieved from http://flirmedia.com/MMC/THG/Brochures/7038/7038_EN.pdf
- FLIR. (2014b). *Technical Note*. <https://doi.org/10.1080/02564602.1995.11416507>
- FLIR. (2016a). Cooled or Uncooled Thermal Cameras. Retrieved January 17, 2017, from <http://www.flir.ca/science/display/?id=65982>
- FLIR. (2016b). FLIR Tools Plus. Retrieved February 15, 2017, from <http://www.flir.com/instruments/display/?id=54865>

- FLIR. (2016c). User Manual. Retrieved from <https://www.google.com/url?sa=t&rct=j&q=&esrc=s&source=web&cd=1&ved=0a>
- FLIR Systems. (2017). FLIR Calibration. Retrieved February 13, 2017, from <http://www.flir.com/surveillance/display/?id=64951>
- Gamidi, S. H. (2009). Non Destructive Testing of Structures. *Indian Inst.of Technol., Bombay*.
- Gertler, J. (2012). U.S. Unmanned Aerial Systems. *Congressional Research Service*, 55. <https://doi.org/7-5700>
- Giel, B., & Issa, R. R. A. (2011). Using Laser Scanning to Assess the Accuracy of As-Built BIM. *Computing in Civil Engineering(2011)*, 665–672. Retrieved from [http://ascelibrary.org/doi/abs/10.1061/41182\(416\)82](http://ascelibrary.org/doi/abs/10.1061/41182(416)82)
- González-Aguilera, D., Rodriguez-Gonzalvez, P., Armesto, J., & Lagüela, S. (2012). Novel approach to 3D thermography and energy efficiency evaluation. *Energy and Buildings*, 54, 436–443.
- Goswami, D. Y., & Kreith, F. (2015). Global Energy Systems. *Energy Efficiency and Renewable Energy Handbook, 2002*.
- GRAYESS Inc. (2016). IRT Stitch. Retrieved January 7, 2017, from <http://www.grayess.com/software/irt-stitch/>
- Grussing, M., & Liu, L. (2013). Knowledge-based optimization of building maintenance, repair, and renovation activities to improve facility life cycle investments. *Journal of Performance of Constructed Facilities*.

- Ham, Y. (2015). Vision-based building energy diagnostics and retrofit analysis using 3D thermography and building information modeling. (*Unpublished PhD Dissertation*)., (University of Illinois at Urbana-Champaign).
- Ham, Y., & Golparvar-Fard, M. (2012). Identification of Potential Areas for Building Retrofit Using Thermal Digital Imagery and CFD Models. In *Computing in Civil Engineering (2012)* (pp. 642–649). Reston, VA: American Society of Civil Engineers. <https://doi.org/10.1061/9780784412343.0081>
- Hegde, G. M., & Ye, C. (2008). SwissRanger SR-3000 range images enhancement by a singular value decomposition filter. In *Information and Automation, 2008. ICIA 2008. International Conference on* (pp. 1626–1631). IEEE.
- Heliguy. (2017). DJI Zenmuse XT Thermal. Retrieved February 13, 2017, from <https://www.heliguy.com/blog/2016/04/28/insider-exclusive-dji-zenmuse-xt-ft-flir-thermal/>
- Holzer, S., Rusu, R., Dixon, M., & Gedikli, S. (2012). Adaptive neighborhood selection for real-time surface normal estimation from organized point cloud data using integral images. *2012 IEEE/RSJ*. Retrieved from http://ieeexplore.ieee.org/xpls/abs_all.jsp?arnumber=6385999
- Hsieh, Y., & Chio, S. (2015). Generation of Digital Surface Temperature Model from Thermal Images Collected by Thermal Sensor on Quadcopter UAV. *acrs2015.ccgeo.info*.
- Kaiser, H. H., & Davis, J. S. (1996). *A foundation to uphold: a study of facilities conditions at U.S. colleges and universities*. APPA.
- Key, J. (2016). EXPERIMENTAL RESEARCH AND DESIGN. Retrieved January 8, 2017, from <https://www.okstate.edu/ag/agedcm4h/academic/aged5980a/5980/newpage2.htm>

- Klein, L., Li, N., & Becerik-Gerber, B. (2012). Imaged-based verification of as-built documentation of operational buildings. *Automation in Construction*, 21, 161–171. <https://doi.org/10.1016/j.autcon.2011.05.023>
- Lagüela, S., Armesto, J., Arias, P., & Herráez, J. (2012). Automation of thermographic 3D modelling through image fusion and image matching techniques. *Automation in Construction*, 27, 24–31. <https://doi.org/10.1016/j.autcon.2012.05.011>
- Lagüela, S., Martínez, J., Armesto, J., & Arias, P. (2011). Energy efficiency studies through 3D laser scanning and thermographic technologies. *Energy and Buildings*, 43(6), 1216–1221. <https://doi.org/10.1016/j.enbuild.2010.12.031>
- Liu, W., Shen, J., & Chen, W. (2009). Image mosaic technology based on overlapped area linear transition method. *2009 2nd International Congress on Image and*.
- Lo, T. Y., & Choi, K. T. W. (2004). Building defects diagnosis by infrared thermography. *Structural Survey*, 22(5), 259–263. <https://doi.org/10.1108/02630800410571571>
- Mackenzie, H. (2013). Canada's infrastructure gap. (ALTERNATIVE FEDERAL BUDGET TECHNICAL PAPER). Canadian Centre for Policy Alternatives.
- Maldague, X. (2001). Theory and practice of infrared technology for nondestructive testing, 684.
- Markets, & Markets. (2014). *Unmanned Aerial Vehicle (UAV) Market by Class, Subsystem, Application, funding, & by Payload - Forecast & Analysis to 2014 - 2020*.
- McDougal, T. (2016). Introduction to Drones and UAVs. Retrieved from <http://www.bhphotovideo.com/explora/video/buying-guide/introduction-drones-and-uavs>

- Morgenthal, G., & Hallermann, N. (2014). Quality Assessment of Unmanned Aerial Vehicle (UAV) Based Visual Inspection of Structures. *Advances in Structural Engineering*, 17(3), 289–302. <https://doi.org/10.1260/1369-4332.17.3.289>
- National Centre for Education Statistics. (2013). *Facilities Information Management: A Guide for State and Local Education*. National Center for Education Statistics.
- Nex, F., & Remondino, F. (2014). UAV for 3D mapping applications: a review. *Applied Geomatics*, 6(1), 1–15. <https://doi.org/10.1007/s12518-013-0120-x>
- Nikon. (2016). Nikon | Imaging Products | Specifications - Nikon D600. Retrieved December 13, 2016, from <http://imaging.nikon.com/lineup/dslr/d600/spec.htm>
- Nishar, A., Richards, S., Breen, D., Robertson, J., & Breen, B. (2016). Thermal infrared imaging of geothermal environments and by an unmanned aerial vehicle (UAV): A case study of the Wairakei – Tauhara geothermal field, Taupo, New Zealand. *Renewable Energy*, 86, 1256–1264. <https://doi.org/10.1016/j.renene.2015.09.042>
- NRC, N. R. C. (2012). *Improving Energy Performance in Canada*. Retrieved from <http://oee.nrcan.gc.ca/publications/statistics/parliament11-12/parliament11-12.pdf>
- Oreifej, O., Cramer, J., & Zakhori, A. (2014). Automatic Generation of 3D Thermal Maps of Building Interiors. *ASHRAE Transactions*.
- Plesu, R., Teodoriu, G., & Taranu, G. (2012). Infrared thermography applications for building investigation. *Buletinul Institutului Politehnic Din Iasi. Sectia Constructii, Arhitectura*, 58(1), 157.


- Roca, D., Martínez-Sánchez, J., Lagüela, S., & Arias, P. (2016). Novel Aerial 3D Mapping System Based on UAV Platforms and 2D Laser Scanners. *Journal of Sensors*.
- RPLS.Network. (2016). 3DReshaper. Retrieved January 4, 2017, from <http://community.pobonline.com/reviews/item/63/75>
- Rufino, G., & Moccia, A. (2005). Integrated VIS-NIR hyperspectral/thermal-IR electro-optical payload system for a mini-UAV. *Infotech@ Aerospace*, 1–9.
- SAAB Aerosystems. (2006). Skeldar V-150. Retrieved January 7, 2017, from <http://defense-update.com/products/s/skeldar150.htm>
- Sadek, A. W., Kvasnak, A., & Segale, J. (2003). Integrated infrastructure management systems: Small urban area's experience. *Journal of Infrastructure Systems*, 9(3), 98–106.
- Safety express Ltd. Concordia university (2016). Retrieved from <http://www.safetyexpress.com/>
- Schreyer, A., & Hoque, S. (2009). Interactive three-dimensional visualization of building envelope systems using infrared thermography and SketchUp. *Proc. of InfraMation, Available Online: Http.*
- Siebert, S., & Teizer, J. (2014). Mobile 3D mapping for surveying earthwork projects using an Unmanned Aerial Vehicle (UAV) system. *Automation in Construction*.
- Snaveley, N., Simon, I., & Goesele, M. (2010). Scene reconstruction and visualization from community photo collections. *Proceedings of the*. Retrieved from http://ieeexplore.ieee.org/xpls/abs_all.jsp?arnumber=5483186
- Stachniss, C. (2015). Photogrammetry I - 08a - Matching - Cross Correlation. Retrieved January 7, 2017, from <https://www.youtube.com/watch?v=Afvg8SB6Fok>

- Stevenson, B. UAV solutions launches phoenix 15 UAS (2013). Retrieved from <https://www.shephardmedia.com/news/uv-online/uav-solutions-launches-phoenix-15-uas/>
- stm. (2016). Maps | Société de transport de Montréal. Retrieved December 13, 2016, from <http://www.stm.info/en/info/networks/maps>
- Teachers Guide to the Infrared. (2016). What is infrared light. Retrieved April 14, 2016, from http://coolcosmos.ipac.caltech.edu/image_galleries/ir_zoo/lessons/background.html
- Teax T. (2014). *User manual User manual for ThermalCapture*. [https://doi.org/No. rev2](https://doi.org/No.rev2)
- Transport Canada. (2016). Drone Safety -. Retrieved January 7, 2017, from <http://www.tc.gc.ca/eng/civilaviation/drone-safety.html>
- U.S. Department of Energy. (2012). Buildings Energy Data Book. Retrieved January 7, 2017, from <http://buildingsdatabook.eren.doe.gov/>
- Vavilov, V. (2010). A pessimistic view of the energy auditing of building structures with the use of infrared thermography. *Russian Journal of Nondestructive Testing*.
- Vollmer, M., & Möllmann, K. (2010). *Infrared thermal imaging: fundamentals, research and applications*.
- Wang, C. (2014). Point Clouds and Thermal Data Fusion for Automated gbXML-based Building Geometry Model Generation. (*Unpublished PhD Dissertation*)., (Georgia Institute of Technology).
- Wang, C., & Cho, Y. (2011). Non-invasive 3D Thermal Modeling for Buildings. In *ASCE, International Conference on Sustainable Design and Construction in Kansas City, MO*.

- Wang, C., & Cho, Y. (2014). Automatic 3D thermal zones creation for building energy simulation of existing residential buildings. *Construction Research Congress*.
- Wang, C., Cho, Y. K. Y., & Gai, M. (2012). As-is 3D thermal modeling for existing building envelopes using a hybrid LIDAR system. *Journal of Computing in Civil Engineering*, 27(6), 645–656.
- Westoby, M., Brasington, J., Glasser, N., & Hambrey, M. (2012). “Structure-from-Motion” photogrammetry: A low-cost, effective tool for geoscience applications. *Geomorphology*.
- Wild, W. (2007). Application of infrared thermography in civil engineering. *Proc. Estonian Acad. Sci. Eng.*

APPENDIX

Table 6-1: Total energy consumption (Mtoe) (Enerdata, 2016)

Total energy consumption (Mtoe)								
	2010	2011	2012	2013	2014	2015	2014 - 2015 (%/year)	2000 - 2015 (%/year)
World	12900	13125	13321	13540	13678	13778	0.7	2.1
OECD	5410	5312	5260	5313	5262	5260	0.0	0.0
G7	3927	3828	3763	3816	3786	3764	-0.6	-0.4
BRICS	4378	4654	4824	4952	5081	5139	1.1	4.8
Europe	1924	1862	1854	1838	1769	1800	1.8	-0.2
European Union	1721	1658	1646	1625	1557	1578	1.3	-0.5
Belgium	61	58	54	56	54	54	0.4	-0.5
Czech Rep.	44	43	43	42	41	40	-2.1	-0.3
France	262	252	252	253	244	246	1.1	-0.2
Germany	327	311	312	318	302	305	1.1	-0.7
Italy	170	167	162	156	146	152	3.9	-0.8
Netherlands	83	77	79	77	73	72	-1.5	-0.2
Poland	101	101	98	98	94	96	1.4	0.5
Portugal	23	23	22	22	21	22	3.4	-0.7
Romania	35	36	35	32	32	33	1.2	-0.7
Spain	128	125	124	115	113	116	3.0	-0.3
Sweden	51	50	50	49	48	47	-2.8	0.0
United Kingdom	202	188	193	191	178	179	0.6	-1.5
Norway	34	28	30	33	31	32	4.7	1.4
Turkey	105	112	117	117	121	127	5.3	3.4
CIS	1010	1056	1072	1055	1051	1028	-2.2	0.9
Kazakhstan	69	77	74	82	82	78	-5.0	5.4
Russia	689	723	741	730	731	718	-1.7	1.0
Ukraine	133	127	123	117	106	92	-13.1	-2.2
Uzbekistan	43	47	48	43	45	45	1.0	-0.8
America	3254	3250	3224	3291	3328	3293	-1.0	0.4
North America	2467	2449	2393	2443	2473	2446	-1.1	-0.2
Canada	251	257	252	253	256	251	-2.2	0.0
United States	2216	2192	2140	2190	2217	2196	-0.9	-0.2
Latin America	787	801	831	848	855	847	-0.9	2.4

Background on the evolution of UAS

The evolution of unmanned aerial systems (UAS) started for more than a century. In the late nineteenth century and beginning of the twentieth century, the technology of flying airships and unmanned balloons was improved and updated. Later, the concept of an unmanned aircraft was developed and took place in 1917 of World War 1 by the US army (Colomina & Molina, 2014). For many decades, the main purpose of aerial aircraft was observed in the military actions and war contexts. For example, UAS were used during the Vietnamese war that took place between 1963 and 1973, also, Israel used UAS in its war against Egypt during the 1973 October war (Gertler, 2012). In the late nineteen-seventies, researchers started to understand the power of UAS in surveillance, control, monitoring, and other related applications that serve the civilian sector. As a result, some initial experiments and trials were occurred, for the first time, in places like Australia, UK, and Japan for applications other than military purposes. Finally, the past decade showed a remarkable enhancement in the manufacturing and improving UAS technology worldwide (Colomina & Molina, 2014). Currently, UAS have invaded the world market in fields related to business, construction, agriculture, safety etc. The future of UAS is promising in all fields, especially in the field of Photogrammetry and Remote Sensing (PARS) and mapping (Eisenbeiß, 2009).

Consequently, UAS have shown a remarkable utilization in PARS and has become a notable practice in aerial imaging. In the beginning, the idea of collecting aerial images has started in the late of the nineteenth century where balloons, kites, and rockets were used for aerial photography. For example, aerial photographs of Paris were captured in 1858 by unmanned balloon (Colomina & Molina, 2014). However, the first experiment in unmanned aerial photographs was held by J. Neubronner in 1903 when he mounted a small camera on the breasts of a pigeon. Later on, manned aerial photographs took place in 1909 by W. Wright when he shot a motion pictures using his home-made airplane (Colomina & Molina, 2014). After that, researchers suggested to evolve the aerial remote sensing using a remotely-piloted aircraft or as later named unmanned aerial remote sensing. In the late of the twentieth century, tests and experiments were established using different types of aircraft (eg. Rotary and fixed-wing, single and multi-rotor, remotely- and auto-piloted platforms) as the key development of UAS and their implementation in PARS (Eisenbeiß, 2009).

In general, UAS efficiency in civilian sectors has been proven in many applications and aspects, which can be illustrated in the following advantages stated by (Eisenbeiß, 2009; Elhassan et al., 2015):

1. UAS is very efficient when used in risky situations and dangerous circumstances, without risking the human-life of staff. For example, it can be after natural catastrophes, war conflict zones and dangerous places in terms of geography, weather, and safety.
2. UAS are small in size and light in weight, thus, can be used in small, unapproachable, and isolated locations such as caves, tunnels, and mining structures.
3. UAS are cost and physical effective when compared to traditional manned aircraft.
4. UAS supports the technology of real-time data collection and live-video record which is connected with the ground station.
5. UAS are time-efficient and user-friendly equipment that needs no previous knowledge and requires no training courses or any special skills for operation.

Types of Unmanned Aerial Systems (UAS):

UAS can be classified into many types by means of different elements, they can be characterized and classified according to several criteria's such as (size, weight, endurance, aerodynamics, range coverage, wind dependency, maneuverability, price, localization and positioning, real-time capabilities, and application accuracy requirements, Etc.). However, there is no unified or standard classification for the types of UAS (Eisenbeiß, 2009). As a result, researchers started to classify UAS into different types according to different variables, for example (Colomina & Molina, 2014) defined three types of UAS with respect to various characteristics of the aerial platform. Categorization and characteristics are shown respectively in Table 6-2; (1) nano-micro-mini UAS, (2) close-short-medium range UAS, and (3) the remaining UAS. In which, the nano-micro-mini UAS have the shortest operation range and the lowest maximum takeoff weight. Thus, it is considered as the most suitable and appropriate type with the PARS needs. From Table 6-2 **Error! Reference source not found.**, (Colomina & Molina, 2014) classified the weight-based range for the maximum take-off weight (MTOW) as follow: micro less than 5 Kg, mini less than 30 Kg, tactile-less than 150 Kg, and high more than 150 Kg.

Table 6-2: Types and characteristics of UAS (Colomina & Molina, 2014)

Types of UAS	Characteristics
1- Nano-micro-mini UAS	<ul style="list-style-type: none"> • Low weight • Low flying altitude • Low payload sizes • Rapid operational categorization • Operating range less than 10 km • Low range endurance • Mini maximum take-off weight (MTOW), less than 30 Kg
2- Close-short-medium-range UAS	<ul style="list-style-type: none"> • Operating range between 10 and 70 km • Fixed and rotary wing developments • High maximum take-off weight (MTOW), between 150 and 1250 kg
3- Rest of UAS	<ul style="list-style-type: none"> • Medium ranges endurance • Highest operating altitude

Table 6-2: comparison between fixed-wing UAS and rotary-wing UAS (Siebert & Teizer, 2014)

Types	Fixed-wing UAS	Rotary-Wing UAS
Airtime	More	Less
Noise	Less	More
Take-off and Landing	Need airstrip	Don't need airstrip

Other classifications of UAS are determined with respect to factors related to the type of UAS-wing. For example, (Siebert & Teizer, 2014) classified UAS into two main types as fixed-wing UAS and rotary-wing UAS. Table 6-2, shows a comparison between the two UAS-wing types by means of airtime, noise, take-off and landing. As a result, fixed-wing UAS have more airtime and less noise when compared with the rotary-wing UAS while fixed-wing UAS requires an airstrip for take-off and landing which is not the case for rotary-wing UAS. Consequently, fixed-wing UAS are considered more suitable for applications related to control and investigation, while the rotary-wing UAS are preferable for applications applied in bounded and restricted spaces since they are more stable, steady, user-friendly and easy to operate by means of take-off and landing.

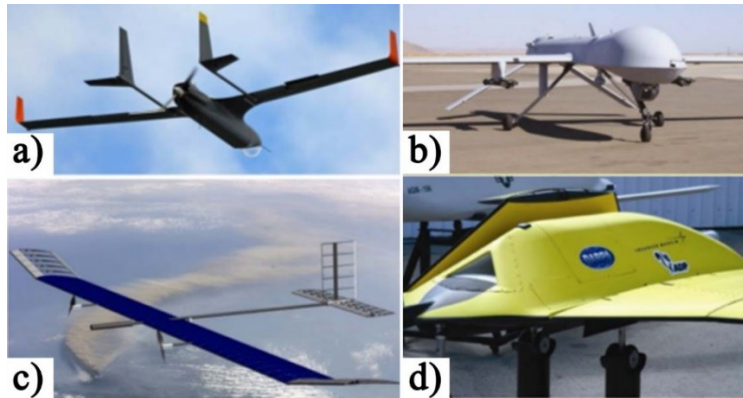


Figure 6-1: Fixed-wing UAS; a) Insitu Inc., USA-Integrator; b) General Atomics Aeronautical Systems, USA-Predator A; c) QinetiQ, UK-Zephyr; d) Lockheed Martin, USA-Morphing UAS. (Colomina & Molina, 2014)



Figure 6-2: Rotary wing UAS; a) Cheerson CX10 nano UAS (Andi, 2015), b) Phoenix 15 micro UAS (Stevenson, 2013), c) Phantom 3 professional mini UAS (dji, 2016), d) Skeldar 150 VTOL and e) Tricopter UAS (SAAB Aerosystems., 2006), f) Matrice 100 (DJI, 2016), g) s1000 octocopter UAS (Dji, 2014), h) MQ-8B Fire Scout by USnavy (Ben, 2015)

In (Figure 6-1), different types of fixed-wing UAS are shown with respect to their sizes and their applications. For example, in (a) the “USA-Integrator” developed by Institute Inc. are mainly used as a weather tracking system for commercial, civil, and military actions. Second, in (b) “the USA-Predator A” designed by General Atomics Aeronautical Systems are manufactured as unmanned combat air vehicle. Third, in (c) the “QinetiQ Zephyr” developed by the UK Company are designed for high altitude long endurance unmanned aircraft. Finally, in (d) the “USA-Morphing UAS” designed by Lockheed Martin are considered as a revolutionary prototype for the next generation of UAS (Colomina & Molina, 2014). While in Figure 6-2, different types of rotary-wing UAS are shown with respect to their sizes and number of copters. The first three figures (a, b and c) represents the different sizes of a rotary-wing UAS mentioned as nano, micro, and mini UAS respectively. While, the other figures (d, e, f, and g) are related to the number of copters mentioned as helicopter, tri-copter, quad-copter and octa-copter respectively. Finally, figure (h) is an example of a rotary-wing UAS that is used in military context applications.

The system configuration of Unmanned Aerial Systems (UAS):

UAS technology is a combination of different systems that are collected together to achieve a specific objective. Technically, UAS composition includes three main components that are (1) ground control station, (2) communication data link and (3) Unmanned Aerial Vehicle (UAV) (Eisenbeiß, 2009). First, the ground control station can be a mobile or immobile device that is used for aircraft remote control monitoring. Second, communication data link is responsible for controlling and monitoring of an aircraft with its ground station device through a connection that links them together. Finally, the UAV is the aircraft itself where it receives the commands sent from the ground central station using sensors that calculate the corresponding flight information related to (Sensing, navigation, and orientation). Then, UAV sends them back to the Flight Control Unit (FCU) that uses them for flight navigation through motors and propellers (Colomina & Molina, 2014). However, other researchers have categorized UAS based on their components. Mainly, UAS can be classified into seven main key components (McDougal, 2016).

Accordingly, the transmitter works as a ground control station which connects the aircraft’s receiver by means of communication data link. In Figure 06-3, (McDougal, 2016) has analyzed and illustrated these components as follow:

1. Main Controller (MC): It is considered as the brain of the UAS, it has a software for control and monitoring.
2. Sensors: The main objective of sensors is to detect the acceleration changes of the UAS, its level, and orientation.
3. Electronic Speed Controllers (ESCs): They are responsible for arranging the power going to motors.
4. Receiver: links the unmanned air vehicle with the radio control system known as the transmitter
5. Motors: brushless motors, in which its parts rotates either clockwise or counter-clockwise with respect to their position and orientation.
6. Propellers: plastic props that are safer and more flexible.
7. Transmitter: A radio control system is a combination of a mobile app and Wi-fi compatible with tablets and smartphones.



Figure 06-3: UAS composition (McDougal, 2016)

Safety and Regulations of Unmanned Aerial Systems (UAS):

UAS have some limitations and special regulations related to civilian applications. First of all, UAS need to be flown with the presence of a backup pilot or a controller in its line of sight. The controller should be aware and have the knowledge of a remote control and monitoring of unmanned aircraft (Eisenbeiß, 2009). Regulations related to UAS differs from one country to another and have different hierarchical classes of local, national and continental authorities. Some regulatory bodies consist of a group of countries, others are related to a specific continent. For example, in North America, the US Federal Aviation Administration (FAA) developed a plan for integrating the civilian use of UAS in the national airspace system without altering its capacity, affecting its safety or increasing the risk (Colomina & Molina, 2014). While in Europe, the European Aviation Safety Agency (EASA) requires all UAS that has a maximum take-off bigger than 150 Kg to be certified by EASA, where all other UAS with a maximum take-off less than 150 Kg are required to be certified only by the national authorities (Eisenbeiß, 2009). Also, other rules and regulations that were developed are related to environmental protection. On the other hand, the European organization for the safety of air navigation, known as Euro-Control, had developed and applied an air traffic management system for both civilian and military users (Colomina & Molina, 2014; Eisenbeiß, 2009)

In Canada, Transport Canada is considered the direct authority that is responsible for the regulations for the control and use of UAS. According to (Transport Canada, 2016), it is prohibited for UAS users to fly close to airports, heliports, aerodromes, forest fires and built-up areas in a radius of 9 km. Also, it is prohibited to fly over military basis, governmental buildings or any restricted areas. Similarly, it is prohibited to carry dangerous goods or to fly over crowds or to be higher than 90 m. However, (Transport Canada, 2016) do not require any permission of aviation if the UAS is used for research work and it weighs less than 2 Kg; but in case it weighs more than 2 Kg and less than 25 Kg, a set of exemption requirements are required that ensures safety precautions and privacy rights. Therefore, Transport Canada must have the contact information for the UAS owner and controller, UAS model, UAS description of the model, and the geographical boundaries of operation before any UAS aviation. Finally, some tips for a safe aviation recommends to fly during daylight and in good weather, the controller must be present in the aircraft line of sight, and to respect the privacy and safety of others (Transport Canada, 2016).

The main objective of the different levels and types of UAS regulatory bodies is to ensure the public safety and to preserve their security and rights. Consequently, associated agencies and authorities enact regulations taking in considerations many safety measurements related to the size, weight and flight technology of UAS. From Table 6-3, some different regulations for UAS civil use in several countries of different continents are mentioned (Nex & Remondino, 2014).

Table 6-3: Regulations for UAS use in several countries (Nex & Remondino, 2014)

Continent	Country	Regulatory bodies for UAS Civil Use (laws and regulations)
North America	Canada	Approach to the Classification of Unmanned Aircraft, 19.10.10
	USA	UAS Certification Status, 18.08.08; Fact Sheet- Unmanned Aircraft Systems, 15.7.10 und NJO7210.766, 28.3.11, 8.2.12 und FAA Bill
Oceania	Australia	CASA Circular, July 2002
Europe	Great Britain	CAP 722, 06.04.10 u. Joint Doctrine 2/11, 30.3.11
	France	Decree concerning the design of civil aircraft flies without anyone on board, August 2010

Applications

Based on the all above mentioned, UAS have invaded the worldwide market and started to be invested in a variety of applications that includes but not limited to construction and engineering (e.g., wind turbines, power lines, bridges, solar panels, and tunnels). Other researchers, used UAS-based thermo-graphic 3D modeling for inspection and condition assessments of building envelopes, building roofs, infrastructures and other structures such as bridges (Colomina & Molina, 2014; Eisenbeiß, 2009). In summary, some of the applications of UAS are as follow:

1. Construction Industry: Using UAS in construction sites allows the collection and documentation of the site aerially, this will enable the site's control and monitoring through the construction process. Also, it will provide and view the as-built situation of construction sites that can be used for up-to-date assessments, volumetric measurements, earth-work monitoring, soil excavation management and any further analysis (Eisenbeiß, 2009).

2. **Surveying:** The implementation of UAS-based photogrammetry and 3D mapping techniques as a replacement for the old manual and traditional practices in surveying is considered more beneficial by means of cost, time, effort, and safety. Similarly, many researchers have conducted studies to prove the efficiency of replacing the old surveying techniques using UAS-based photogrammetry for indoor environments. Also, (Siebert & Teizer, 2014) introduced the sfm algorithm principle in UAS-based photogrammetry using related software (e.g, Agisoft PhotoScan and Autodesk Recap 360).
3. **Agriculture Analysis:** UAS-based imagery can be a powerful technique in vegetation control, by replacing the old-fashioned techniques that depend on the visual assessment of inspectors (Colomina & Molina, 2014; Eisenbeiß, 2009; Siebert & Teizer, 2014).
4. **Mining:** UAS are a very powerful tool when tested in confined spaces or other inaccessible places that are difficult for a human to reach. Mining is one of these places in which UAS can be very helpful, it is also considered as safer in dangerous locations (Eisenbeiß, 2009).
5. **Emergency Response and Prevention:** UAS are very helpful when tested in post-disaster assessment, by collecting very high-quality critical data that can be stored and enabled for later accurate measurements. Many researchers and studies were conducted using UAS in emergency response, (Rufino & Moccia, 2005) used UAS to enhance control management of forest fires. Other applications of testing UAS in emergency responses can be related to crime scenes documentation, intelligence, surveillance, and reconnaissance.
6. **Aerial Photogrammetry:** Image-based modeling using UAS images can be used for a variety of applications, such as documentation of archaeological and cultural heritage sites, creating 3D city models that are related to other aspects of the city and urban planning, architecture and design, and many other applications (Eisenbeiß, 2009).
7. **Environmental Monitoring:** UAS can be a powerful tool for viewing and monitoring key resources, endangered species, their habits and behavior and much more in the environmental applications. Also, it is used to monitor hazardous places that are difficult for a human to achieve such as ice melting monitoring in Antarctica and in the North Pole. Similarly, (Eisenbeiß, 2009) mentioned how UAS images were used for documentation of large rock slide areas in Randa, Switzerland.